Material properties of skin in a flying snake (*Chrysopelea ornata*)

Sarah Bonham Dellinger

Thesis submitted to the faculty of the Virginia Polytechnic Institute and State University in partial fulfillment of the requirements for the degree of

Master of Science
In
Engineering Mechanics

John J. Socha, Chair
Raffaella De Vita
Pavlos P. Vlachos

April 27, 2011
Blacksburg, VA

Keywords: flying snakes, skin, material properties, digital image correlation
© Sarah Bonham Dellinger 2011

Material properties of skin in a flying snake (*Chrysopelea ornata*)

Sarah Bonham Dellinger

ABSTRACT

The genus *Chrysopelea* encompasses the "flying" snakes. This taxon has the ability to glide via lateral aerial undulation and dorsoventral body flattening, a skill unique to this group, but in addition to other functions common to all colubrids. The skin must be extensible enough to allow this body shape alteration and undulation, and strong enough to withstand the forces seen during landing. For this reason, characterizing the mechanical properties of the skin may give insight to the functional capabilities of the skin during these gliding and landing behaviors. Dynamic and viscoelastic uniaxial tensile tests were combined with a modified particle image velocimetry technique to provide strength, extensibility, strain energy, and stiffness information about the skin with respect to orientation, region, and species, along with viscoelastic parameters. Results compared with two other species in this study and a broader range of species in prior studies indicate that while the skin of these unique snakes may not be specifically specialized to deal with larger forces, extensibility, or energy storage and release, the skin does have increased strength and energy storage associated with higher strain rates. The skin also has differing properties with respect to dorsoventral location, and regional differences in strength in the circumferential orientation. This may indicate that, although the properties of the skin may not be different, the rate at which the skin is strained in the different species may vary, thus altering the apparent properties of the skin during specific behaviors.

Dedication

To Matthew…

For all your love and support, thank you.

Acknowledgements

First, I would like to thank the members of my committee, Dr. Pavlos Vlachos and Dr. Raffaella De Vita for their continuous help throughout this study. I would also like to acknowledge the other members of the DARPA snake team and AEThER lab for their helpful suggestions and assistance with image correlation. Next I must thank, my advisor, Dr. Jake Socha, not only for his for his continual guidance and assistance in this study, but also for helping me to see the bigger picture. I would also like to thank Carolyn Roberts for her assistance with dissection and experimental testing. Funding for this project was provided by DARPA.

I would also like to thank my family, biological or not, for constantly encouraging me through this. Lastly, I would like to not only thank anyone who has sent up a prayer for me, but most especially the One answering them.

Table of Contents

List of Figures

List of Tables

List of Symbols

$\varepsilon'_{11}, \varepsilon'_{22}$	Linear Lagrangian strain
e'_{11}, e'_{22}	Linear Eulerian strain
$\varepsilon_{11}, \varepsilon_{22}$	Nonlinear Lagrangian strain
e_{11}, e_{22}	Nonlinear Eulerian strain
X_i	Reference frame coordinates
x_i	Moving frame coordinates
u_i	Displacement
λ_1, λ_2	Stretch ratio
σ	Stress
w	Initial width of sample
t	Thickness of sample
A_o, $A(t)$	Initial, current area of sample
W	Strain energy
E	Modulus

Chapter 1: Introduction

1.1 Overview

The functional demands of the skin of the 'flying' snakes (g. *Chrysopelea*) are unique. These snakes employ aerial in combination with dorsoventral body flattening to create a gliding behavior. In general, snake skin functions as a protective barrier from the elements [1], a fluid barrier to preserve body hydration level [2], and camouflage [3]. In macrostomates (snakes which ingest large prey whole), the skin allows the body to expand to accommodate a food bolus [4]. Although these functions are seen in all colubrids, the skin of gliding snakes performs other additional functions, such as simultaneous stretching in the circumferential and longitudinal directions to accommodate the body flattening and undulation associated with gliding behavior [5, 6]. The skin must also withstand landing forces, which can be orders of magnitude greater than body weight [7]. In tree snakes, the skin is also thought to function as a vasoconstrictor, preventing blood from pooling in the portion of the body closer to the ground (most likely the caudal end), though this may be affected more by the skin's connection to underlying musculature than the properties of the skin [8]. Because of these unique functional demands, the mechanical properties of the skin may influence these behaviors.

To date, there have been few studies performed on the mechanical properties of snake skin. Prior investigation of snake skin in relation to feeding behavior [9] and locomotion (terrestrial and aquatic) [10] has been performed, and determined that skin is specialized to handle large food objects with larger low-stress circumferential strains in the pre-pyloric region and may also be specialized for different types of locomotion (terrestrial, aquatic, arboreal, etc) as indicated by some differences in properties between snakes using different modes of locomotion. However, the integration of skin and underlying tissue may present even more evidence for locomotor specialization [10]. No tests have been performed on the skin of gliding snakes, and therefore it is not known if, and in what ways, the skin is specialized for the specific functional demands of takeoff, gliding, and landing.

To characterize how the skin of flying snakes performs as a mechanical system, several parameters are examined here. The research presented will focus on strength, extensibility, energy storage and return, stiffness, as well as rate and time dependent responses. Each property

reveals details about the mechanical capabilities of the skin. Strength is indicative of the stress the skin can withstand without breaking. Similarly, extensibility is indicative of the distensibility of the skin before it fails. Although the modulus of elasticity and strain energy are functions of stress and strain, they also have their own functional correlates. Considering the skin to contain bundles of fibers oriented in certain directions, the modulus, or stiffness, of the material can be indicative of the orientation of fibers with respect to the load being applied. Lastly, strain energy relates the amount of energy that can be returned to the system after the skin is stretched or absorbed if failure occurs. If a large portion of the energy is returned, it can assist in passively returning to the initial configuration. If little energy is returned, the snake must actively return the body to the starting configuration, expending additional energy.

From a mechanical point of view, this tissue is complex. It can be thought of as a composite structure with both elastic/rigid (scales) and viscoelastic (protein fibers, matrix, and connective tissue) structures. However, before the individual portions of the skin are analyzed to determine functional capabilities, the structure as a whole should be examined.

1.2 Contributions and Hypotheses

This thesis seeks to analyze patterns of load and deformation of the overall system when the skin is stretched to failure. Although previous studies have been performed on snake skin, there are currently no data on *Chrysopelea*. Secondly, methodological issues have been presented in each that should be overcome to accurately characterize the response of the material by accounting for hydration, viscoelasticity, and other aspects of biological tissues that are often unaccounted for. Methodological problems of prior studies include failure/shearing of samples at the grips, samples slipping from the grips, inconsistency in sample shape, lack of hydration during testing, lack of preconditioning, stress concentration due to gripping techniques, and strain calculation inaccuracies due to test shape and gripping methods [9, 10]. This study presents a method of testing and analysis that considers the nonlinearity and viscoelasticity of the tissue, along with considerations for standard tensile test techniques that will address some of these issues.

The hypotheses of this thesis are as follows: 1) flying snake skin should be stronger and have greater energy absorption capabilities to deal with the dynamic deformation of the skin during

gliding behaviors, especially landing, 2) the skin of gliding snakes may have greater energy return than non-gliding snakes (as gliding snakes also move on land, the energy return may play more of a role in terrestrial locomotion, since the ground friction force is likely greater than any drag forces seen in aerial locomotion), 3) the skin should be more extensible in multiple directions at once to accommodate simultaneous body shape change and undulation behaviors, and possibly more uniformly extensible if body shape change yields greater strains than other strains typically seen, and 4) the properties of skin may be strain rate dependent as the functional demands may vary with rate. To address these hypotheses, the properties of snake were examined using uniaxial tensile tests. Skin was tested at two strain rates to failure, and also for creep, relaxation, and hysteresis responses. Statistical comparisons were performed by examining three different orientations in two regions along the snake (based on results from [9], properties vary with respect to cranio-caudal body location), and also across species. Lastly, results from *C. ornata* are compared to other colubrid snakes to determine if there are differences in mechanical properties between aerial and terrestrial locomotors.

1.3 Organization of Thesis

In Chapter 1, a brief introduction to the background of flying snakes and skin mechanical properties is given, along with problems that will be addressed. The hypotheses being tested are also presented, with a basic overview of methods. Chapter 2 presents a review of the relevant literature on flying snakes, mechanical testing of soft biological tissues, snake skin structure, snake skin material properties, and a brief overview of digital image correlation, specifically as applied to biological tissues. The methods used for testing and analysis are given in Chapter 3. Chapter 4 presents a comprehensive mechanical view of three species of snake skin based on quasi-static, dynamic, and cyclic tests. Chapter 5 discusses the biological and mechanical implications of this study. Suggestions for future work and improvements to this study are presented in Chapter 6.

Chapter 2: Background and Review of Literature

As the premise of this thesis is to not only present a comprehensive characterization of snake skin, but to do this across both aerial and terrestrial locomotors, an overview of flying snakes is given. This chapter begins by reviewing the previous work performed in the areas of snake skin structure, snake skin mechanics, and other reptile skin mechanics. The kinematics work performed on gliding snakes is also included as a reference for the animals of particular interest in this study, *Chrysopelea*. Relevant work in the area of digital image correlation is also included, especially as applied to biological tissue.

2.1 Flying Snakes

The genus *Chrysopelea* encompasses the 'flying' snakes, a group of Southeast Asian arboreal colubrid snakes. Like many other gliders, a major feature of snake gliding is an increase in surface area from the normal configuration, although the exact aerodynamic mechanisms are not understood. Unlike animals that are capable of true flight, 'flying' snakes are not able to generate enough lift to gain altitude relative to the starting height, though positive accelerations may be seen [11].

Of these species, *Chrysopelea paradisi* is the premier glider, with glide angles around 28° and a maximum gliding distance of 21 m (with takeoff height of 9.8 m) [5]. To take off, the animal hangs in a J-shape loop from a branch, and launches itself upward [12]. However, the animal can also glide when it 'falls' from the same height as previous J-shape launches. Gliding behavior includes a combination of aerial undulation, body flattening, and tail motion, and possibly other unidentified small-scale behaviors. When the body is flattened, the ribs likely move in the dorso-cranial direction, causing the body width to almost double [5, 6]. This creates an airfoil shape that allows the wing loading of the snake to be decreased, and increases the lift coefficient relative to a cylindrical shape [13]. The typical undulations seen in the animal have a lateral amplitude of approximately 0.1 m and frequency of 1-2 Hz [11]. These parameters are later used to estimate the average strain rate of skin during undulation. Finally, preliminary consideration of landing behaviors has estimated landing forces of 12-20x body weight [7].

Factors such as the change in body shape along with aerial undulation, as well as landing behaviors, make this taxon an interesting subject of study, particularly in terms of functional capabilities of the skin.

2.2 Snake Skin Structure & Function

The skin of snakes is composed of several components, the majority being keratin, collagen, and elastin [10, 14, 15]. Among the keratin proteins are the α protein (single-strand structure) and β protein (structure similar to feather) [16]. The skin is made up of several layers, each with varying protein content [15]. However, variances in nomenclature among structural studies make characterization of the skin difficult.

From micrographs of the skin (see [17] for images) and Figure 2-1, we can see that there are several distinct regions in the skin. The skin itself is connected to the underlying musculature via connective tissue. It is thought that the compliance of this connection is correlated with the mode of locomotion used by snakes. Tree snakes have less compliance in this connection than non-arboreal species, especially in the caudal end of the snake. The tightness of the skin-musculature connection in tree snakes is thought to prevent blood pooling near the tail of the snake while climbing [8]. Scales are centrally integrated with the underlying dermis, with the edges of the scale overlying an inter-scalar region of skin that appears to be folded [17]. The dermis located below the scale is slightly thicker than other regions (i.e. below the free margin/inter-scalar skin)[14]. In an unloaded state, the free margins of the scales overlap one another, and this pattern of overlap can vary with species. When a load is applied to the skin, these folded inter-scalar regions unfold. To achieve this unfolding, only minor loads are needed [17]. When the skin is loaded further, the inter-scalar skin begins to stretch, while the skin beneath the scales may remain somewhat unstretched. This stretching of the skin between the scales is thought to contribute to some of the non-linearity in the stress-strain response of the skin, particularly in the low-stress region [15, 17]. Figure 2-2 shows separate views of skin in normal and stretched configurations.

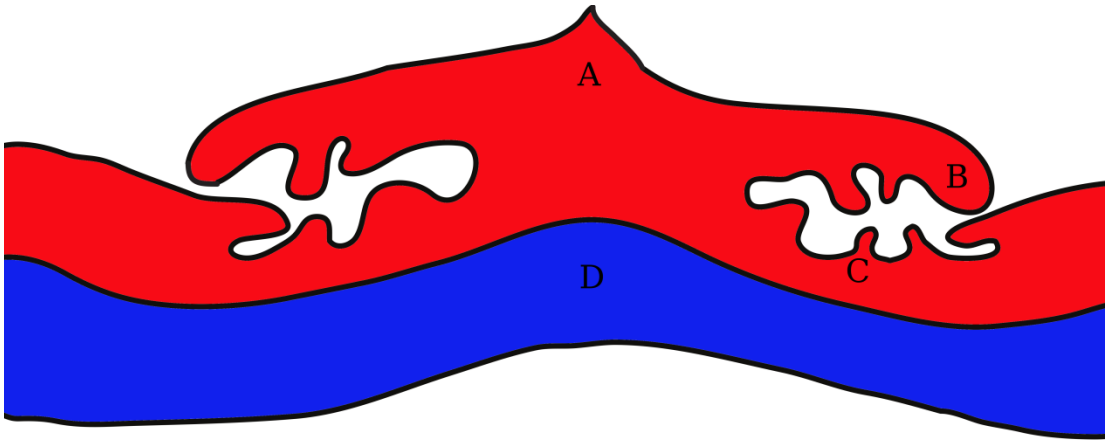

Figure 2-1: Snake skin structure (derived from [14, 17]). The scale region is indicated by (A), free margin is indicated by (B), inter-scalar skin is indicated by (C), and underlying dermis are shown in blue at (D). The percentage of scale characterized as free margin varies among species, and along the snake [14].

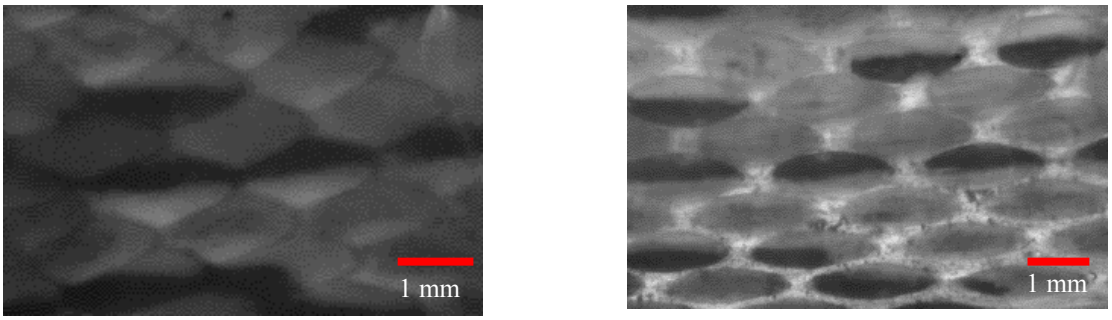

(a) (b)

Figure 2-2: External surface of *Elaphe guttata* skin in an unloaded (a) and loaded (b) state. In early loading to stresses which are still in the toe region, the inter-scalar skin unfolds as seen in (b).

2.3 Mechanical Properties of Biological Tissues

Mechanical testing has long been used as a method of determining the elastic properties of soft tissues. However, there are many challenges that come with this. First, many biological materials are non-linear, and in some cases, stress is an exponential function of strain. This reflects that the stiffness of the material changes over the range of strains or stresses applied. Biological material properties also depend on the recent strain history of the tissue. Preconditioning is a pre-test method used to decrease the low-strain hysteresis response of the tissue to a relatively steady state value and is recommended when using any biological tissue due to strain history dependence [18].

Similar to some other materials (i.e. hyperelastic materials such as rubber), biological materials tend to change dimensions in more than one direction when tested in uniaxial tension. As they are often assumed to be incompressible (since they are mostly composed of water), it can be assumed that the product of the stretch ratios along the major loading axes is equal to 1. For this reason, the cross-sectional area of some biological tissues (i.e. directions 1 and 3 in Figure 3-5) is a function of the stretch ratio in the direction of loading, $\lambda_2 = \frac{1}{\lambda_1 \lambda_3}$. In cases where small strains are observed and the change in area is negligible, infinitesimal (or small) strain theory is used. However, in biological materials that experience strains of over 5-10% before failure, small strain theory should not be used. Along with large strains in the direction of the load, the tissue also experiences strain perpendicular to the load, further invalidating infinitesimal strain theory [18].

Many biological materials may also not be described as Hookean because stress increases at a faster rate with increasing strain, instead of the constant rate of linear elastic solids. Also, *in vivo* tissues are in a constant state of 'prestress' (prestress indicating that that the tissues are partially loaded under normal conditions), which also is not accounted for in Hooke's law [18]. A further assumption in testing of biological materials is that the tissue is homogeneous at the macro-scale, even though biological materials are known to be non-homogeneous at the macro- and micro-scale [19], and clearly snake skin falls at the end of the spectrum of non-homogeneous tissues..

The implications of these assumptions and simplifications are discussed later.

2.4 Skin Material Properties

2.4.1 Snakes

To date, only two studies on the material properties of fresh snake skin are known to have been performed [9, 10] . From these studies, it is known that the material properties of snake skin vary across species and location on the body of the snake. These property differences are thought to be associated with varying morphologies and locomotor behaviors. Both of these studies give a starting point for future snake skin material properties research, and some issues within these will be addressed in this study.

The first study by Jayne [10] focused on locomotor behavior and how costocutaneous muscles affect the stiffness of the skin. This study showed that, when skin is loaded in the longitudinal direction (snout-vent), the ventrolateral skin was the most compliant (or extensible) compared to the other regions (dorsal and ventral), whereas the dorsal skin was the least extensible. Although it may seem intuitive that snakes of a similar size would have similar skin properties, this was found not to be the case. The relatively high stiffness of the skin in general was attributed to collagen fibers. This study also noted a 'step phenomenon' that occurs at approximately 15% strain where the load instantaneously decreases slightly as the skin is stretched, which Jayne attributed to the stratum corneum often separating from other layers of skin [10]. However, because this step is referenced by other studies on mammalian skin [20], this may not be the actual cause of the phenomenon seen in snake skin.

A more recent study by Rivera et al. [9] focused on skin properties in the circumferential direction in one species of snake. This is important as many snakes, especially colubrids, are macrostomates [21]. As the actual movement mechanism of the snake is different in this direction, the properties may differ from those loaded longitudinally, suggesting an anisotropic material. In this study, the skin was shown to have varying properties with respect to location along the body. Maximum stress of the samples ranged from approximately 8-15 MPa and the elastic modulus at 2.0 MPa ranged from approximately 5-12 MPa. The modulus also increased two to three times from snout to vent, and the overall strain at a particular stress decreased from snout to vent. Because of these regional differences in properties, particularly strain, it can be inferred that the extensibility of the skin could be related to the size of prey normally ingested, specifically in the pre-pyloric region. However, further study is necessary for a definite comparison, as only one species was examined. Also, the 'step phenomenon' mentioned above was not mentioned in this work [9], indicating that its occurrence may be a function of direction.

In addition to the two studies on fresh skin, a recent study examined tanned cobra skin [22], specifically looking at anisotropy in the skin and how this relates to movements seen in the body in various directions. To focus on possible anisotropy, uniaxial tensile tests to failure were performed on rectangular sections of cobra leather cut at various angles along the body of the snake. The results showed that failure stress increased as the angle rotated from transverse (circumferential) to cranial-caudal (longitudinal), while failure strain had the opposite effect. The differences with changes in orientation angle were more prominent in the dorsal location than the

abdomen, indicating that the skin in this area is more anisotropic. Failure stress was also shown to decrease in cranial-caudal samples when moving from the spine outward, and increased slightly in the transverse segments. Again, the opposite relationship was seen in failure strains [22].

2.4.2 Similar Tissues

Similar material property experiments have been performed on the skin of other reptiles, particularly various gekkonid lizards [23, 24]. The resulting stress-strain curves showed the typical J-shape curve of many nonlinear biological materials with maximum strains of approximately 30-60%, maximum stresses between 1.3 and 11.5 MPa, elastic moduli of 7-42 MPa, and failure energies of 0.3-2.4 $MJ \cdot m^{-3}$. In one species, no noticeable difference was seen with respect to body location or loading direction, indicating an isotropic material. However, the mode of failure was different between the two species, with one failing almost instantaneously and the other tearing [23]. A later study showed another species with failure strains of approximately 40%, maximum stresses of approximately 0.5 MPa, elastic moduli of 2.2 MPa, and failure energies of 0.11 $MJ \cdot m^{-3}$. Again, these properties did not seem to vary with direction or location, but did differ somewhat from the previous study. The species in this study, *Teratoscincus scincus*, is thought to have fragile skin. The fragile nature of the skin is thought to be an anti-predator defense (allowing regional loss of skin) with other possible behavioral influences [24].

Previous investigation of shark skin indicated that as the swimming speed of the shark increased (along with strain rate), the apparent stiffness of the skin also increased. At higher speeds, the energy loss tended to be less than at low speeds. The fibers in the skin were found to be oriented helically around the shark's body, creating a criss-cross pattern, which aids in restoration of normal body shape when the body bends during swimming [25]. Other studies on swimming animals have shown the effects of the angle of these collagen fibers and how this relates to the energy storage of the tissue. Altered fiber angles may increase or decrease the energy storage capabilities of the tissue, thus specializing the tissue for specific motions [26, 27]. Bat wing skin has also been shown to have differing properties with respect to fiber angle. When the difference between loading angle and fiber angle was compared to mechanical properties,

failure strain increased, while modulus and strength decreased as the crossed angle differences increased [28].

Differences in properties may be particularly important among animals that use undulatory locomotion, as the skin must transmit forces along the length of the animal. Because the moment arm of the force transmitted by the skin is greater than that of underlying musculature or connective tissue, the skin is at an advantage in terms of energy transfer. When the different dorsoventral locations are considered, the ventrolateral location has the greatest advantage as it is furthest from the body midline [29]. However, not all animals with crossed fiber orientations perform external force propagation, as suggested by biaxial tests. A parameter indicative of force distribution capability is the retraction of one direction of skin when pulled in another during biaxial testing. In the Norfolk spot and skipjack tuna, contraction did not occur, so the skin is assumed to have little force transmission capability [27].

2.5 Digital Image Correlation (DIC)

Digital image correlation is a non-contact technique used to determine regional deformation. Although digital image correlation has been used for fluid mechanics measurements (i.e. digital particle image velocimetry [30]), some recent studies of biological tissues have also used this method to analyze tissues using optical rather than physical techniques (i.e. extensometers), including arteries [31, 32], cartilage [33], ligaments [34], and skin [35]). DIC has proven to be an accurate measurement of displacement between sequential images in situations where the material has high contrast areas [36]. Advantages of using DIC to calculate strain rather than the traditional method of using sample displacement include the ability to examine the heterogeneous nature of biological tissues, the high resolution of small displacements [35], and analysis of regions far from the grips, as gripping effects can impact the properties measured [37]. DIC also allows calculations of displacements in multiple directions, allowing two-dimensional strain measurements [34]. However, the field being analyzed must remain in the field of view of the camera [35], and correlations may not measure extremely large (due to image regions moving out of the test window) [35] or small deformations (specifically sub-pixel displacements) [38] with great accuracy.

Standard DIC using cross-correlation is generalized as the Fourier-based cross-correlation between two signals (image at 'undeformed' configuration and image at 'deformed' configuration). After correlation, a smoothing filter is added to achieve a generalized cross-correlation. With the addition of other optimizing filters and a phase correlation transform, a robust phase correlation was developed. Compared to a standard cross-correlation, this robust phase correlation was found to be more accurate, and is implemented in this study. However, there is still a slightly negative bias error [30]. Errors in image correlation can be caused by any number of things including the quality and contrast of the speckle pattern on the sample, the sample orientation not being perpendicular to the focal axis of the camera, distortions in the images due to the lenses, and noise inherent in the signal. Correlation errors can occur due to the sample region size, differences in correlation techniques, interpolation, and the shape function used [39].

Chapter 3: Methods

To determine the mechanical properties of snake skin, freshly excised skin was tested uniaxially in tension in four types of tests: strain to failure, creep, relaxation, and hysteresis. Digital image correlation was used to analyze the images to determine the two-dimensional displacement of a sample during testing. The results from this correlation were converted to strain in the horizontal and vertical directions, giving a comprehensive view of the response of snake skin to a tensile load/extension. Because the skin changed dimensions greatly in both the horizontal and vertical directions, both Lagrangian and Eulerian stress values were considered, and a comprehensive analysis of the following parameters was performed: strength, extensibility, strain energy, stiffness, and some basic viscoelasticity parameters. All animal procedures were approved by the Virginia Tech Institutional Animal Care and Use Committee (Project 10-098-ESM) and ARO (#57949-LS-DRP).

3.1 Animals

The animals used for this analysis come from the colubrid family. The 'flying' snake *Chrysopelea ornata* is the focus of this study, and is also compared to the non-gliding colubrids *Elaphe guttata* (now *Pantherophis guttatus*) and *Thamnophis sirtalis*. A modified cladogram showing the hypothesized evolutionary relationship of the snakes is shown in Figure A-1. The mass and snout-vent length of each snake are listed in Table 3-1.

Each snake (except one) was euthanized and then immediately tested. The snakes' shed cycles were tracked, and we deliberately avoided selection for testing during or near the onset of shedding. To euthanize, the animals were given an intra-coelomic injection of Fatal-Plus (350 mg/ml sodium pentobarbital) using a dosage of 1 mL/100 kg body mass. All samples were tested within 72 hours of euthanization based on a time dependency study described in Appendix B. In the case of *Chrysopelea ornata* 2, the animal died of unknown causes and was immediately frozen. All samples from this specimen were tested within 72 hours of thawing the animal.

Table 3-1: Snake mass and length data

Snake	*Mass (g)*	*Snout-Vent Length/Tail Length (cm)*
Chrysopelea ornata 1	33.9	65/27
Chrysopelea ornata 2	88.0	82/29
Chrysopelea ornata 3	49.0	67/24
Elaphe guttata 1	173.9	79/14
Elaphe guttata 3	110.5	65/15
Elaphe guttata 5	83.6	62/13
Elaphe guttata 6	105.0	63/15
Elaphe guttata 8	101.8	69/12
Elaphe guttata 9	110.7	74/15
Thamnophis sirtalis 2	18.7	40/11
Thamnophis sirtalis 5	13.7	37/10

3.2 Sample Preparation

To begin removal of the skin, the specimen was decapitated using a razor blade at approximately the 5^{th} -7^{th} ventral scale. The skin was slit through the edge of the ventral scales along the length of the body (or in small circumference sections, the midline of the ventral scales). The skin was then pulled slightly to expose the connective tissue between the skin and underlying musculature. This exposed tissue was removed using a razor blade and micro-scissors. The skin was then placed on a sheet of paper towel dampened with snake Ringer's solution (119 mM NaCl, 4.1 mM KCl, 2.5 mM $CaCl_2$, 1.5 mM $MgCl_2$, 15 mM glucose, 5 mM sodium pyruvate, and 10 mM HEPES [40]) to keep the skin from stretching and help keep the sample moistened during the rest of sample preparation. The skin was cut into approximately 15 x 30 mm^2 rectangles oriented in the longitudinal and circumferential directions (longitudinal samples came from both the ventral and ventrolateral regions). A dog-bone shape was cut from these rectangular sections so that middle section (gage length) was approximately 10 mm long and 6-8 mm wide. Small pieces of 100 grit sandpaper (approximately 15 x 6-8 mm^2) were glued to the ends of the specimen on both sides to give a more solid surface for gripping and to prevent

the skin from being crushed within the grips. A sheet of thin plastic was glued to the scale side of the sample over the sandpaper to keep the specimen in a configuration as close to the original as possible. This also allowed for easier insertion into the grips of the tensile tester and prevented stretching of the sample for the remainder of sample preparation.

The testing setup was composed of two Photron APX-RS high speed cameras, an Instron ElectroPuls E1000 tensile tester with 250 N Dynacell load cell (Instron, Norwood, MA), desktop computer, and mirror. Bluehill 2 (Instron, Norwood, MA) and Photron FASTCAM Viewer (PFV) (Photron, San Diego, CA) software were used to control and record the data synchronously from the Instron and cameras, respectively. An incandescent light was also placed between the two cameras. The inner surface of the sample was viewed with a 105 mm lens, and the outer surface with a 200 mm lens. Cameras were placed just far enough from the sample so that the images were in focus at the lowest focal distance of the lens (generally about 1.5-2 feet from the sample). A frame rate of 250 fps were used for all tests with the exception of the fast rate tests, which used a frame rate of 1200 fps. The shutter speed used for all tests was 1/250 seconds, and aperture was adjusted based on ambient light conditions to yield a high contrast image. The sample was held by custom-made grips and submerged in a bath of Ringer's solution for the duration of testing. Both cameras were leveled prior to testing.

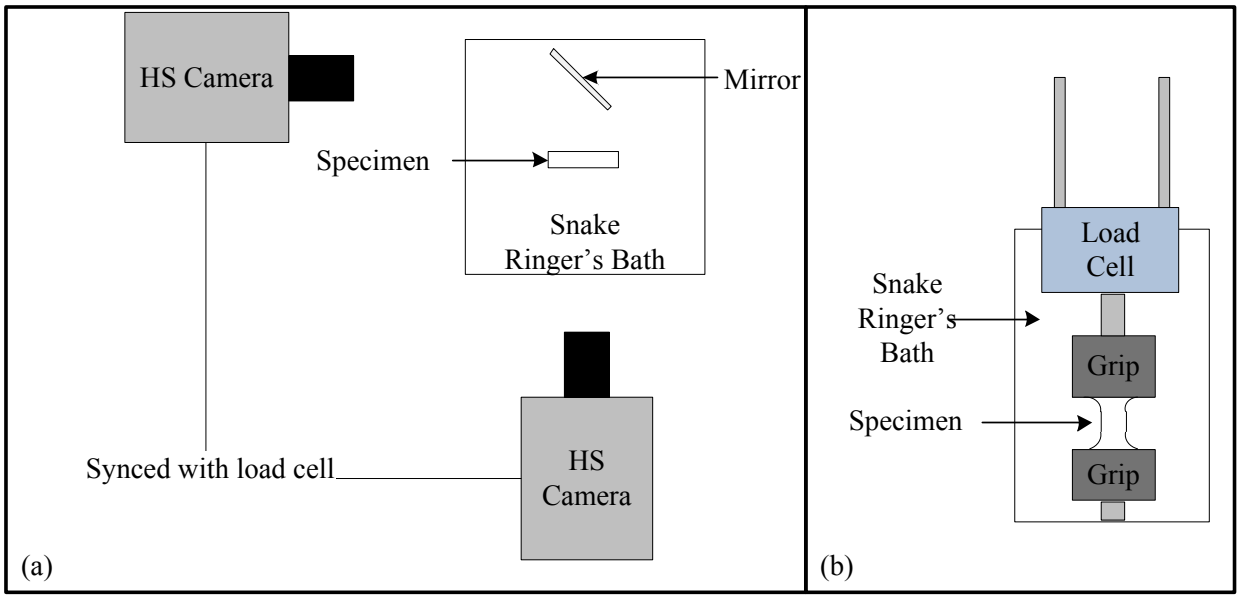

Figure 3-1: Top view (a) and front view (b) of testing setup

Before testing, samples were imaged to determine initial dimensions and speckle coated to provide a trackable surface during analysis. All samples were kept in an airtight storage bag humidified with Ringer's solution in a refrigerator until the next phase of preparation. Samples were imaged using a Zeiss Stemi 2000-C microscope (Carl Zeiss, Germany) at 51.2X magnification and Nikon digital camera to measure the thickness of each sample. This was done by placing the skin between two thin pieces of plastic for alignment. These pieces were oriented perpendicular to the field of view of the camera so that the space between the two pieces (or the skin) could be viewed. Samples were held lightly so that the plastic was flush against both surfaces of the skin without causing compression of the skin.

The thickness dimension was obtained by taking three calibrated measurements between the two pieces of the plastic at the middle of the frame and at two points equidistant from this measurement (see Figure 3-2) and averaging to get a nominal thickness for the entire sample. Measurements were taken in this way for several reasons: a) the skin is non-uniform, and taking a single measurement in an inter-scalar region may change the results by under-estimating the area, causing an increased stress estimation, b) using calipers presents issues in that the area of contact is much smaller than the plastic, so applying equal amounts of pressure to 'contact' may compress the skin more so than spreading the force over the entire sample, and c) digital measurements can easily be repeated multiple times (even after the sample has been tested) if necessary to achieve greater confidence in the measurement.

Following this measurement, the inner surface of the skin was allowed to dry slightly until tacky (usually less than 5 minutes), speckle coated with an airbrush, allowed to dry for approximately 30 seconds, and re-hydrated with Ringer's solution. After speckle-coating, a sample was either placed in the grips, hand-tightened to hold the sample, or returned to the refrigerated bag. The width measurement was performed using a similar method with the initial image of the tensile test. Measurements were taken at the smallest width area of the gage section of the sample (see Figure 3-3).

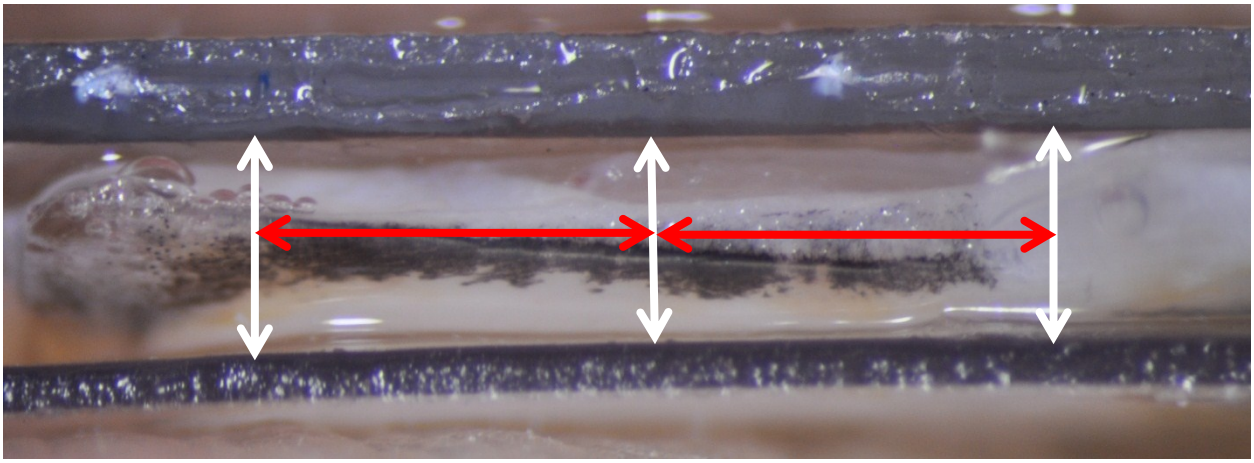

Figure 3-2: Thickness measurement technique. White lines indicate the actual thickness measurement. Red lines are of equal length to space the measurements at equal distances from the center measurement.

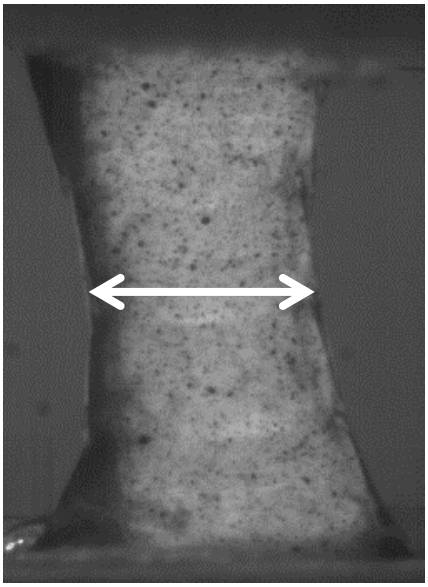

Figure 3-3: Width measurement technique of a ventral sample. A single measurement is taken at the smallest width, which was generally in the middle of the gage section.

3.3 Uniaxial Tensile Testing

Following the standard of other biological tissue testing, all samples were preconditioned. Preconditioning is performed to give all samples an identical immediate history and ensures the tissue is at a steady state at the preconditioning strain level [18]. While this does remove some viscoelastic effects that may be seen during testing, it ensures that the last extension seen by each sample is the same. This is especially important as some samples may be handled differently

during preparation due to different preparers, difficulties in skin removal, sample cutting and gluing, or other later testing setup procedures. To precondition, each sample was cyclically loaded using a sine wave extension pattern with an amplitude of 0.5 mm and frequency of 1 Hz for 10 periods. This gave the sample an approximately 10% amplitude preconditioning strain, which is well within the physiological range of each loading direction (in many cases, negligible load was seen during preconditioning). The sample was held stretched at 0.5 mm for approximately 15 seconds following the last cycle, and then returned to the initial position. The sample was allowed to rest in this position for 5 minutes before testing.

To maintain testing conditions as close to physiologic as possible, the base set of tensile tests to failure was performed at a strain (extension) rate based on the behavior of gliding undulation. To estimate a strain rate comparable to aerial undulation, the body of the snake was modeled as a sine wave with a known undulation frequency (approximately 1 Hz for this case), arc length (one segment = 16 cm; see Figure 3-4), and peak-to-peak amplitude of 6.5 chords (13.65 cm). Values for this from model were derived from a previous study on snake flight kinematics [11]. Knowing arc length and amplitude, the equation of the function of the center-line of the snake was determined to be $x = 6.825\cos(\frac{y}{9})$. The width of the snake (2.1 cm) was used to model the left and right sides of the snake (black lines) with respect to the center-line function (red line) in Figure 3-4. By computing the length of the left and right sides between points a and b, the difference in length of a section of snake skin during points in the undulation cycle was found. Using the undulation frequency, a strain rate of 9.4%·s^{-1} was found to be an approximate lower bound on the undulation strain rate. When this strain rate is applied to a specimen with a gage length of 10 mm, the extension rate of an average specimen is 0.94 mm·s^{-1}. Data for these low rate uniaxial tests were recorded at 50 Hz.

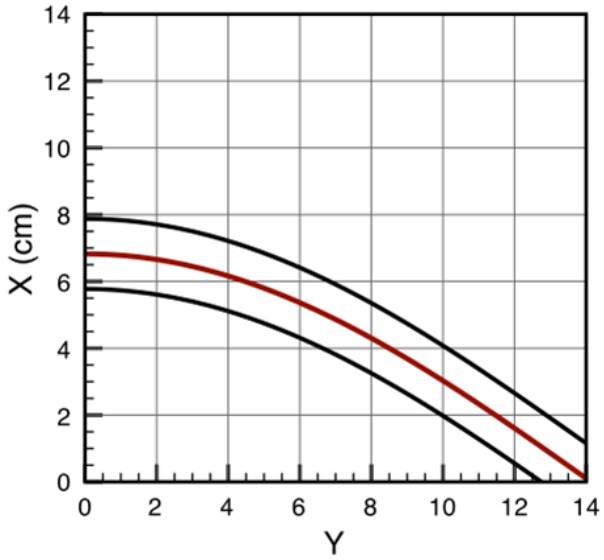

Figure 3-4: Model of snake section. Center red line indicates the midline of the snake. Edges of the snake are indicated by black lines. The difference in lengths of black lines corresponds to the change in length calculated.

For tests of other behaviors typical of a flying snake, particularly landing, a higher strain rate was used. Specifically, a strain rate for landing was assumed to have a minimum value at least 10x that of the undulation rate. For these tests, the extension rate used was 9.4 $mm \cdot s^{-1}$. Data for these tests were recorded at 500 Hz.

Because stress and strain could not be directly controlled, creep, relaxation, and hysteresis tests were run to fixed loads and extensions. These values were picked from previous uniaxial tensile tests to failure so that the point chosen on the load-extension curve was far enough in the curve to see some linear elastic effects, but not far enough to reach the yield or failure region. A first series of tests to determine the variability in tests within a snake was performed with multiple samples in each orientation from EG9. Following this, one sample from each orientation was tested from each snake, generally from the pre-pyloric region. Creep tests were run with the same initial setup through preconditioning. Following the 5 minute period after preconditioning, the sample was loaded at 0.9413 $mm \cdot s^{-1}$ to a predetermined load. The loads for each orientation are listed in Table 3-2. Following this initial extension phase, the sample was held at a constant load for 30 minutes. The camera settings used were the same as those for a normal uniaxial tensile test, but here data were sampled at 5 Hz. Relaxation tests were performed using the same protocol as in the previously described uniaxial tests. However, instead of testing until sample failure, the samples were held at a constant extension level for 30 minutes. The extensions for each orientation are listed in Table 3-2. Data for these tests were sampled at 50 Hz, but images

were only recorded until the constant extension was reached. Hysteresis tests were run to the same extensions as the relaxation tests, but then immediately unloaded. These load-unload cycles were repeated 50 times, and data were sampled at 10 Hz.

Table 3-2: Creep and Relaxation Test Parameters

	Longitudinal	***Circumferential***	***Ventral***
Creep Load (N)	1.0	0.5	2.0
Relaxation Extension (mm)	5.0	10.0	4.0

3.4 Test Analysis

Here, the following directional notation (x_n) will be used, with x_1 oriented in the direction of the width of the sample, x_2 oriented in the direction of the load applied, and x_3 oriented in the direction of the thickness. These relationships to the sample orientation are shown in Figure 3-5.

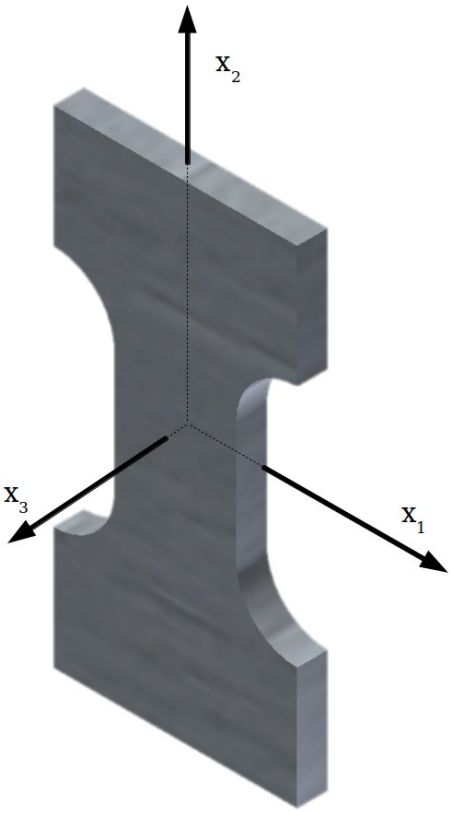

Figure 3-5: Sample orientation and directional nomenclature.

Several assumptions were made to simplify analysis. First, the thickness of the skin was assumed to be constant for any extension due to inability to view thickness change during testing (see Appendix B for more details). Second, the material was assumed to be uniform. This was done to characterize the material on the macroscale, rather than looking at each individual portion (i.e. scales vs. inter-scalar skin) and follows the standard of other biological tissue studies. We also neglect scale size and number of scales, as all samples were cut to the same dimensions (scale size and number may have little impact on the response of the skin [10]). Unlike many other biological tissue studies, the material deformation was not assumed to be isochoric (constant volume deformation) due to inter-scalar skin folding, and plane deformation was assumed.

Digital image correlation was used to determine the displacement of small regions in the series of images from each test. Prana, a particle image velocimetry (PIV) program implementing DIC [4] was used to analyze the images from each test, and the setup details can be found in Appendix B. The robust-phase correlation in Prana that implements optimizing filters and phase transforms in addition to the standard cross-correlation was used to determine the displacements [30]. To analyze a series of images from a normal strain rate test, the two-dimensional displacement field was calculated from correlations between every 10 images. This was done to provide large enough displacements to yield sufficient accuracy in displacement estimation over the entire analysis region while still yielding high resolution in the load data. The output of this procedure gave an 8 x 8 pixel grid over the entire image of displacements between each correlation step. A 5 x 5 pixel rectangular grid was super-imposed on the image (see Figure 3-6) to enable ‘tracking’ of various features. The grid region was centered on the sample both horizontally and vertically. It was also centered over scales so that if possible, the top and bottom of the grid regions fell on the same portion of the scales. This approach attempted to avoid bias in the strain measurements due to different concentrations of skin regions being analyzed (i.e. to avoid 2 inter-scalar regions with 3 scale regions).

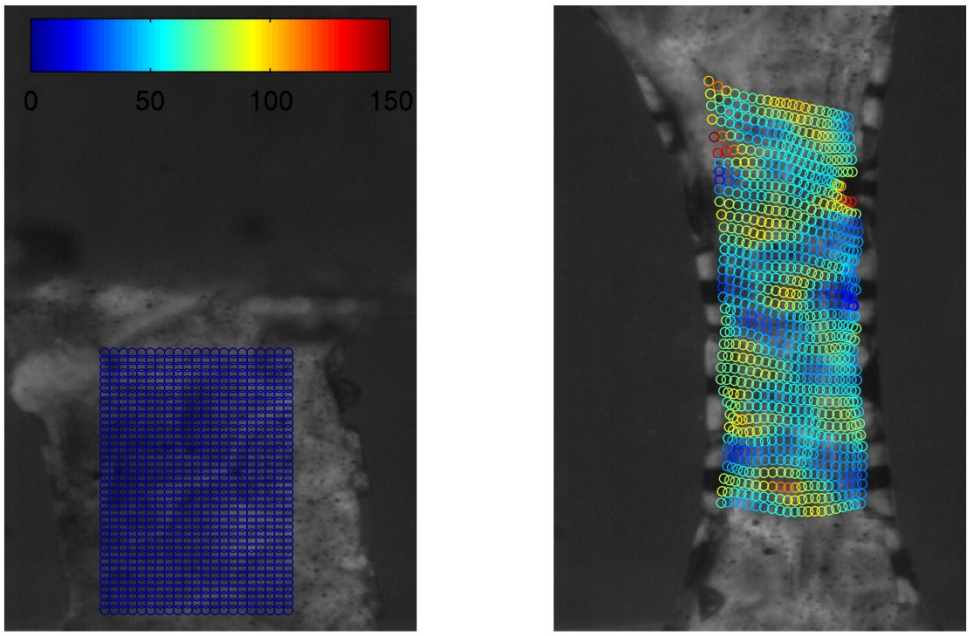

Figure 3-6: Sample grid at initial configuration (left) and during testing (right). Local axial strain between grid points is shown by the color of the circles and ranges from 0% (blue) to 150% (red) as indicated by the left figure.

To track the displacement of these super-imposed grid-points through the duration of the test, a 4th-order Runge-Kutta integration technique was used on each point x. The details of this integration are given in Equations 3-1 and 3-2, where T is the step size. T was set to a value of $(f_s \cdot T_{corr})^{-1}$ for all tests, where f_s is the sample frequency of the test, and T_{corr} is the image step size used during correlation.

$$x_{n_{s+1}} = x_{n_s} + \frac{1}{6}k_{1_{x_n}} + \frac{1}{3}k_{2_{x_n}} + \frac{1}{3}k_{3_{x_n}} + \frac{1}{6}k_{4_{x_n}} \tag{3-1}$$

The function $f_{x_1,x_2}(x_1,x_2,t)$ is the interpolation of the 3-D displacement matrices $U(X_1,X_2,t_s)$ and $V(X_1,X_2,t_s)$ at the x_1,x_2,t point given. The x_n components of k_m (where $m=1:4$) were computed separately for application to each x_n function.

$$\begin{aligned}
k_{1_{x_1,x_2}} &= f_{x_1,x_2}(x_{1_s}, x_{2_s}, t_s) \\
k_{2_{x_1,x_2}} &= f_{x_1,x_2}\left(x_{1_s} + \frac{Tk_1}{2}, x_{2_s} + \frac{Tk_1}{2}, t_s + \frac{T}{2}\right) \\
k_{3_{x_1,x_2}} &= f_{x_1,x_2}\left(x_{1_s} + \frac{Tk_2}{2}, x_{2_s} + \frac{Tk_2}{2}, t_s + \frac{T}{2}\right) \\
k_{4_{x_1,x_2}} &= f_{x_1,x_2}(x_{1_s} + Tk_3, x_{2_s} + Tk_3, t_s + T)
\end{aligned} \tag{3-2}$$

Both Lagrangian and Eulerian strains were calculated for each sample grid region. If the superimposed grid had *N·M* points, *(N-1)·(M-1)* strain values could be calculated. The equations used for these are listed below, where ε_{ij} is the Lagrangian tensor and e_{ij} is the Eulerian tensor. In this case, ∂X is the distance between two grid points in the original configuration, ∂x is the distance between two grid points in the current configuration, and ∂u is the difference in displacement between two grid points (see Figure 3-7).

$$\varepsilon_{ij}(t) = \frac{1}{2}\left[\frac{\partial u_j(t)}{\partial X_i} + \frac{\partial u_i(t)}{\partial X_j} + \frac{\partial u_k(t)}{\partial X_i}\frac{\partial u_k(t)}{\partial X_j}\right] \tag{3-3}$$

$$e_{ij}(t) = \frac{1}{2}\left[\frac{\partial u_j(t)}{\partial x_i(t)} + \frac{\partial u_i(t)}{\partial x_j(t)} + \frac{\partial u_k(t)}{\partial x_i(t)}\frac{\partial u_k(t)}{\partial x_j(t)}\right] \tag{3-4}$$

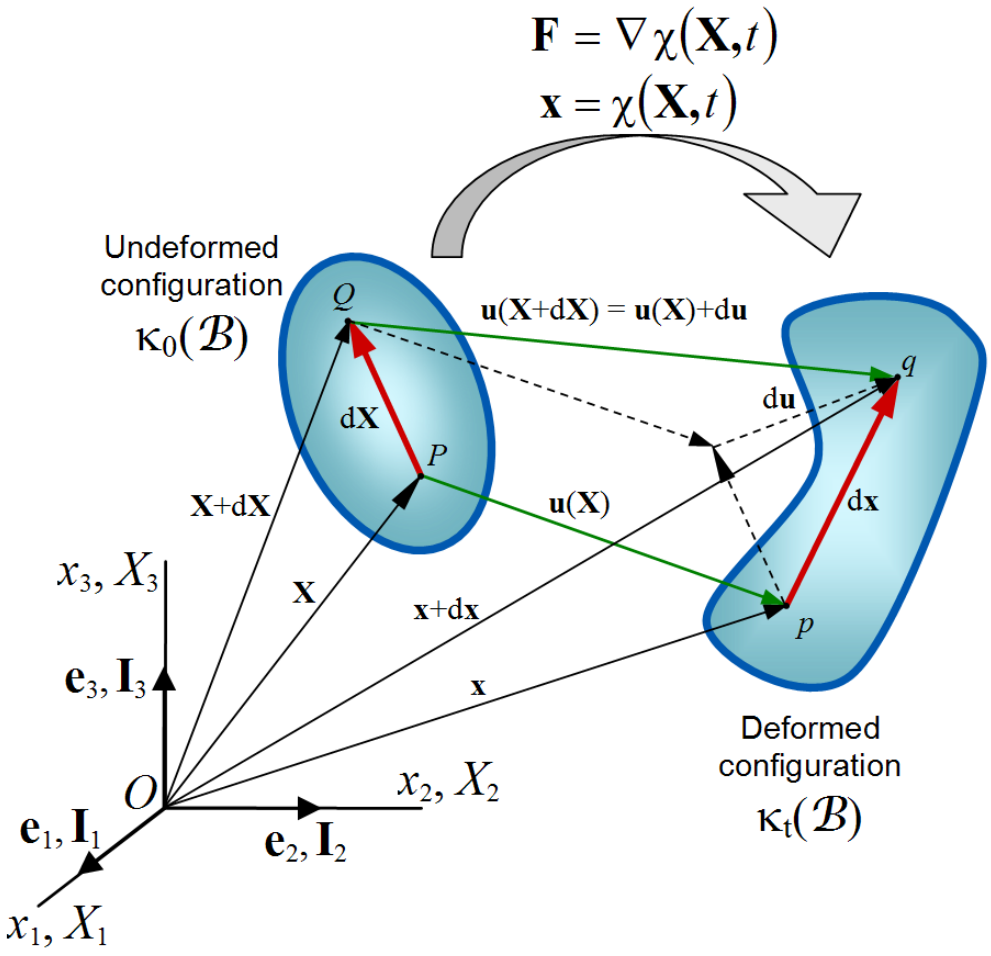

Figure 3-7: Deformation of a continuum body [41] (creative commons). Note that the indices (*i,j =1, 2, 3*) do not match this diagram. However, the deformation of this body in terms of notation is the same.

We assumed no thickness change in the samples during testing. For this reason, the *i=3,j=3* terms were neglected. This leaves the following equations for non-linear strains in the horizontal (*i=1,j=1*) and vertical (*i=2,j=2*) directions. Shear strains ($i \neq j$) were not calculated, reflecting the assumption of plane deformation only.

$$\varepsilon_{11}(t) = \frac{\partial u_1(t)}{\partial X_1} + \frac{1}{2}\left[\frac{\partial u_1(t)}{\partial X_1}\frac{\partial u_1(t)}{\partial X_1} + \frac{\partial u_2(t)}{\partial X_1}\frac{\partial u_2(t)}{\partial X_1}\right] \tag{3-5}$$

$$\varepsilon_{22}(t) = \frac{\partial u_2(t)}{\partial X_2} + \frac{1}{2}\left[\frac{\partial u_1(t)}{\partial X_2}\frac{\partial u_1(t)}{\partial X_2} + \frac{\partial u_2(t)}{\partial X_2}\frac{\partial u_2(t)}{\partial X_2}\right] \tag{3-6}$$

$$e_{11}(t) = \frac{\partial u_1(t)}{\partial x_1(t)} + \frac{1}{2}\left[\frac{\partial u_1(t)}{\partial x_1(t)}\frac{\partial u_1(t)}{\partial x_1(t)} + \frac{\partial u_2(t)}{\partial x_1(t)}\frac{\partial u_2(t)}{\partial x_1(t)}\right] \tag{3-7}$$

$$e_{22}(t) = \frac{\partial u_2(t)}{\partial x_2(t)} + \frac{1}{2}\left[\frac{\partial u_1(t)}{\partial x_2(t)}\frac{\partial u_1(t)}{\partial x_2(t)} + \frac{\partial u_2(t)}{\partial x_2(t)}\frac{\partial u_2(t)}{\partial x_2(t)}\right] \tag{3-8}$$

Linearized forms of the equations were also computed, specifically of ε_{22}.

$$\varepsilon'_{22}(t) = \frac{\partial u_2(t)}{\partial X_2} \tag{3-9}$$

The stretch ratio used to calculate the change in area during testing was calculated from the Lagrangian components of the strain.

$$\lambda_1 = \varepsilon_{11} + 1 \tag{3-10}$$

The area of the sample throughout the test was calculated using the following formula, where *w*=initial width of the sample and *t*=thickness of the sample.

$$A(t) = A_o\lambda_1 = wt\lambda_1 \tag{3-11}$$

Stress throughout the trial was calculated as the force over area of the sample. Load data were smoothed using a moving average over a span of 3 points before use in stress calculation. Lagrangian stress, or engineering stress, was calculated as force divided by the original area (Equation 3-12).

$$\sigma(t) = \frac{F(t)}{A_o} \tag{3-12}$$

However, Eulerian stress takes into account the change in area (Equation 3-13).

$$\sigma(t) = \frac{F(t)}{A(t)} = \frac{F(t)}{A_o \lambda_1} \tag{3-13}$$

To view the stress-strain response with the same initial toe region without including negligible-stress extension that could be attributed to the inter-scalar skin unfolding, the data were aligned so that a value of 0.1 MPa Lagrangian stress corresponded to a strain value of 0 %. The strain measurements were converted back into the original pixel displacements, so that the initial displacement was equal to 5 pixels (see Equation 12). This is similar to pre-loading a sample, as is done with some biological tissues [42], but takes into account the varying thicknesses of samples within an orientation and region. The pixel displacement at a stress of 0.1 MPa was found and used as the new reference displacement. Using these displacements, the new strains were found using the same equations as before (Equations 3-5:3-8).

$$d_{pixel} = 5 * \varepsilon'_{22} + 5 \tag{3-14}$$

Strain energy is defined here as the integral of the linear stress-strain relationship to failure where failure is demonstrated by maximum stress. This formulation of strain energy is used to compare the response of the skin to strain in a single direction. Although the specimen is known to strain in multiple directions during testing, when computing the hysteresis response, the nonlinear value keeps increasing throughout the test. Because strains are calculated using the cumulative total of displacements, displacements are negative in hysteresis tests when the sample is unloaded, but when squared the values are positive. This causes the increasing strain values seen in Figure 3-8.

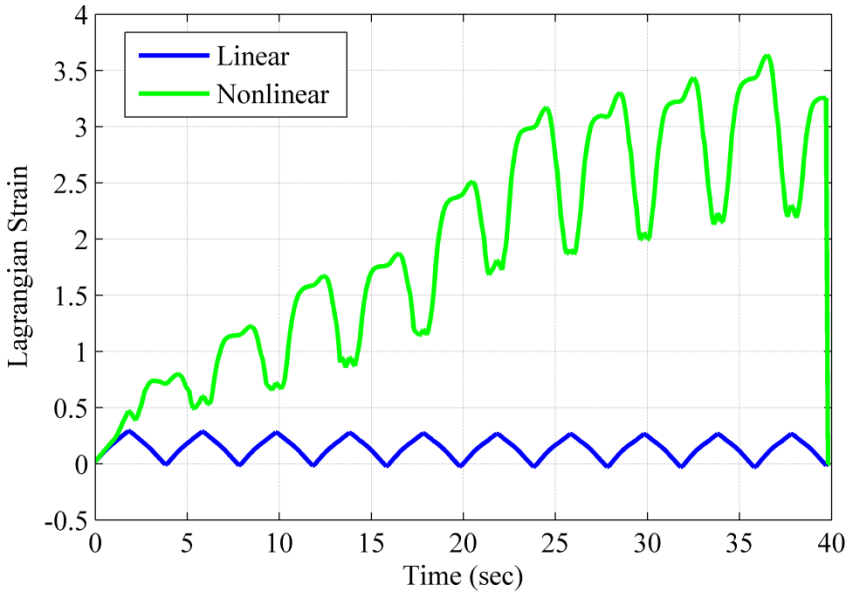

Figure 3-8: Nonlinear and linear strain in hysteresis testing..

By using this formulation of strain in strain energy calculations, we are assuming a linear material. However, this is still indicative of the energy the skin can absorb to failure.

$$W = \int_0^{\varepsilon_{22max}} \sigma_{22}\, d\varepsilon'_{22} \tag{3-15}$$

The Young's modulus of the material, *E*, was estimated using a second order central difference differentiation technique on the nonlinear Lagrangian stress-strain data.

Unless otherwise specified, these formulations of stress, strain, and strain energy are used to analyze all tests. Whenever a Lagrangian formulation is used in one parameter, it is used for the rest, and the same applies to Eulerian formulations. Both linear and nonlinear values of strain, before and after normalization, are given. Nonlinear strain gives a more accurate representation of the true strain, but for purposes of comparison to previous studies (pre-loaded and not), linear values are also given.

To compare values for significance due to region, orientation, and species, t-tests with $\alpha = 0.05$ were performed on each comparison of parameter combinations using the assumption of unequal variance between data sets, and unequal data set size. An ANOVA was also performed using all data, and a Tukey test was performed to determine the significance of each parameter.

Chapter 4: Results

The results of all valid tests performed are shown below. In most cases, the variance among samples is much larger than the experimental error. For this reason, known values of measured uncertainty and error are given in Appendix B, but not directly applied to the analyses described later.

4.1 Uniaxial Tensile Tests

Comparisons of several parameters within each species are listed below. Unless otherwise noted, strains refer to non-linear Lagrangian strain. This value attempts to more fully characterize the non-linear behavior of biological tissue, and does not make the small strain assumption that is sometimes incorrectly made when linear strain measurements are used on many biological tissues. However, linear values of maximum strain are also presented for purposes of comparison to previous work and other tissues. Linear strains are also used in the calculation of strain energy, for reasons that were explained in Chapter 3. Lagrangian and Eulerian calculations of stress are given for several reasons. First, this shows the differences between engineering and true stress. Second, most prior studies calculate Lagrangian stress; however, given the large decrease in width of the samples during testing, Eulerian stress gives a more accurate representation of the stress applied at any given point in the test.

4.1.1 Chrysopelea ornata

Table 4-1 lists the number of each test run in the comparisons below for *C. ornata*. The post-pyloric region tests are lower in number due to the location of the pylorus along the length of the snake. P-values for all statistical comparisons can be found in Appendix C, along with ANOVA results for global parameters.

Table 4-1: Number of normal rate uniaxial tests ran in each scenario for *Chrysopelea ornata*.

	Longitudinal	*Circumferential*	*Ventral*
Pre-Pyloric	15*	16	14
Post-Pyloric	8	6	8

*This section had an additional sample with a scar in the middle of the test region

Figure 4-1 shows representative plots from each orientation and region of *C. ornata*. Plots of all tests along with averages and standard deviations can be found in Appendix C. These stress-strain curves show the non-linear shape typical of biological materials. In almost every case the modulus does begin increasing near the beginning of the test, and in some cases may even decrease slightly near the end of the test**.** The variability in stiffness also seems to be greater in the pre-pyloric samples than the post-pyloric. All orientations exhibit a typical non-linear shape, but there is greater variability in the strain of the circumferential and ventral orientations, with several tests reaching strains of over 1.0. These tests may somewhat account for the large deviations in average maximum strain seen later.

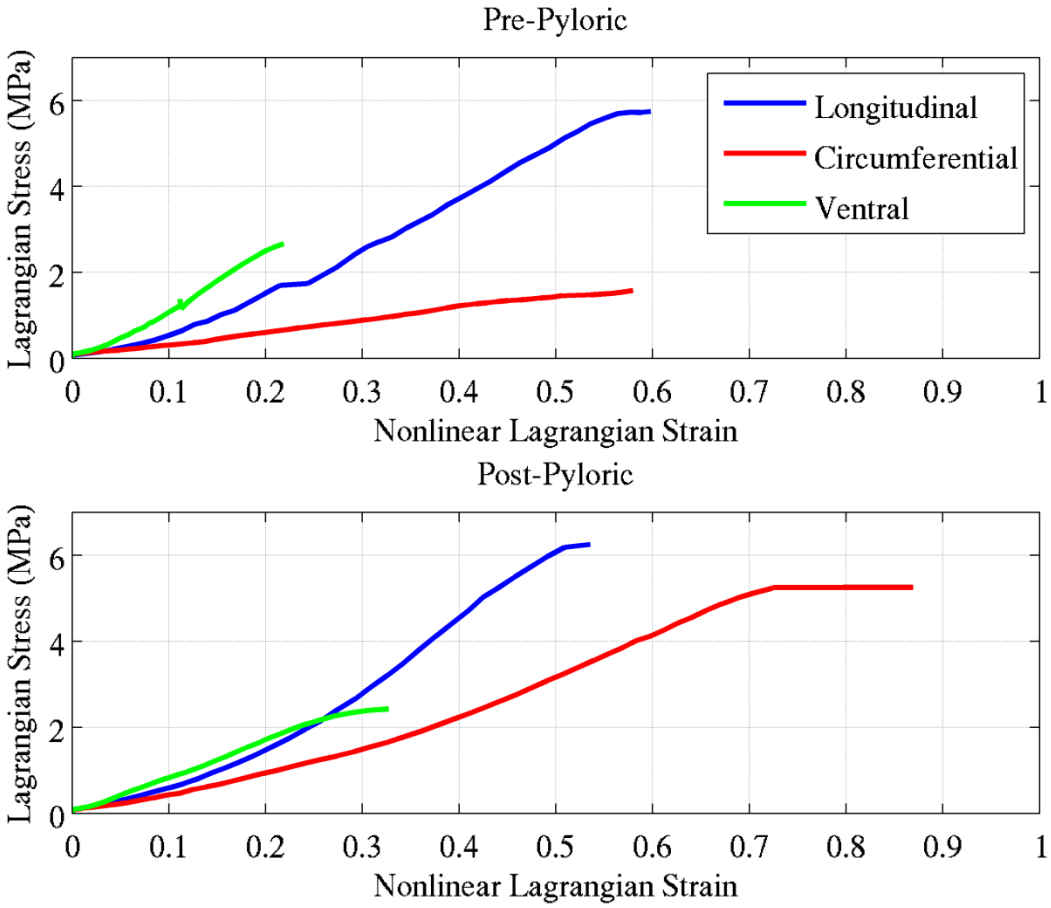

Figure 4-1: Representative *C. ornata* plots from each orientation and region of *C. ornata*

The maximum stresses for each loading direction and location can be found in Table 4-2 for both Lagrangian and Eulerian reference frames. Based on a t-test to compare the average maximum stresses seen in each direction and location, the following results were found. When examining the Lagrangian calculations, the longitudinal was found to be statistically different from the circumferential and ventral maximum stresses in the pre-pyloric region. In the post-pyloric region, the ventral was found to be different from the longitudinal, and likely different from the circumferential. When regions were compared, longitudinal and circumferential orientations had significant or near significant differences.

In the post-pyloric region, the longitudinal and circumferential Eulerian calculations were not found to have a difference on average. However, ventral averages were different from both longitudinal and circumferential in both regions. When comparing pre- and post-pyloric regions,

the longitudinal orientation was found to have a statistically different average, while the circumferential orientation was only likely different.

As seen in Table 4-2, strain energy increases overall from the pre-pyloric to post-pyloric regions in the longitudinal and circumferential orientations, but not the ventral. When comparing orientations, the longitudinal was different from the ventral in the pre- and post-pyloric regions, and the circumferential was different from the ventral orientation in the post-pyloric region. The circumferential was also different comparing pre- and post-pyloric regions. All other orientation and region comparisons were not significant.

For purposes of showing how much the skin stretches before a significant load is applied, one can compare the average strains before and after normalization. The difference between the two values in the same reference frame is the amount the skin can stretch (or inter-scalar skin can unfold) without a significant amount of fibers being recruited to carry a load. By comparing the values in Table 4-2 using a derivation found in Appendix C to convert normalized strains back to the reference configuration, we can see that pre- and post-pyloric skin stretches equal amounts in the longitudinal and ventral orientations before a load is seen; the circumferential pre-pyloric skin stretches more than the other orientations in that region, and more than the corresponding post-pyloric skin. Results for this comparison can be found in Appendix C.

When comparing the maximum extensibility of orientations and regions, several differences are seen. The circumferential orientation was different from the ventral in both regions and formulations (except pre-pyloric linear). The longitudinal was different from the circumferential and ventral in the post-pyloric linear comparisons, and in the pre- and post-pyloric regions in nonlinear comparisons. In all orientations, the regional comparisons were not significantly different in both linear and nonlinear calculations, with the exception of circumferential samples.

Elastic modulus, or stiffness, of the skin was also examined. By comparing the maximum moduli, we see that both longitudinal and circumferential orientations have greater values in the post-pyloric region, while the ventral modulus is less in the post-pyloric region. The stiffness at the beginning of the stress strain curve is also shown to indicate how much the stiffness changes over the test range for each orientation, demonstrating the nonlinearity of the response. Ventral samples have the greatest increase in stiffness, while circumferential has the least; in the pre-pyloric region, the circumferential stiffness barely changes relative to the change of other regions and orientations. When a statistical comparison was performed, the circumferential modulus was

different from the longitudinal and ventral in the pre-pyloric region. The circumferential was different from the ventral in the pre-pyloric region. The ventral was also different when comparing regions.

Table 4-2: Maximum values of *C. ornata* parameters (unless otherwise indicated). Values are given with (SD).

	Longitudinal		***Circumferential***		***Ventral***	
	Pre	***Post***	***Pre***	***Post***	***Pre***	***Post***
Strength - Lagrangian (MPa)	**3.63** (1.38)	**6.06** (3.31)	**2.15** (1.11)	**6.29** (4.07)	**2.67** (0.95)	**2.54** (0.89)
Strength - Eulerian (MPa)	**4.79** (1.52)	**9.08** (4.62)	**3.13** (1.72)	**9.22** (6.17)	**3.21** (1.25)	**3.36** (1.23)
Strain Energy (MJm^{-3})	**0.46** (0.24)	**0.73** (0.54)	**0.30** (0.16)	**1.37** (0.86)	**0.29** (0.20)	**0.28** (0.095)
Extensibility – linear – raw	**0.58** (0.14)	**0.56** (0.14)	**1.09** (0.50)	**0.69** (0.058)	**0.51** (0.35)	**0.49** (0.090)
Extensibility – nonlinear – raw	**1.00** (0.36)	**0.94** (0.28)	**10.51** (13.24)	**2.80** (1.13)	**1.73** (2.61)	**0.91** (0.31)
Extensibility – linear – normalized	**0.31** (0.067)	**0.31** (0.061)	**0.32** (0.079)	**0.48** (0.056)	**0.24** (0.16)	**0.24** (0.028)
Extensibility – nonlinear – normalized	**0.45** (0.11)	**0.53** (0.087)	**0.62** (0.12)	**0.82** (0.12)	**0.32** (0.24)	**0.34** (0.033)
Elastic Modulus (MPa) - initial	**10.18** (0.96)	**4.29** **(1.48)**	**1.77** (0.58)	**3.51** (0.96)	**5.85** (4.04)	**4.08** (2.07)
Elastic Modulus (MPa)	**16.36** (8.79)	**21.02** (10.67)	**6.97** (3.73)	**16.67** (15.68)	**21.34** (11.87)	**14.18** (7.44)

The properties of the skin may also be altered when damage occurs due to scar tissue or torn fibers. In a sample which had an area of scar tissue in the middle of the test section, the extensibility and strength of the skin were measured. When compared to the average values for other tests (longitudinal orientation in the pre-pyloric region), the values did not fall within one standard deviation of the values, and in most cases did not fall within two standard deviations.

Table 4-3: Maximum values for the damaged specimen. This sample had scar tissue in the middle of the sample region, and the values here are representative of this region, as the sample failed at the scar.

Extensibility - Linear	*Extensibility - Nonlinear*	*Strength - Lagrangian (MPa)*	*Strength - Eulerian (MPa)*	*Strain Energy (MJm^{-3})*
0.14	0.17	0.888	1.07	0.069

4.1.2 Elaphe guttata

Table 4-4 lists the number of each test run in the comparisons below for *E. guttata*. P-values for all statistical comparisons can be found in Appendix C, along with the results of an ANOVA.

Table 4-4: Number of normal rate uniaxial tests ran in each scenario for Elaphe guttata

	Longitudinal	*Circumferential*	*Ventral*
Pre-Pyloric	27	23	10
Post-Pyloric	27	18	12

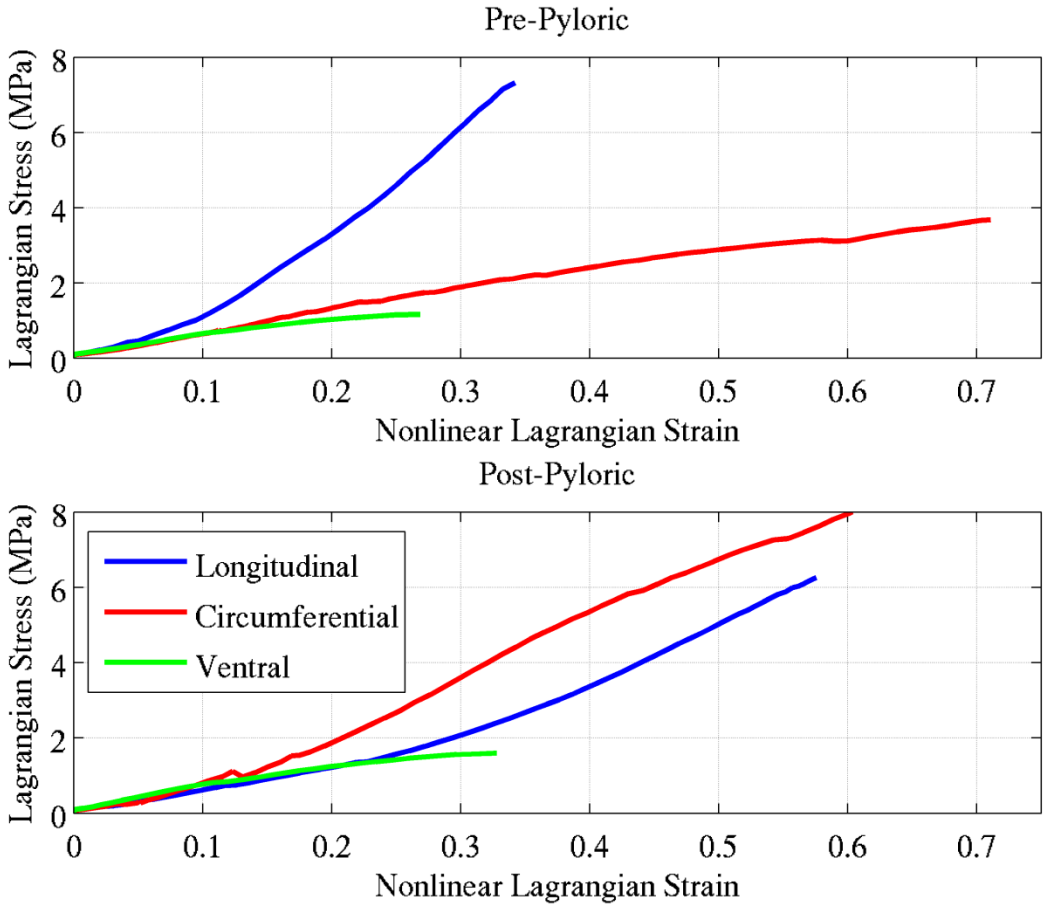

Figure 4-2: Representative curves from each orientation and direction of *E. guttata*

As before, the results were compared using a t-test. In the Lagrangian stress data, the longitudinal pre-pyloric was found to be statistically different from the circumferential and ventral. However, in the post-pyloric region, the longitudinal was different from the ventral, as was the circumferential. When comparing regions, the only significant difference was found in

the circumferential samples. This was also the case with the post-pyloric samples. When comparing regions, differences were seen in the longitudinal and circumferential orientations.

In maximum strain energy, as with stress, the ventral was different from the longitudinal and circumferential orientations in both regions. The circumferential was also different when comparing regions.

As with *C. ornata*, the circumferential skin seems to stretch the most of any orientation before a significant stress is applied in the pre-pyloric region, but all values were similar in the post-pyloric region.

After performing statistical comparisons among the linear extensibilities, several differences were seen. All orientation comparisons were different in the pre-pyloric region for linear values, and the ventral was different from the other orientations in the post-pyloric region. Nonlinear circumferential values were different from other orientations in the pre-pyloric region, and ventral values were different from other orientations in the post-pyloric region. The only difference when comparing regions for individual orientations occurred in the longitudinal orientations, for both linear and nonlinear calculations.

In *E. guttata* samples, stiffness in the post-pyloric region is only greater in the circumferential orientation, compared to both circumferential and longitudinal in *C. ornata* samples. When examining the modulus at the beginning of the stress-strain response, there is a slight decrease from pre-pyloric to post-pyloric regions in the longitudinal orientation, and a slight increase in the circumferential orientation. In this species, the overall modulus increases the most over the test in the longitudinal orientation and least in the ventral (compared to the ventral and circumferential orientations respectively in *C. ornata* and *T. sirtalis*). When a statistical comparison of maximum modulus was performed, almost every comparison was found to be significant. All pre-pyloric circumferential samples were different from longitudinal and ventral orientations. Post pyloric comparisons of ventral to both longitudinal and circumferential were also significant. When comparing regions, circumferential and ventral orientations had different averages.

Table 4-5: Maximum values of *E. guttata* parameters (unless otherwise indicated). Values are given with (SD).

	Longitudinal		***Circumferential***		***Ventral***	
	Pre	***Post***	***Pre***	***Post***	***Pre***	***Post***
Strength - Lagrangian (MPa)	**6.76** (4.51)	**7.36** (3.52)	**2.84** (1.66)	**7.27** (3.67)	**2.07** (1.02)	**1.96** (0.64)
Strength - Eulerian (MPa)	**9.11** (6.62)	**10.51** (5.09)	**3.93** (2.43)	**10.42** (5.83)	**2.84** (1.34)	**2.78** (0.92)
Strain Energy (MJm^{-3})	**0.81** (0.71)	**0.95** (0.50)	**0.57** (0.36)	**1.34** (0.80)	**0.23** (0.16)	**0.23** (0.12)
Extensibility – linear – raw	**0.53** (0.21)	**0.73** (0.15)	**0.86** (0.21)	**0.76** (0.26)	**0.61** (0.17)	**0.65** (0.11)
Extensibility – nonlinear – raw	**1.04** (0.90)	**1.77** (1.91)	**1.68** (0.46)	**2.53** (1.46)	**1.26** (0.60)	**1.35** (0.65)
Extensibility – linear – normalized	**0.31** (0.11)	**0.37** (0.069)	**0.37** (0.076)	**0.40** (0.083)	**0.23** (0.10)	**0.23** (0.074)
Extensibility – nonlinear – normalized	**0.44** (0.18)	**0.61** (0.13)	**0.65** (0.14)	**0.66** (0.13)	**0.35** (0.14)	**0.38** (0.096)
Elastic Modulus (MPa) - initial	**5.44** (4.06)	**3.16** (1.84)	**3.44** (1.46)	**4.76** (2.21)	**4.99** (2.38)	**4.88** (1.68)
Elastic Modulus (MPa)	**28.67** (12.11)	**23.67** (12.32)	**10.20** (5.44)	**20.70** (11.45)	**21.27** (14.65)	**9.38** (4.15)

4.1.3 Thamnophis sirtalis

Table 4-6 lists the number of each test run in the comparisons below for *T. sirtalis*. Because of the small sample sizes, the comparisons made may not have strong statistical confidence. However, some overall comparisons can be made, and P-values for these can be found in Appendix C.

Table 4-6: Number of normal rate uniaxial tests ran in each scenario for Thamnophis sirtalis

	Longitudinal	*Circumferential*	*Ventral*
Pre-Pyloric	6	5	3
Post-Pyloric	2	3	3

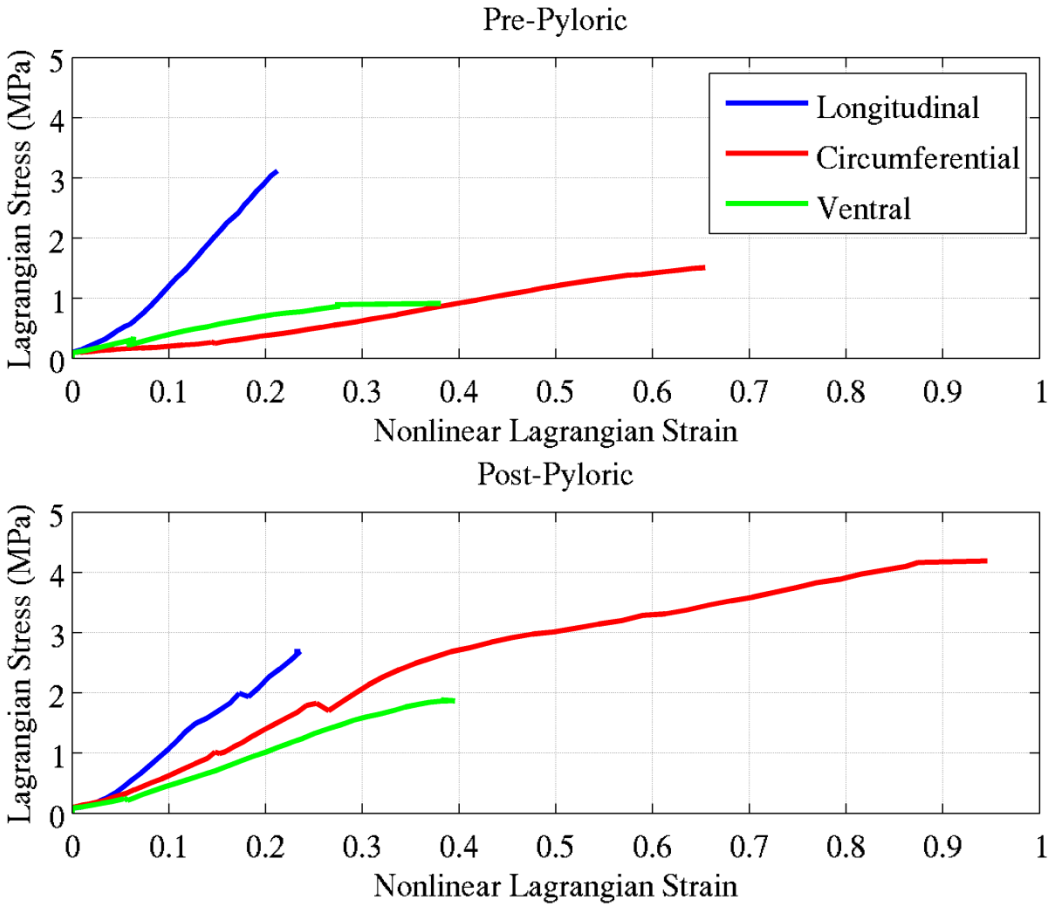

Figure 4-3: Representative curves from each orientation and direction of *T. sirtalis*

No maximum Lagrangian stresses regional or orientational comparisons were significant in *Thamnophis sirtalis* specimens (longitudinal and ventral pre-pyloric comparisons were likely significant, along with post-pyloric circumferential and ventral). However, when comparing the Eulerian formulation of stress, the circumferential and ventral post-pyloric were found to be likely different. Also, the circumferential pre- and post-pyloric values were likely different, along with the ventral Eulerian stress.

When making orientation and regional comparisons of strain energy, circumferential and ventral pre-pyloric samples were likely different. Circumferential samples were also likely different when comparing regions.

Similar to both *C. ornata* and *E. guttata*, when determining the strain a particular orientation of skin can reach before a significant stress is seen, the largest strain is seen in the circumferential orientation, particularly in the pre-pyloric region, and the least strain is seen in

the longitudinal orientation. In the post-pyloric region, ventral samples have the greatest non-load bearing strain, but low sample numbers may make these values insignificant.

Table 4-7: Maximum values of *T. sirtalis* parameters (unless otherwise indicated). Values are given with (SD).

	Longitudinal		***Circumferential***		***Ventral***	
	Pre	***Post***	***Pre***	***Post***	***Pre***	***Post***
Strength - Lagrangian (MPa)	**3.55** (2.40)	**6.22** (4.99)	**1.78** (0.63)	**3.98** (1.14)	**1.06** (0.51)	**1.87** (0.48)
Strength - Eulerian (MPa)	**4.71** (4.09)	**8.80** (7.27)	**2.20** (0.80)	**5.22** (1.45)	**2.59** (0.63)	**2.59** (0.64)
Strain Energy (MJm^{-3})	**0.36** (0.35)	**0.78** (0.86)	**0.41** (0.31)	**1.19** (0.46)	**0.14** (0.093)	**0.25** (0.12)
Extensibility – linear – raw	**0.42** (0.067)	**0.42** (0.022)	**1.14** (0.35)	**0.86** (0.10)	**0.77** (0.096)	**0.67** (0.22)
Extensibility – nonlinear – raw	**0.66** (0.31)	**1.62** (1.43)	**2.99** (1.46)	**3.15** (1.55)	**1.88** (0.72)	**1.21** (0.43)
Extensibility – linear – normalized	**0.21** (0.046)	**0.23** (0.089)	**0.42** (0.099)	**0.51** (0.089)	**0.23** (0.058)	**0.26** (0.068)
Extensibility – nonlinear – normalized	**0.28** (0.11)	**0.33** (0.14)	**0.71** (0.19)	**0.80** (0.14)	**0.37** (0.10)	**0.42** (0.14)
Elastic Modulus (MPa) - initial	**6.09** (1.31)	**8.38** (4.05)	**1.74** (0.38)	**3.29** (0.52)	**2.35** (1.18)	**3.81** (1.84)
Elastic Modulus (MPa)	**19.65** (9.08)	**27.58** (15.85)	**4.36** (1.18)	**11.24** (0.49)	**6.81** (3.31)	**8.09** (3.09)

As with the other snakes, the pre- and post-pyloric region maximum strains do not appear to be different in each direction. Statistical tests showed that the circumferential was different from the ventral in both linear and nonlinear calculations in the pre- and post-pyloric regions (except linear pre-pyoric). The circumferential was also different from the longitudinal orientation in both calculations. No other comparisons were significant.

Similar to *C. ornata*, peak modulus increased when moving from the pre-pyloric region to post-pyloric in both the longitudinal and circumferential orientations. When comparing the change in stiffness over the course of the tests, the ventral samples again seem to have the greatest increase in stiffness, with the circumferential having the lowest. Statistical comparisons of peak modulus were also performed and indicated that the peak pre-pyloric longitudinal modulus was different from the ventral and circumferential orientations. However, in the post-

pyloric region, no peak values were significantly different. Also, circumferential peak values were different across regions.

4.1.4 All snakes

When comparing the same direction and region across all snakes, the following significant differences were noted. In the pre-pyloric region, Lagrangian stress was only different when comparing the longitudinal *C. ornata* and *E. guttata* specimens. Pre-pyloric Eulerian stress was different when comparing the longitudinal *C. ornata* and *E. guttata* specimens, longitudinal and circumferential *E. guttata* and *T. sirtalis* samples, ventral *E. guttata* and *T. sirtalis* samples, and ventral *C. ornata* and *T. sirtalis* samples. In the post-pyloric region, the only difference occurred in and Eulerian stress in the circumferential comparing *E. guttata* and *T. sirtalis*.

When maximum strain in the pre-pyloric region was compared, few differences were seen. Considering both linear and non-linear Lagrangian strain, the only differences were between the longitudinal orientations comparing *C. ornata* to *T. sirtalis* and *E. guttata* to *T. sirtalis*. *C. ornata* was also different from *T. sirtalis* in the linear circumferential orientation. In the post-pyloric region, the longitudinal and circumferential *C. ornata* and *E. guttata* linear and nonlinear values were different.

Differences in strain energy occurred in the pre-pyloric region comparing the longitudinal *C. ornata* and *T. sirtalis* samples to the *E. guttata* samples, as well as the circumferential *C. ornata* and *E. guttata* comparison.

Modulus calculations showed many differences. In pre-pyloric comparisons, the only comparisons that were not different were circumferential and longitudinal *C. ornata* to *T. sirtalis*. In the post-pyloric region, ventral *C. ornata* to *E. guttata* comparisons, along with circumferential *T. sirtalis* to *E. guttata*, were significant.

However, the post-pyloric stresses, strains, and strain energies are on average greater than the pre-pyloric values in every case as seen in the figures below, with the exception of a few ventral comparisons (although not statistically significant in every case). Although modulus comparisons showed many differences, trends are not as obvious in these values as most other parameters. Plots are shown to give a visual comparison of the values.

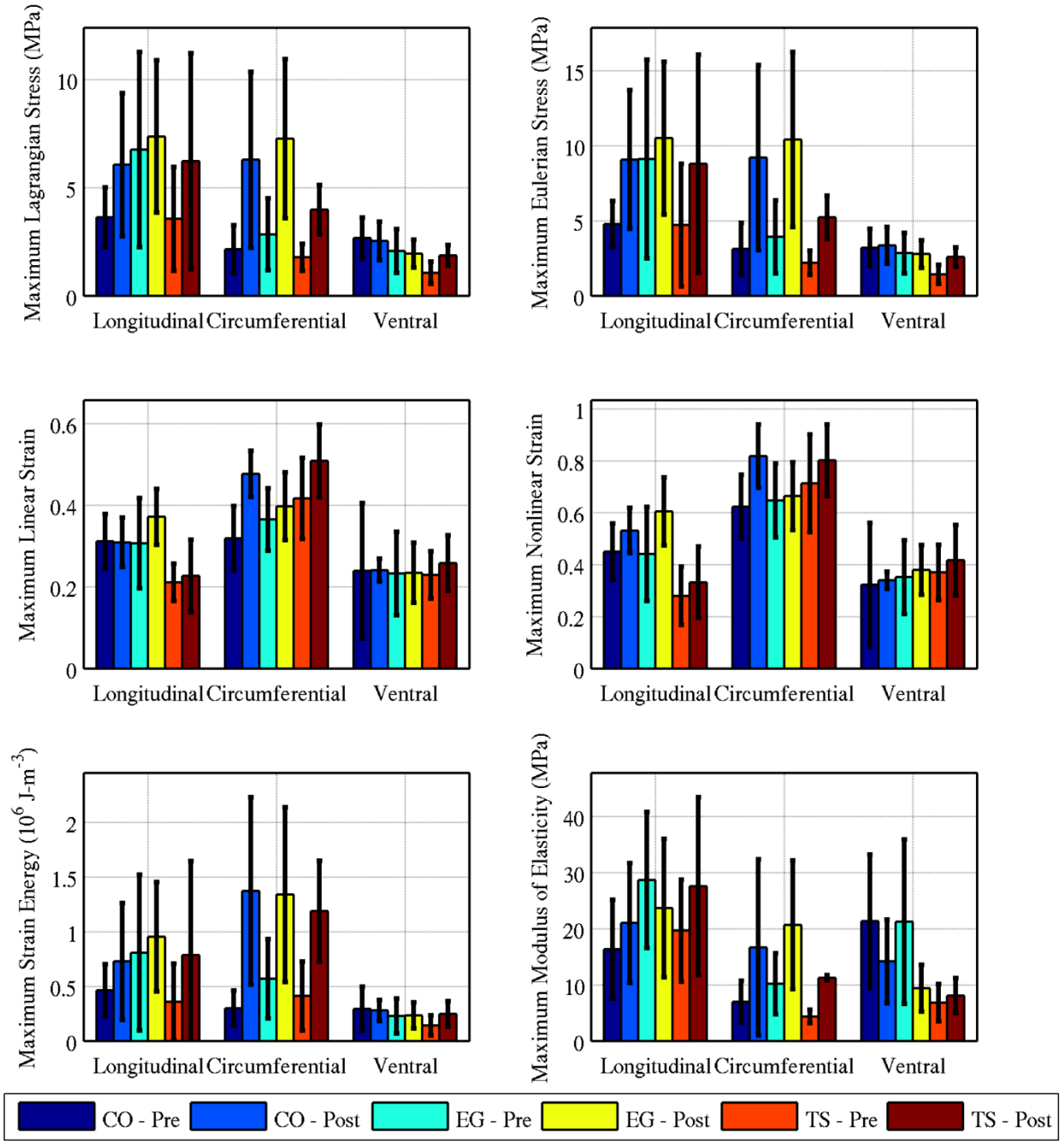

Figure 4-4: Average values for parameters. Error bars indicate one standard deviation. Sample numbers used here are the same as those used in calculations above.

4.2 Strain Rate Effects

To determine if the mechanical properties of the skin were rate-dependent, neighboring 'normal' (0.94 $mm \cdot s^{-1}$) and 'fast' (9.4 $mm \cdot s^{-1}$) rate samples were paired. The table below shows the numbers for each direction and species. The hypothesis tested here is to examine if the strength of the skin at the faster rate is greater than that of the normal rate. To do this, a paired t-test was performed on each section of data listed below using $\alpha = 0.05$ and a left tail (i.e. the mean of the normal rate values minus the fast rate values is less than zero). Note that the comparisons here are not done with the average values for all specimens, but the average of differences between neighboring specimens. For this reason, not all of the normal strain rate test data are used in this analysis.

Table 4-8: Number of sample pairs in each orientation and region

	C. ornata		*E. guttata*	
	Pre-pyloric	Post-pyloric	Pre-pyloric	Post-pyloric
Longitudinal	3	2	8	9
Circumferential	3	3	6	8
Ventral	3	4	2	2

To first analyze the skin at the higher extension rate of 9.413 $mm \cdot s^{-1}$, the same parameters calculated for low strain rate tests are reported for this data. As seen in Table 4-9 and Table 4-10, the same trends in the normal strain rate data are seen here. There is an increase from pre-pyloric to post-pyloric samples in each orientation, and the Eulerian stress is much greater than the Lagrangian stress. In these data, the standard deviations are high, likely due to the lower sample numbers. The stress-strain curves for these tests are also shown. Because the strains are all similar and stresses have significant differences, the strain energies can also be seen to have differences similar to those of the stress comparisons (as elastic strain energy is a linear function of stress and strain; the viscoelastic component was not considered here). However, comparing the peak elastic moduli to those from the normal rate, there seems to be no clear trend for a higher or lower stiffness, especially given the standard deviations.

Table 4-9: *C. ornata* average maximum stress

Strength (SD) - MPa		*Longitudinal*	*Circumferential*	*Ventral*
Lagrangian	Pre-Pyloric	8.04 (1.29)	4.21 (3.19)	5.88 (2.02)
	Post-Pyloric	6.45 (3.32)	8.44 (2.15)	5.66 (2.43)
Eulerian	Pre-Pyloric	11.05 (2.17)	5.75 (4.27)	7.70 (3.30)
	Post-Pyloric	9.82 (5.28)	12.24 (2.94)	7.46 (3.65)

Table 4-10: *E. guttata* average maximum stress

Strength (SD) - MPa		*Longitudinal*	*Circumferential*	*Ventral*
Lagrangian	Pre-Pyloric	7.34 (3.04)	3.86 (2.26)	4.02 (0.51)
	Post-Pyloric	13.67 (4.83)	9.54 (5.48)	4.25 (0.37)
Eulerian	Pre-Pyloric	10.08 (4.51)	5.38 (2.74)	5.07 (0.61)
	Post-Pyloric	19.63 (7.02)	13.66 (8.11)	5.37 (0.53)

Table 4-11: *C. ornata* maximum strain

Extensibility (SD)		*Longitudinal*	*Circumferential*	*Ventral*
Linear	Pre-Pyloric	0.38 (0.01)	0.35 (0.07)	0.22 (0.0097)
	Post-Pyloric	0.33 (0.027)	0.40 (0.022)	0.25 (0.054)
Nonlinear	Pre-Pyloric	0.56 (0.035)	0.58 (0.13)	0.29 (0.034)
	Post-Pyloric	0.55 (0.072)	0.68 (0.044)	0.35 (0.098)

Table 4-12: *E. guttata* maximum strain

Extensibility (SD)		*Longitudinal*	*Circumferential*	*Ventral*
Linear	Pre-Pyloric	0.30 (0.070)	0.42 (0.17)	0.26 (0.057)
	Post-Pyloric	0.35 (0.059)	0.37 (0.088)	0.42 (0.038)
Nonlinear	Pre-Pyloric	0.43 (0.12)	0.75 (0.26)	0.35 (0.086)
	Post-Pyloric	0.55 (0.11)	0.61 (0.14)	0.62 (0.069)

Table 4-13: Peak strain energy at fast strain rate

Max Strain Energy (SD) – $10^6 J \cdot m^{-3}$		*Longitudinal*	*Circumferential*	*Ventral*
C. ornata	Pre-Pyloric	1.29 (4.29)	0.65 (0.53)	0.52 (0.04)
	Post-Pyloric	0.78 (0.37)	1.38 (0.41)	0.64 (0.35)
E. guttata	Pre-Pyloric	0.97 (0.73)	0.98 (0.90)	0.43 (0.12)
	Post-Pyloric	1.68 (0.71)	1.71 (1.16)	0.90 (0.14)

Table 4-14: Peak elastic modulus at fast strain rate

Peak Modulus (SD) – MPa		*Longitudinal*	*Circumferential*	*Ventral*
C. ornata	Pre-Pyloric	21.07 (3.08)	9.22 (5.10)	39.44 (27.27)
	Post-Pyloric	18.16 (7.70)	17.45 (5.85)	22.82 (4.89)
E. guttata	Pre-Pyloric	27.19 (6.19)	9.19 (3.76)	21.09 (4.80)
	Post-Pyloric	40.27 (13.83)	23.07 (13.53)	15.43 (2.50)

Preliminary statistical analysis of each orientation and region showed that most of the comparisons do not show a significant increase in maximum Lagrangian stress from the normal rate to the fast rate. However, almost all orientations do show a positive difference, indicating that on average, the skin stretched at a faster rate has a higher maximum stress than skin stretched at the normal rate in the same location. Because the test numbers are small, the comparisons were run combining all test pairs from a species. If we disregard the orientation of the skin and focus primarily on the difference in properties, the difference is statistically significant in both snakes. The average increase in *C. ornata* was 1.28 (2.78) MPa, $p = 0.038$, and the average increase in *E. guttata* was 1.78 (3.26) MPa, $p = 0.0015$. The same analysis was performed on the maximum strain. However, no significant differences were found in any of the orientation comparisons, or comparing all samples in a species.

Table 4-15: Increase in property values from normal to fast strain rate. Significant differences ($p < 0.05$) are given in bold.

Parameter Value Increase	*C. ornata*	*E. guttata*
Strength - Lagrangian (MPa)	**1.23 (2.78), p=0.038**	**1.78 (3.26), p=0.001**
Strength - Eulerian (MPa)	**1.64 (3.98), p=0.048**	**2.50 (4.75), p=0.001**
Strain Energy ($MJ \cdot m^{-3}$)	0.063 (0.60), p=0.330	**0.36 (0.56), p<0.001**
Extensibility - Linear	0.022 (0.099), p=0.179	0.021 (0.11), p=0.139
Extensibility - Nonlinear	-0.039 (0.17), p=0.172	0.029 (0.19), p=0.173
Modulus (MPa)	4.84 (18.29), p=0.180	**6.34 (11.60), p=0.001**

Similar differences were seen when comparing strain energy and modulus. If we again ignore orientation and look at all samples, we see that *C. ornata* samples do not increase significantly in either parameter, while *E. guttata* samples do.

If the values in Table 4-15 are viewed in percent increase from the 'normal' strain rate value, the percentage increases are similar when comparing species, particularly in strength parameters.

Table 4-16: Increase in property values from normal to fast rate in percent. Significant differences ($p < 0.05$) are given in bold

Percent Increase	*C. ornata*	*E. guttata*
Strength - Lagrangian	**36.28 (63.78)**	**35.72 (55.01)**
Strength - Eulerian	**36.03 (65.35)**	**34.68 (55.83)**
Strain Energy	48.61 (110.45)	**70.36 (99.88)**
Extensibility - Linear	-1.82 (35.38)	11.20 (34.68)
Extensibility - Nonlinear	-2.04 (35.76)	9.80 (34.89)
Modulus	28.33 (64.09)	**39.45 (64.54)**

4.3 Hysteresis Tests

To examine the energy storage properties of the skin, the energy lost due to hysteresis was examined. The sample size of tests is small (see Table 4-17), so no statistical comparisons are made. However, an overview of the response seen in the tests is shown.

Table 4-17: Hysteresis test numbers

	C. ornata		*E. guttata*	
	Pre-pyloric	Post-pyloric	Pre-pyloric	Post-pyloric
Longitudinal	1	-	1	1
Circumferential	1	1	1	1
Ventral	1	2	1	1

To view the response of the skin, the first ten cycles were examined (this encompasses the majority of aerial undulation behavior). The stress and strain responses are shown below. The stress begins to decrease with each cycle as is expected. However, peak strain also decreases to what seems to be a steady state value. While this is not expected if examining extension, the strain response of the skin during the first few cycles of testing is somewhat varied and can result in the portions of the skin buckling due to a lack of recovery. This phenomenon will be explained later.

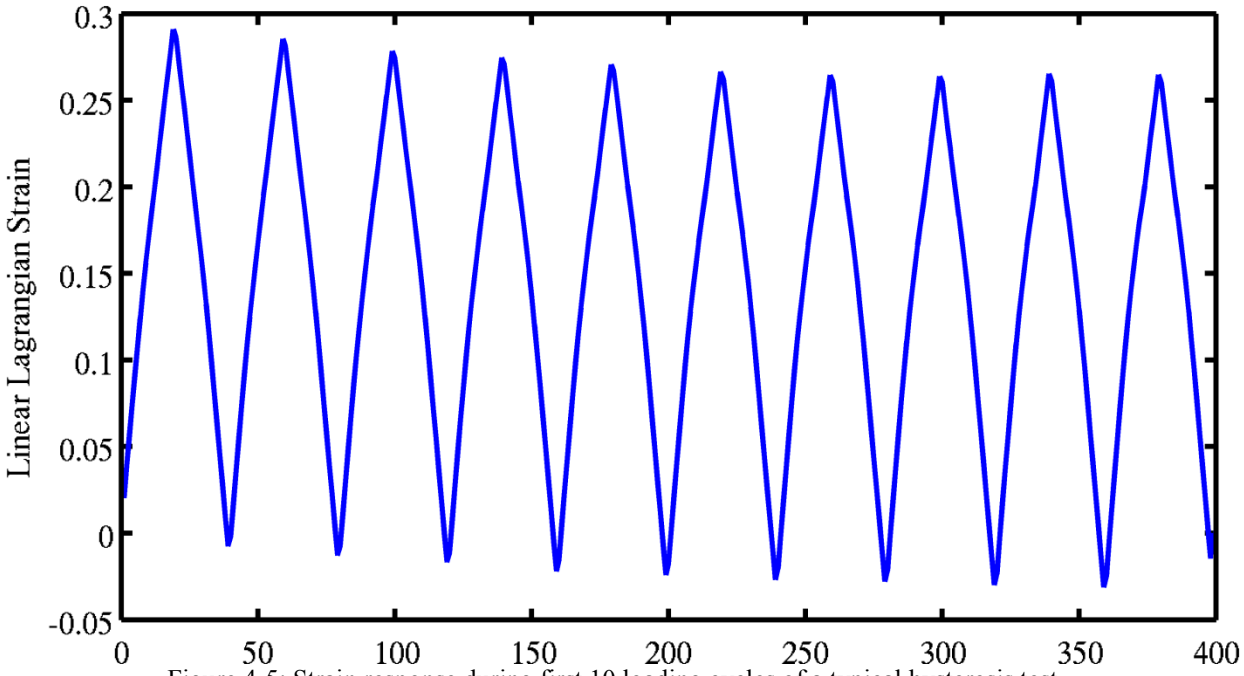

Figure 4-5: Strain response during first 10 loading cycles of a typical hysteresis test.

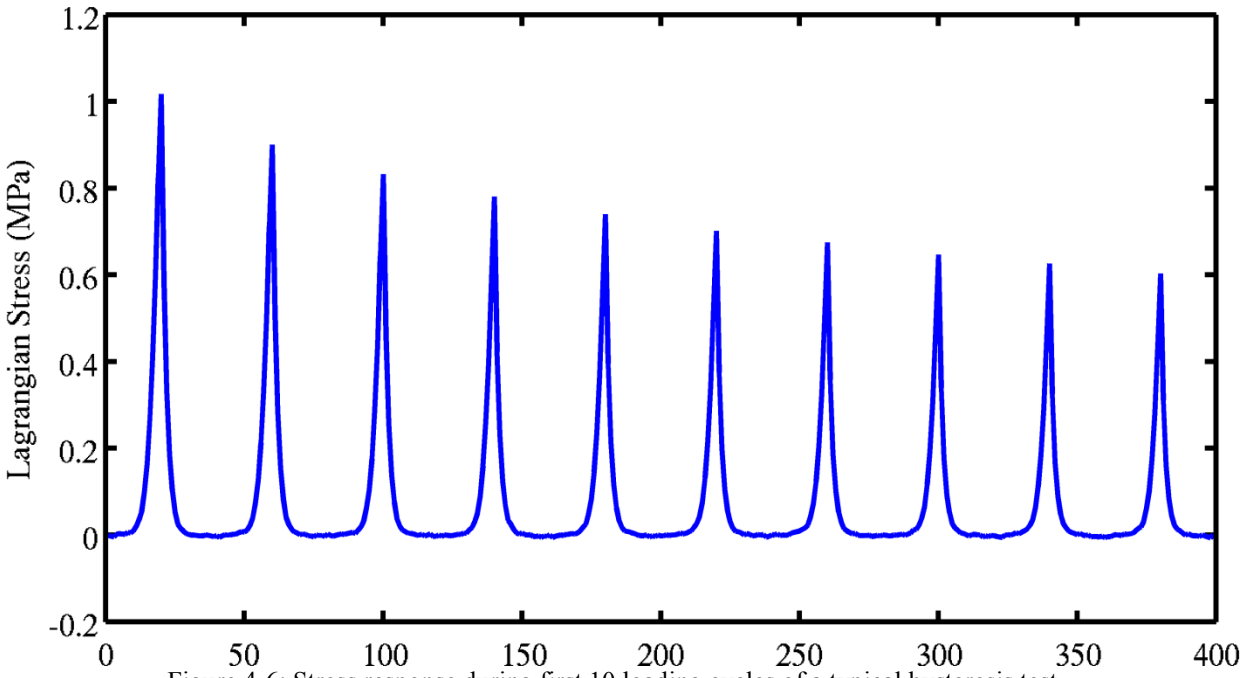

Figure 4-6: Stress response during first 10 loading cycles of a typical hysteresis test.

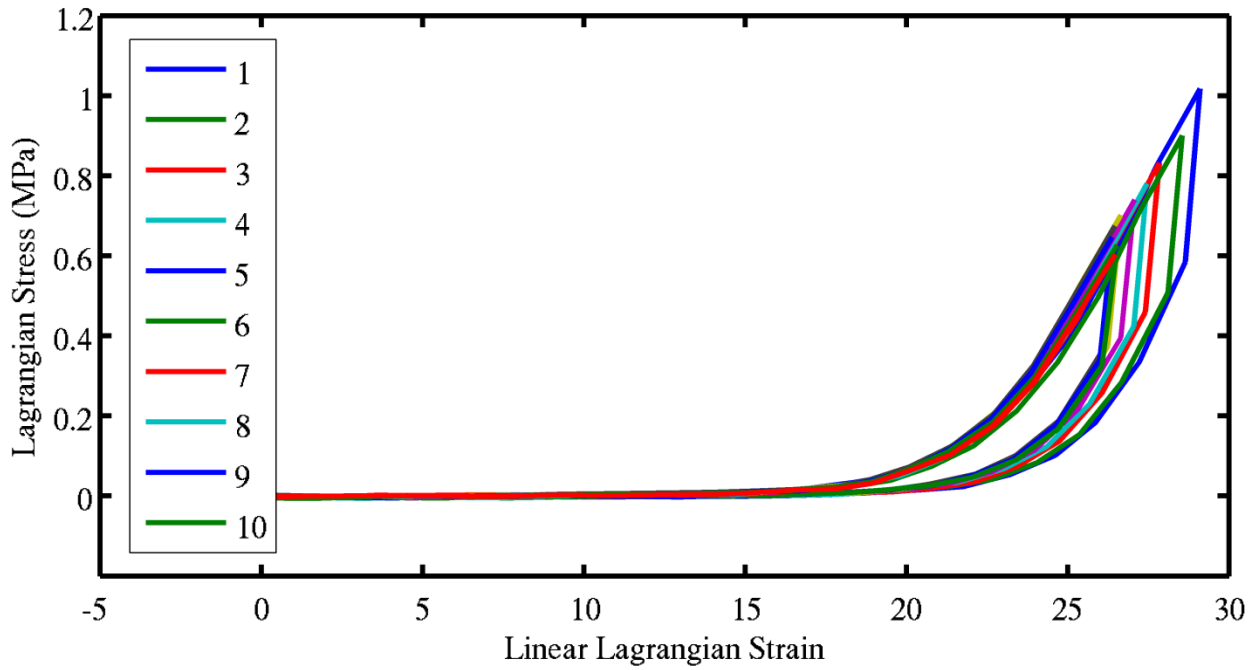

Figure 4-7: Stress vs. Strain response of typical trial. Only the first 9 full cycles are plotted, with the loading portion of the 10th cycle. However, we can see that the curves have the shape typical of a biological tissue exposed to cyclic loading. Color codings correspond to different cycles.

To compare how well each section of skin stores energy, the difference in area under each loading and subsequent unloading cycle was compared. This value represents the energy lost in each cycle. When compared visually in the figures below, there is no obvious difference seen when comparing species. All *E. guttata* orientations seem to have approximately the same energy storage capabilities indicated by an energy loss of 20-40% in all orientations and regions. Both ventral and longitudinal *C. ornata* energy losses seem to be in the 40-60% range. However, the circumferential samples have much lower energy loss, ranging from 0-30%. As the circumferential stresses are much lower than the other orientations, this does have some inaccuracy due to the noise in the load signal at low values where the signal-to-noise ratio is lower than other orientations. There is also one case which has a negative energy loss, caused by an extremely low signal-to-noise ratio.

Because stress and strain values both approached a constant value near the end of the cycles analyzed, the remaining cycles are not analyzed (they also yield little information about gliding behavior). Also, the energy return, the most important portion of these results, is nearly constant across these cycles in each test.

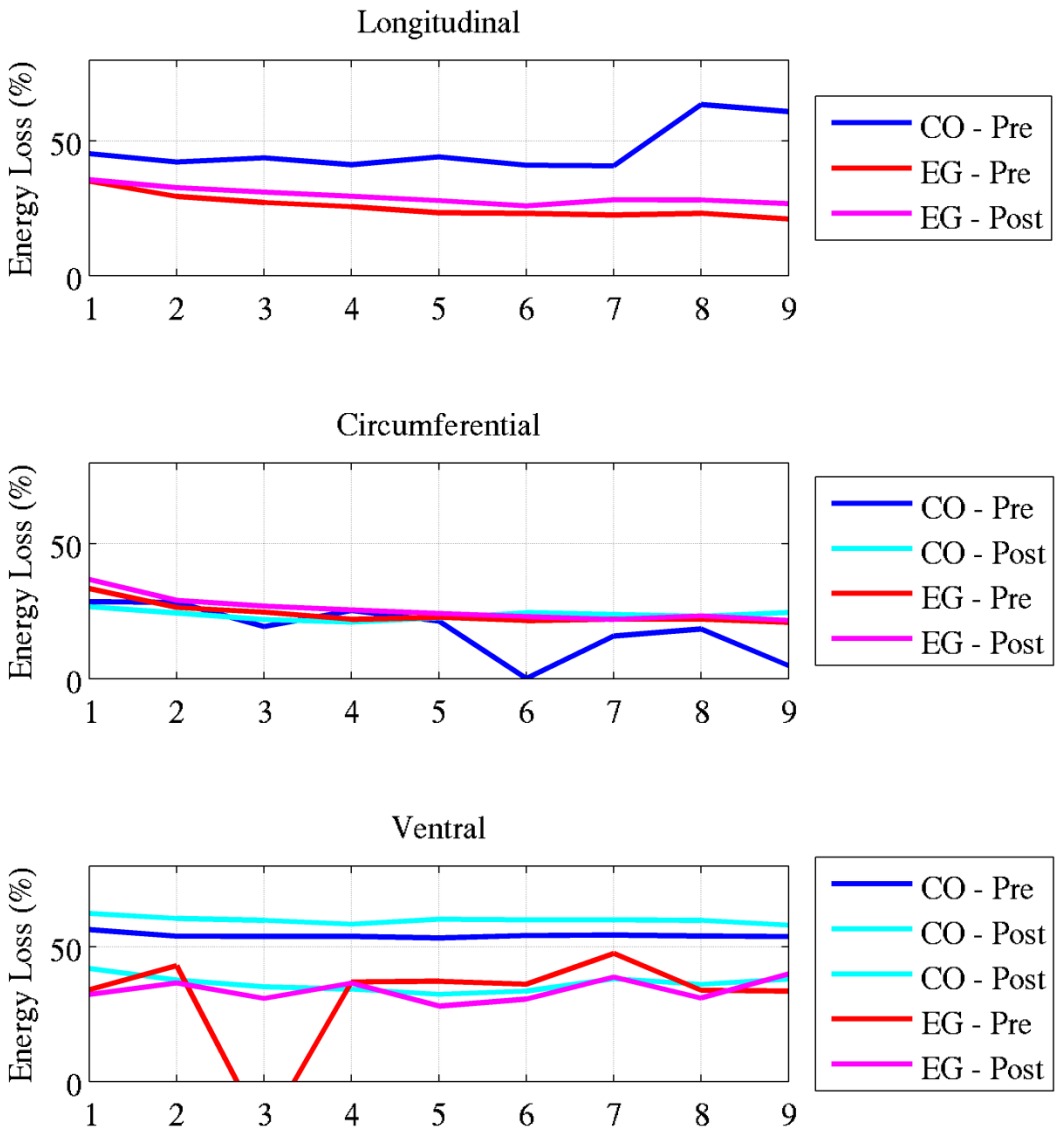

Figure 4-8: Energy loss in the first 9 cycles of hysteresis tests. In most cases, there is no clear difference between directions or orientations, specifically comparing the two species. Here Lagrangian stress is used instead of Eulerian for the strain energy calculations. The strain calculations for approximately the first 5 cycles are not steady-state, so there is some question if the Eulerian stress is representative of the stress that is applied. The point that falls below 0% energy loss in the ventral samples is likely due to a very low signal-to-noise ratio.

4.4 Relaxation Tests

Relaxation tests were performed to determine how the skin responds to being held at a fixed extension for a period of time (in this study, 30 minutes). Because the strain could not be controlled by the test setup, the strain corresponding to each extension is listed below. There are slight variations in strain for similar extensions due to differences in sample size, scalation, etc. However, every effort was made to keep these values as similar as possible. Table 4-20 lists the stress and strain reached at the end of the initial extension phase.

As previously stated, strain could not be directly controlled, so the extension to reach a certain point on the stress-strain curve was estimated. Table 4-18 shows the average strain seen at each extension. Based on these values, the 4 mm extensions yielded 0.062 strain·mm^{-1}, 5 mm extensions yielded 0.065 strain·mm^{-1}, and 10 mm extensions yielded 0.043 strain·mm^{-1}.

Table 4-18: Relaxation test comparison of extension and strain

Extension	*Strain*
4 mm	0.25 (0.041)
5 mm	0.32 (0.041)
10 mm	0.43 (0.11)

When examining the normalized response of the tests (where maximum stress has been scaled to 1.0) in Figure 4-9, there are no obvious differences between the responses of different species and orientations. Table 4-19 shows the percentage decrease in stress over 30 minutes. Because of the low sample numbers, statistical comparisons are not performed. However, we can see that the amount of stress relaxation in each snake and direction is approximately the same, given the deviations.

Table 4-19: Percentage decrease in stress over 30 minutes

Percent Stress Decrease (SD)	*C. ornata*	*E. guttata*
Longitudinal	83.70 (5.20)	73.72 (5.09)
Circumferential	76.27 (0)	72.82 (9.55)
Ventral	70.37 (3.75)	74.84 (10.99)

Table 4-20: Stress and strain at end of initial extension phase of relaxation tests

Test ID	*Species*	*Snake #*	*Orientation*	*Region*	*Max Stress (MPa)*	*Strain*
4	*C. ornata*	3	Circumferential	Pre-Pyloric	-	0.23
5	*C. ornata*	3	Ventral	Pre-Pyloric	0.95	0.22
6	*C. ornata*	3	Longitudinal	Pre-Pyloric	1.16	0.31
20	*C. ornata*	3	Circumferential	Pre-Pyloric	5.15	0.47
216	*E. guttata*	8	Ventral	Pre-Pyloric	0.13	0.29
223	*E. guttata*	8	Longitudinal	Pre-Pyloric	6.47	0.34
272	*C. ornata*	1	Longitudinal	Pre-Pyloric	1.30	0.28
273	*C. ornata*	1	Ventral	Pre-Pyloric	0.50	0.30
274	*C. ornata*	1	Circumferential	Pre-Pyloric	-	0.66
317	*E. guttata*	9	Ventral	Pre-Pyloric	0.15	0.19
318	*E. guttata*	9	Circumferential	Pre-Pyloric	1.09	0.40
319	*E. guttata*	9	Ventral	Pre-Pyloric	0.10	0.24
320	*E. guttata*	9	Longitudinal	Pre-Pyloric	0.50	0.32
321	*E. guttata*	9	Circumferential	Pre-Pyloric	0.72	0.46
322	*E. guttata*	9	Longitudinal	Pre-Pyloric	0.90	0.40
323	*E. guttata*	9	Longitudinal	Post-Pyloric	0.26	0.33
324	*E. guttata*	9	Ventral	Post-Pyloric	0.18	0.24
325	*E. guttata*	9	Circumferential	Post-Pyloric	0.99	0.40
326	*E. guttata*	9	Longitudinal	Post-Pyloric	1.12	0.28
327	*E. guttata*	9	Ventral	Post-Pyloric	0.99	0.21
328	*E. guttata*	9	Circumferential	Post-Pyloric	5.17	0.45
329	*E. guttata*	9	Circumferential	Post-Pyloric	7.64	0.44
330	*E. guttata*	9	Circumferential	Pre-Pyloric	0.97	0.39
331	*E. guttata*	9	Ventral	Pre-Pyloric	0.43	0.29

* Tests with '–' indicate that the maximum stress could not be calculated using the same method as the rest of the tests due to the fact that the stress increased throughout the test. This may have been due to the extremely low load applied at this extension, or slight variations in the testing setup (lighting) that do not affect the rest of the tests due to load or duration.

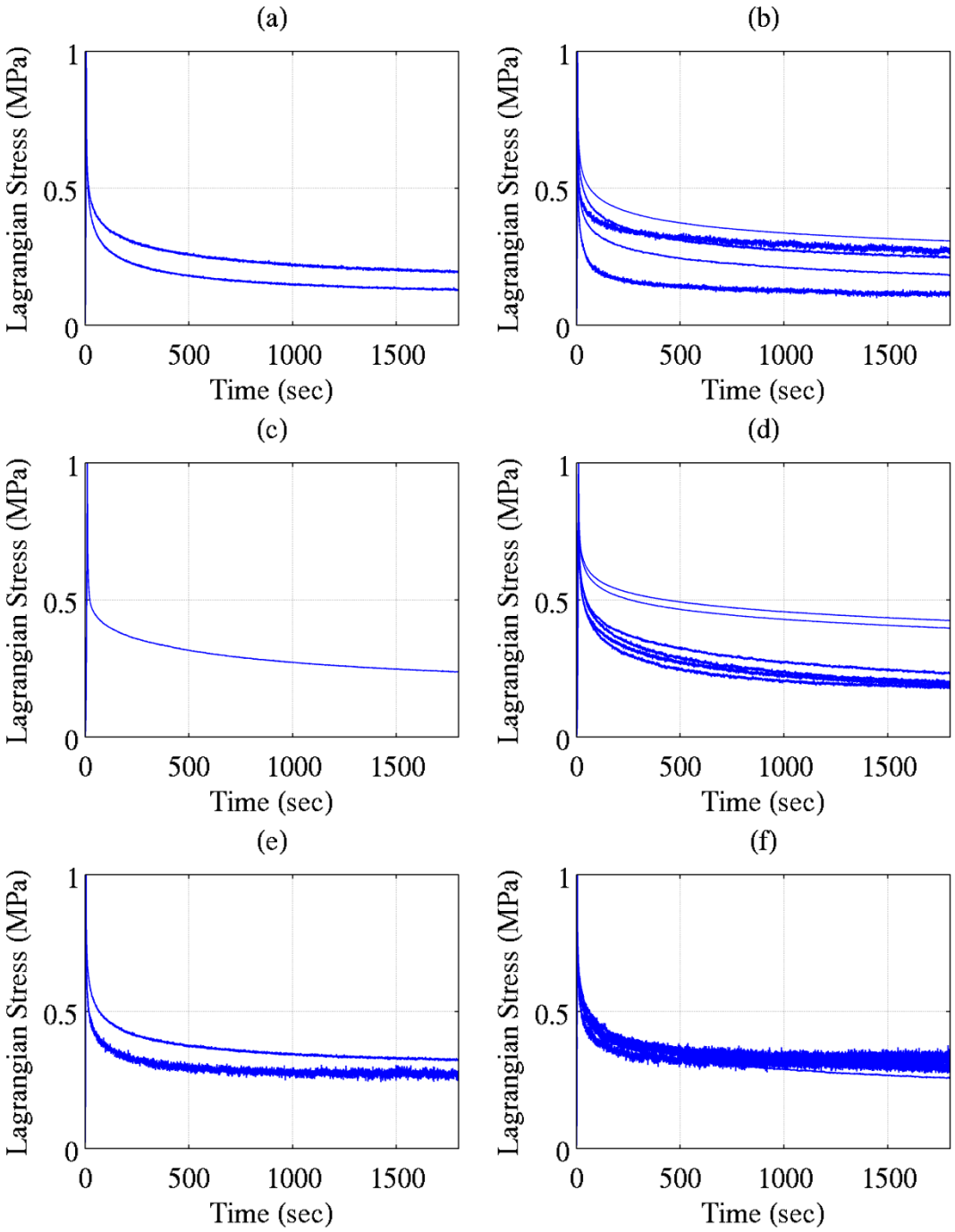

Figure 4-9: Normalized relaxation stress versus time. Longitudinal *C. ornata* in (a), *E. guttata* in (b); circumferential *C. ornata* in (c), *E. guttata* in (d); ventral *C. ornata* in (e), *E. guttata* in (f).

By computing the relaxation rate using the same method as Provenzano [42], the parameters for a single term power law function $\sigma_{norm} = at^b$ for stress versus time are shown in Table 4-21. Normalized data were used because the variation in stresses is great, and the relaxation rate calculation is identical if either normalized or actual Lagrangian stress is used. An exponential fit

was also attempted as shown in a study on tissue gels and heart tissue [43], but yielded poor results. As demonstrated by the R^2 value, the relaxation of snake skin is well defined by the power law used to define the relaxation of other soft tissues.

Table 4-21: Power law fit parameters.

		a	*b*	R^2
C. ornata	Longitudinal	1.004	-.247	0.990
	Circumferential	.9507	-.1811	0.968
	Ventral	0.810	-0.138	0.929
E. guttata	Longitudinal	0.8172	-.180	0.965
	Circumferential	1.157	0.199	0.988
	Ventral	0.820	-0.141	0.905

4.5 Creep Tests

Creep can be divided into 3 distinct phases: primary, secondary, and tertiary. The analysis presented focuses on the first two phases of creep, primarily the second phase. The first stage represents the transient creep response after the end of the initial loading phase. However, after a constant load state is achieved, the steady-state response takes over, and the rate of deformation or strain decreases to a somewhat constant value. The figures below depict the strain response of the skin to a constant load held for 30 minutes. The early response of the skin shows the primary and transition to secondary creep responses.

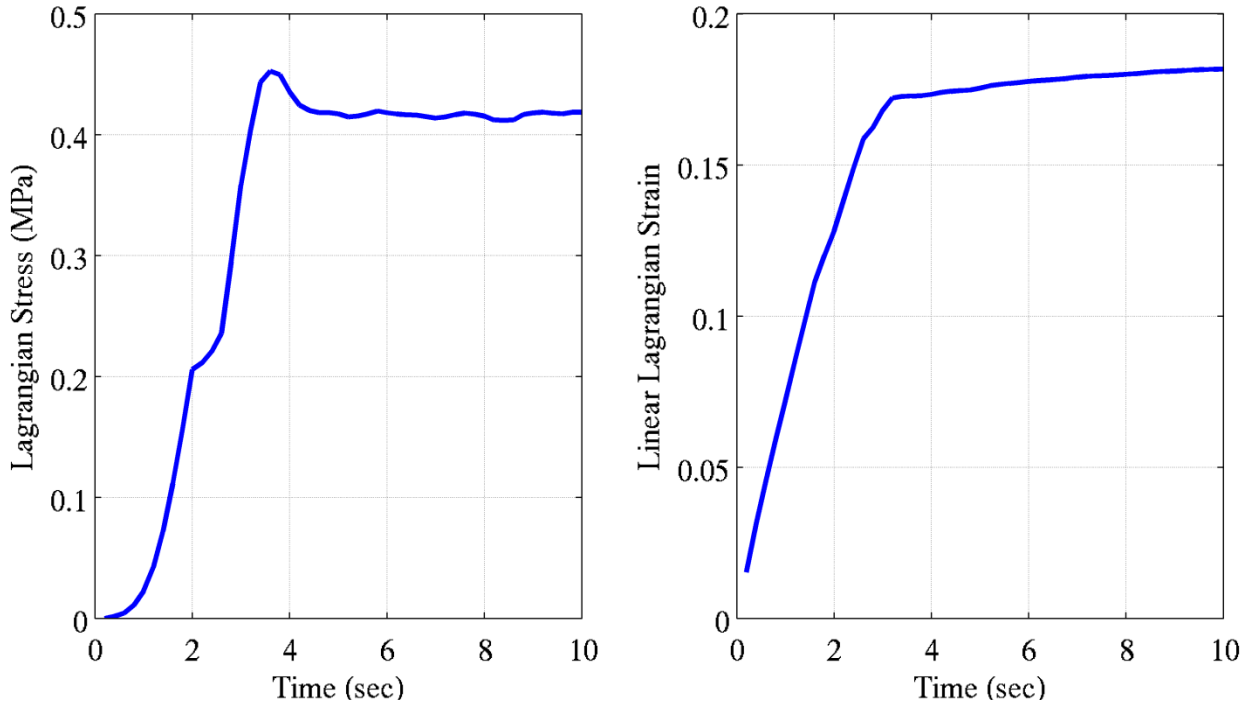

Figure 4-10: Primary and early secondary stress and strain during creep test. The peak at approximately 4 seconds (seen in the stress response) is due to the test control and occurs in most creep tests, but more so at lower stresses. The primary creep response is easily seen in the strain response.

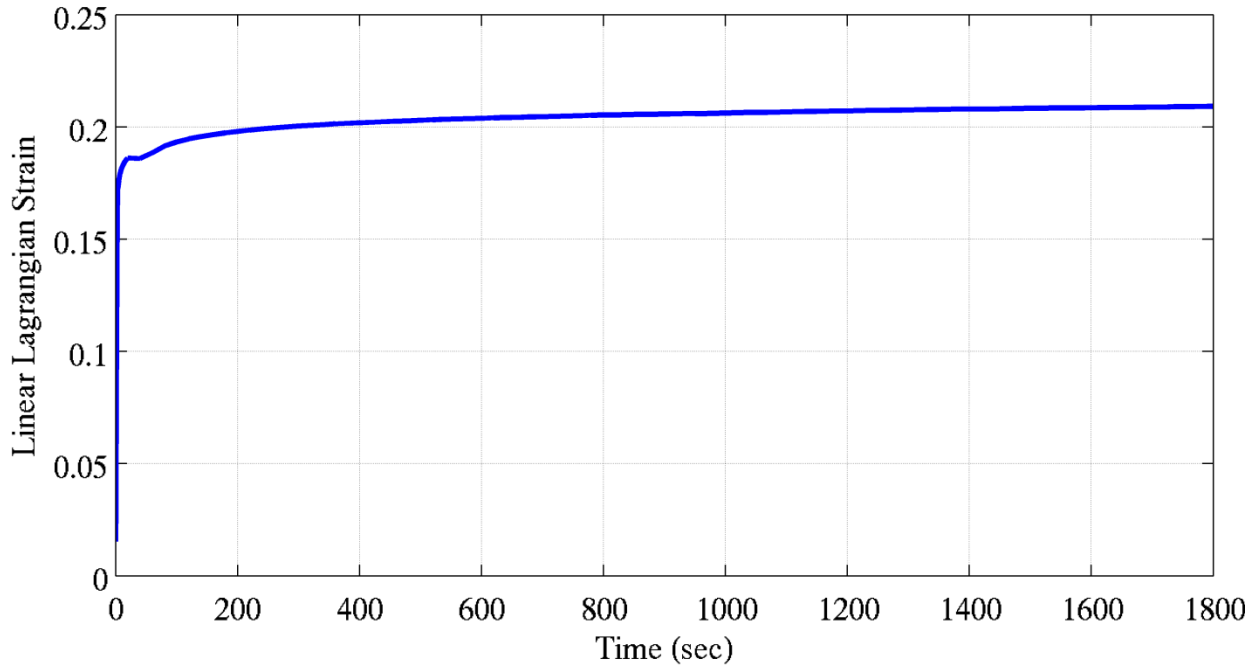

Figure 4-11: Sample creep strain response. The majority of the graph shows the secondary creep response. Here, the switch from primary to secondary seems to be at approximately 400-600 seconds in this test.

A decrease in traditional strain rate (Δstrain/Δtime) is seen in all sample configurations of both *C. ornata* and *E. guttata* in Figure 4-12. In almost all cases, the strain rate decrement is

approximately one order of magnitude over 30 minutes. However, there seems to be no significant difference when comparing snakes or orientations (regional differences were not examined due to low sample numbers. Though it is somewhat visible in Figure 4-11, the switch from primary creep to secondary is more visible in the strain rate plots. Here we can see that the switch generally occurs between 500 and 1000 seconds, with the exception of ventral samples, which tend to switch just before 500 seconds.

A power law, similar to that used for the relaxation response, can also be used to model the creep response with good results. Once again, the power law had very high R^2 values (> 0.95 in all tests, and most > 0.99). By comparing this value to the strain at the end of the initial ramp phase in Figure 4-13, some interesting groupings are seen. Both longitudinal and circumferential orientations seem to have a decrease in creep rate with an increase in initial strain. There may also be a slight decrease in the ventral samples, but not as apparent as the others, especially the circumferential orientation. At equal initial strains, the ventral samples seem to have the lowest creep rates. Longitudinal values are generally higher than ventral until much higher initial strains are seen. The circumferential orientation has the overall highest creep rate values, but has the least consistency in creep rate at any given strain value.

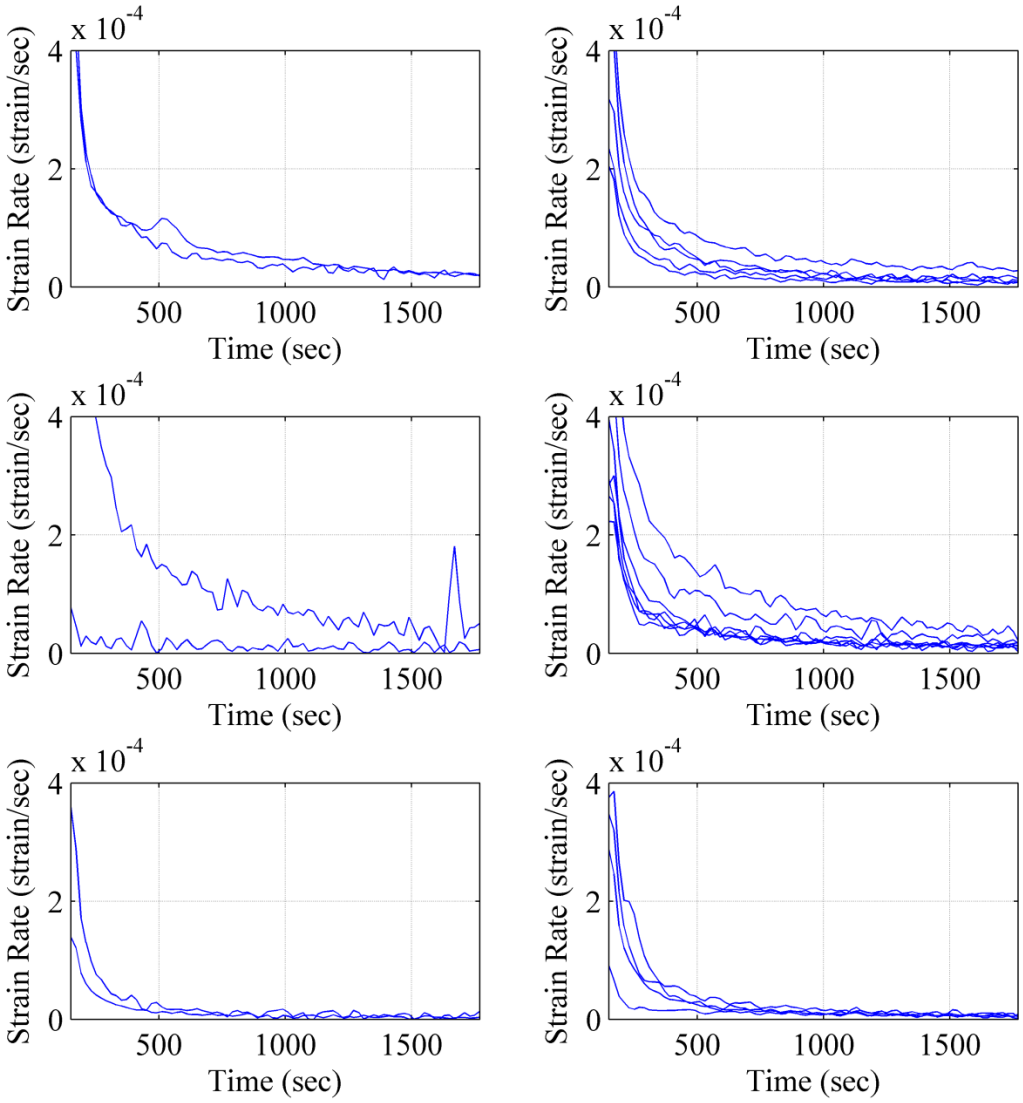

Figure 4-12: Strain rate versus time. *Chrysopelea ornata* samples are seen in the left column, with *E. guttata* in the right. The first row represents longitudinal data, the second row is circumferential, and final row is ventral. The decrease in strain rate is clearly seen in all samples, and most seem to approach a steady state value.

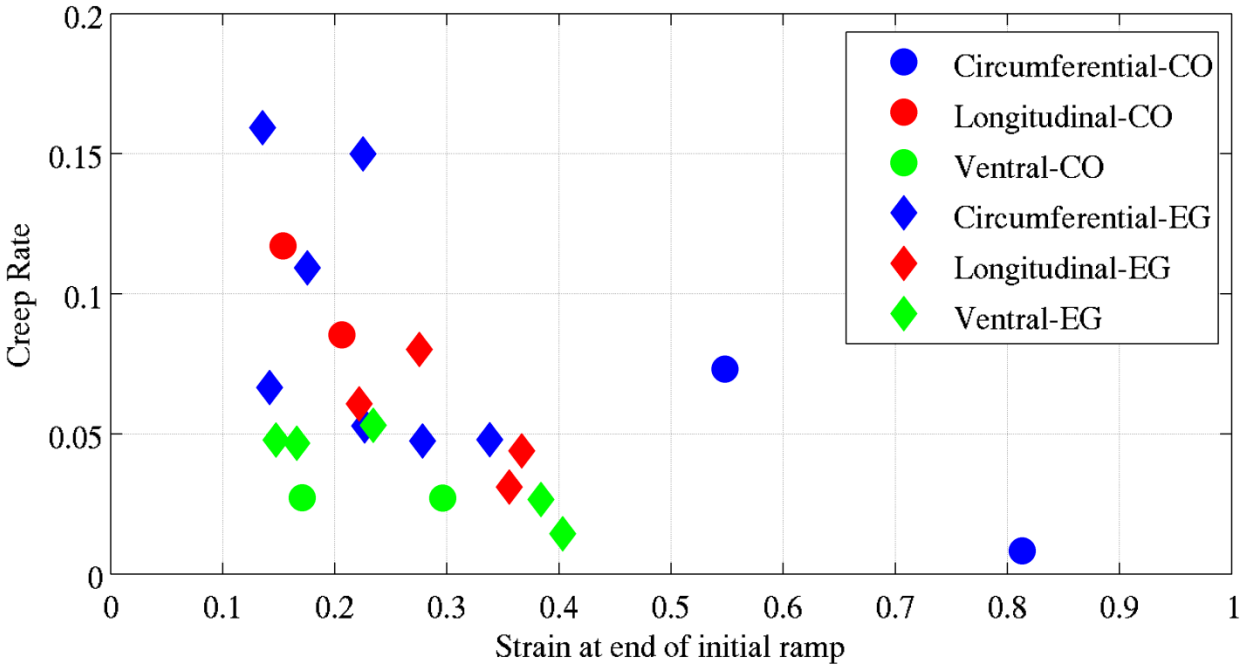

Figure 4-13: Creep rate derived from power law fit versus initial strain. A decrease in creep rate from small strains to large strains is noted, and directional clusters are also noted encompassing both species. At equal strains, ventral samples have the lowest creep rate, and circumferential has the overall highest values, but are very spread out.

Chapter 5: Discussion and Conclusions

The results of this study provide a comprehensive overview of the mechanical properties of snake skin in *C. ornata* and *E. guttata* (along with minimal data from *T. sirtalis*). Although comparisons showed few trends when comparing individual properties of species across the range of tests, differences were seen between the two strain rates. In particular, the strength, modulus, and energy absorption capabilities of skin were larger when tested at higher rates. However, this should give insight into the response of snake skin to quasi-static and dynamic loading scenarios, with some inferences to why values are different (or not).

5.1 Uniaxial Tensile Tests

Although it has been shown that there are definite statistical differences in mechanical properties in circumferential samples when comparing regions [9] and probable differences in dorsoventral sample properties [10] (both longitudinal and ventral in this study), no large-scale comparison of a combination of regional and orientation effects has been performed, with the exception of tanned cobra skin [22]. As previously stated, the low sample numbers of *T. sirtalis* may indicate that the statistical confidence of these comparisons is less than that of *C. ornata* and *E. guttata*. For that reason, they are discussed, but are not given equal weight.

5.1.1 Species comparisons

Several consistencies are noted when comparing maximum Lagrangian stress across orientation, region, and species. First, this stress value is significantly different in the longitudinal and ventral regions for 5 of 6 comparisons within species (not in the *T. sirtalis* post-pyloric). Circumferential samples were also different when comparing pre-pyloric and post-pyloric regions. In all comparisons of circumferential and ventral orientations in the post-pyloric region there was a significant difference. Also, 2 of 3 pre-pyloric longitudinal and circumferential comparisons were significant. From this, we see that all three of these species appear to have circumferential strength characteristics that were not seen by Rivera et al. [9]. Differences in longitudinal and ventral orientations are consistent with the results from Jayne

[10], and signify that there is definitely a significant difference in these orientations. When Eulerian stress, which accounts for the change in area of the sample during testing, was compared, fewer differences were seen. The circumferential pre-pyloric vs. post-pyloric relationship still holds, and 5 of 6 longitudinal-ventral comparisons are significant, but the ventral was also different from the circumferential in 3 of 6 cases.

Overall, this shows that while all three species are known members of the taxon Macrostomata, they do not show peak stress values similar to those in prior studies focusing on specialization for large prey ingestion. It seems that there is a difference between longitudinal and ventral samples overall, but there seems to be no clear locomotor advantage for this. However, if one considers the demands of different dorsoventral regions, the longitudinal skin is stretched more during lateral undulation. As the circumferential values were also generally different from ventral values, but not from longitudinal values, another unanswered question is presented: What functional or mechanical difference occurs between circumferential and ventral that does not between circumferential and longitudinal? This may be due to dorsoventral location on the body, but further investigation is needed, possibly considering fiber orientation. All other inter-species stress comparisons yielded no definitive results for global comparisons of snake skin properties. When comparing these properties across species, there seemed to be no trend in differences, with the exception of longitudinal values in the pre-pyloric region. The majority of all other comparisons were not directly significant, so no definitive conclusions can be made about those comparisons individually. From an ANOVA test, we can see that region and orientation have an effect on the maximum stress a particular sample of snake skin may see. However, due to low sample numbers and high variability, this may not affect a particular snake, region, or orientation.

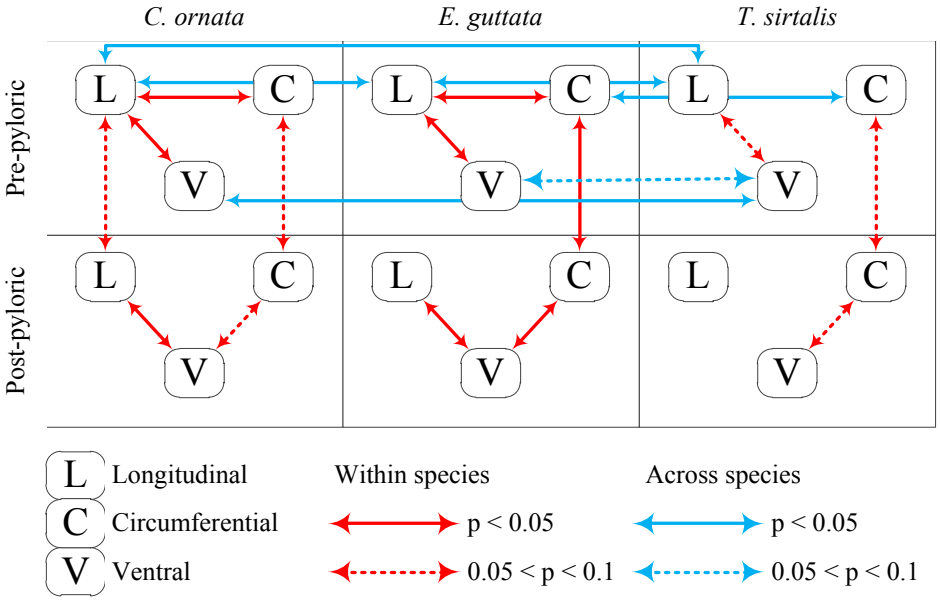

Figure 5-1: Overview of Lagrangian stress statistical comparisons

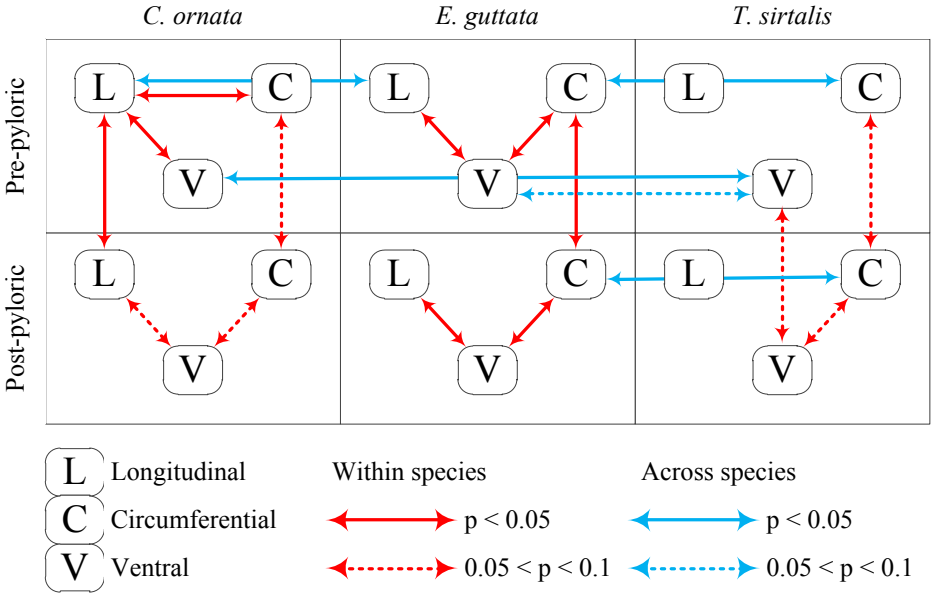

Figure 5-2: Overview of Eulerian stress statistical comparisons

As with the stress comparisons, particularly Eulerian, the linear ventral strain was different from both the longitudinal and circumferential orientations in both regions in 4 of 6 total comparisons. However, no comparisons of circumferential strain showed a significant difference. Although Rivera et al. showed that post-pyloric samples have significantly lower strain values than pre-pyloric specimens, this data has been normalized, and remembering the comparisons of

normalized and non-normalized strains, we see that differences in maximum strains are due to low-stress extension, consistent with [9]. In the nonlinear formulation, the longitudinal-ventral comparison was not as significant, but the ventral-circumferential was more significant with 6/6 comparisons showing differences. In many cases, the longitudinal was also different from the circumferential, with circumferential values being greater. This once again supports large prey consumption functional necessities. Given that longitudinal values are also greater than ventral, it implies that this skin can be stretched more than the ventral skin. As the longitudinal samples were taken from different dorsoventral regions, this makes sense, as the change in length at a greater radius given lateral curvature (recalling Figure 3-4) would be greater than that along the midline, where the ventral samples originate.

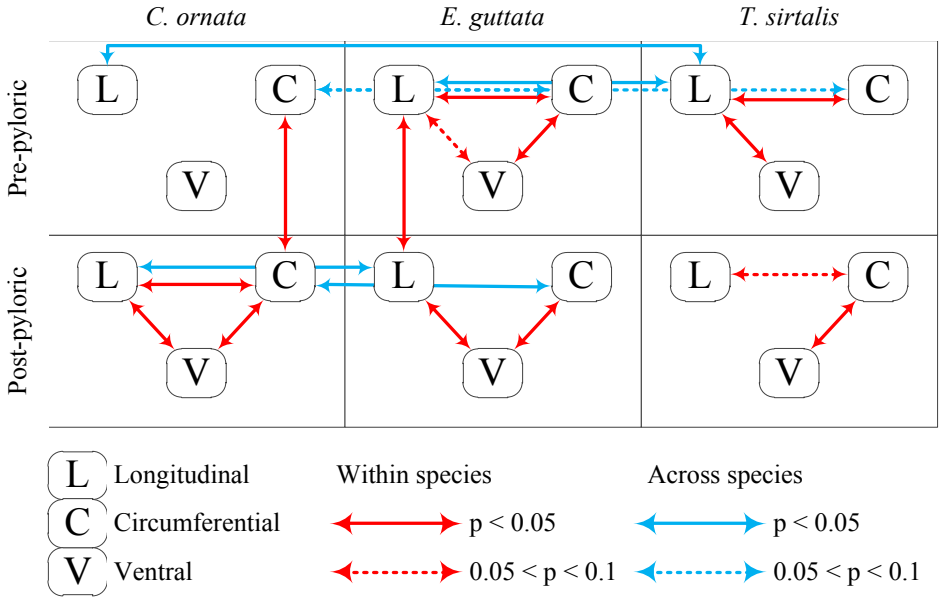

Figure 5-3: Overview of linear Lagrangian strain comparisons

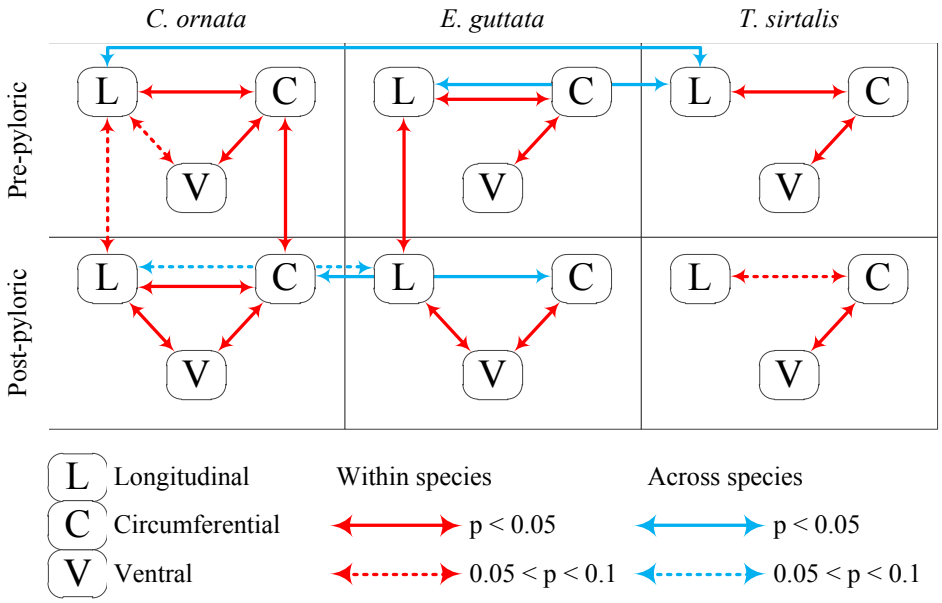

Figure 5-4: Overview of nonlinear Lagrangian strain comparisons

When examining the extensibility of the skin, several things may be noted. First, in *C. ornata*, all raw strain comparisons between orientations are either significantly or likely significant. In *E. guttata*, the differences vary from pre-pyloric to post-pyloric region and from linear to nonlinear strain calculations. In *T. sirtalis*, comparisons to circumferential samples were also either significant or likely significant. Overall, this indicates that there are clearly orientation differences in extensibility (before normalization). However, after normalization, there are very few differences in extensibility comparing similar orientations across regions. To explain this, we must look at the extensibility of the skin before a significant load is applied. By comparing the normalized extensibilities to the non-normalized values, we can examine the average extensibility of the skin before a significant load is applied. In *C. ornata*, the circumferential pre-pyloric value is approximately twice that of the longitudinal and ventral, while the post-pyloric value is similar to the other orientations. The same relationship is true of the *E. guttata* and *T. sirtalis* specimens, although the ventral values are also slightly higher than the longitudinal in these species. From this, we can see that this relationship agrees with previous data [9].

Like the stress and strain comparisons, differences in strain energy were seen in 4 of 6 longitudinal-ventral comparisons (not *T. sirtalis*) and 3 of 6 circumferential-ventral comparisons. Given that lateral undulation is used in all species tested, larger strain energies in the longitudinal

orientation implies that, upon release of extension, longitudinal skin has the capability of returning more energy to the system.

There was also a regional difference in the circumferential samples, which is indicative of several things. First because of the significant differences between stress and strain, particularly in the regional comparisons, it seems that stress is more likely to impact differences in strain energy than strain, particularly in the circumferential direction. However, neither stress nor strain seems to be an indicator of strain energy in the cranio-caudal direction. As few differences were seen when performing interspecies comparisons, we can assume that strain energy is not an indicator of differences between species. However, longitudinal differences in the pre-pyloric region agree with the assumption that strength affects strain energy differences more than extensibility.

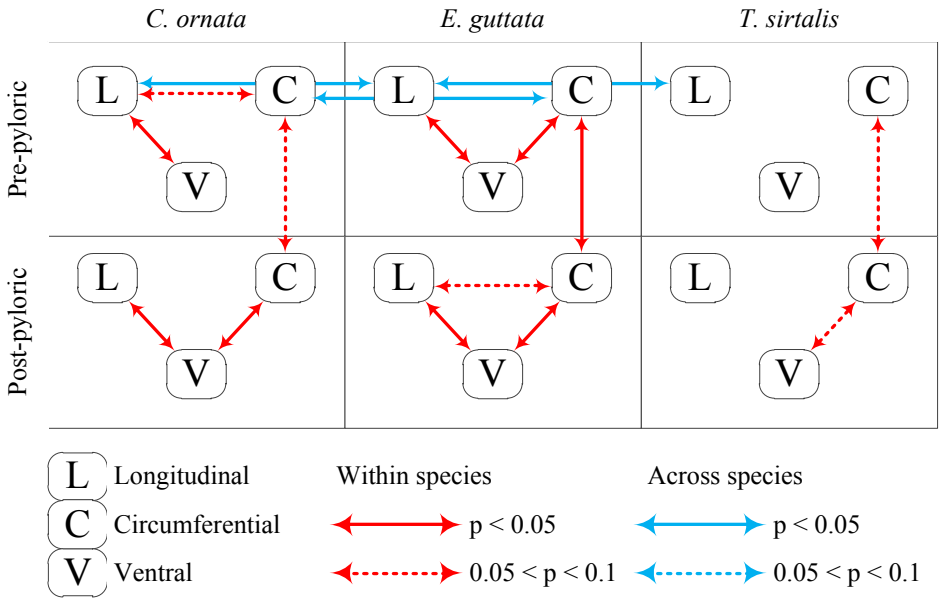

Figure 5-5: Overview of strain energy comparisons

While strain energy can be used to describe several aspects of energy consumption and storage in the skin, we will first look at strain energy absorbed to failure (maximum stress or strain) in the skin. Given that a gliding snake must likely withstand landing forces at least one order of magnitude greater than its body weight, one might expect that the skin might have increased energy absorption during landing to absorb energy so that more important internal organs aren't damaged. By comparing the averages among species, we see that in the longitudinal orientation, the *C. ornata* strain energy average values are slightly less than the *E.*

guttata samples, and similar to the *T. sirtalis* samples in both regions. Ventral values are generally constant across species, as are circumferential values. Relative to body mass, we see an overall increase in strain energy, especially in the pre-pyloric longitudinal values, but more data across a broader species and mass range is needed to fully support this relationship.

Modulus of the skin can be used to show the amount the skin will stretch if a load is applied. Because the modulus of the skin increases with increasing stress (and strain), this shows that the tissue is nonlinear, further justifying the use of nonlinear strain estimation. Also, it presents biological significance and agrees with collagen fiber recruitment theory [42, 44]. As the skin is stretched, there are initially few fibers recruited to bear a significant load. When the skin is stretched further, more fibers are recruited to bear additional load, but the rate of strain remains constant. Therefore, the stiffness of the material must increase with an increase in strain. As stiffness varies between orientation and region in some cases, this may indicate different fiber orientations or amount of fibers.

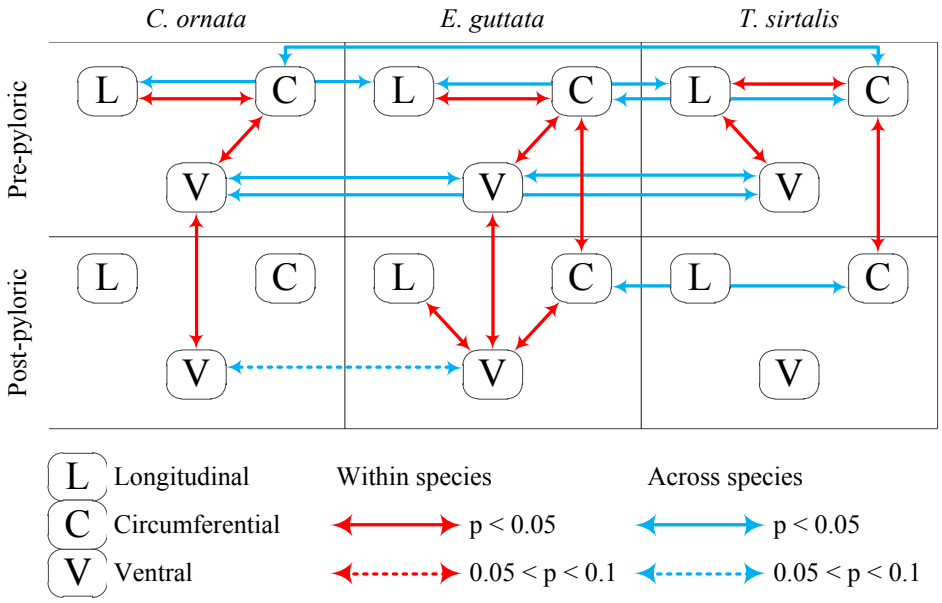

Figure 5-6: Overview of elastic modulus comparisons

When statistical comparisons of elastic modulus were made, circumferential and ventral values were different comparing regions in 2 of 3 comparisons. Comparisons between species showed more differences than any other property measured. 4 of 6 ventral species comparisons were significant, and 2 of 3 pre-pyloric longitudinal comparisons were different. Both comparisons of circumferential values were significant when comparing *E. guttata* and *T.*

sirtalis. Overall, this shows that the elastic modulus of the skin has much more variability across region and species than other values. This is most likely due to the fact that this value, as with strain energy, is dependent on both stress and strain, although the specific dependence is slightly different.

In some tests, there were anomalies that occurred in the stress-strain curve. In many tests, a step in the curve was seen, particularly at lower strains. This has been observed in snake skin before, and is thought to occur when skin layers pull apart [10]. Although this could not be directly confirmed during testing, layers of the skin pulling apart is a reasonable cause for this behavior. A decrease in strain also occurred at the beginning of hysteresis tests. This is possibly due to the inability of the skin to retract completely in the first few cycles, so some skin may buckle out of plane, causing issues with strain measurements. However, after several cycles, it appeared to settle to a steady-state response, oscillating about a seemingly constant value (although the sample does not return to a value of zero strain). Because this issue is most easily seen in hysteresis tests, it could also be due to the fact that the DIC slightly underestimated the displacement in most cases, which may account for some of this behavior (however, because the peak strains do approach steady-state values, this is less likely than the former assumption).

5.1.2 Comparison to other similar tissues

When comparing values from this study to previous work on snake skin [10], some differences must be noted. First, testing rates were different: this study used rates of 0.941 $mm \cdot s^{-1}$ and 9.41 $mm \cdot s^{-1}$. Jayne used a rate of 0.05 $strain \cdot s^{-1}$, which corresponds to 3.5 $mm \cdot s^{-1}$ for a 70 mm gage length. Although fresh tissue was used, there was no indication of keeping the sample hydrated in a buffer solution during testing. For this reason, comparisons were made to see if the values at this median strain rate fell between the two rates tested in this study, specifically comparing *C. ornata* to a closely related tree snake, *Ahaetulla prasina* (for relationship, see Figure A-1). For both strain rates tested in this study, ventral and longitudinal peak stresses in *C. ornata* fell below the average values in *A. prasina* (the only comparison in which the values from this study at the 'normal' and 'fast' rates encompassed the values from Jayne's study was the ventral peak stress of *Nerodia fasciata*). However, given the variance in peak stresses given in Jayne's study, the values presented for each species appear to be well within reasonable confidence intervals for this tissue. Stiffness was also examined and showed a similar

relationship to previous values. When comparing linear failure strains, values for the current study ranged from 0.4 to 0.8 on average in the cranio-caudal direction and fell within reasonable values for all species presented in Jayne's study.

Although direct comparisons were not made to results from Rivera et al. [9], when looking at raw strain values, all three species demonstrated the same difference in failure strain values when comparing pre-pyloric and post-pyloric regions. *E. guttata* did not decrease as much as *C. ornata* and *T. sirtalis*, but a slight decrease was noted from snout to vent. We also found significant differences when comparing maximum stresses across regions in the circumferential orientation. In all cases here, the tissue was not only stronger in the post-pyloric region, but also had greater failure strain energies and larger moduli. However, Rivera et al. reported strains of 1.6 and 1.8 at 1.0 and 2.0 MPa stress respectively. Given that average linear failure strains were less than these values, as were the maximum stresses seen (approximately 10 MPa in the comparison work, compared to approximately 2-4 MPa in the *T. sirtalis* data from the current study), differences in testing and analysis are assumed here, especially since this common species was included in both studies. Hydration during testing, along with sample shape, is thought to be a major factor concerning these differences. Sample shape is more likely since failure strain values fell within the same range of values of Jayne's study which also used dog-bone shaped samples, compared to rectangular samples in [9].

Direct comparisons of values could also not be made to the work by Niitsuma et al. [22]. However, similar relationships between longitudinal and circumferentially oriented specimens were seen in all snakes, with higher stresses in the longitudinally oriented specimens, and larger failure strains in the circumferentially oriented samples. Niitsuma et al. suggest that the anisotropy in mechanical properties is due to the orientation of collagen fibers. SEM photographs in the cobra study indicate that collagen fiber bundles are oriented in the longitudinal orientation along the snake (also in [45]). Their study also indicated that maximum stress was lower near the abdomen and higher near the spine, especially in the longitudinal direction. In this study, we found consistent results with ventral peak stresses less than longitudinal values (in most cases, this was a statistically significant difference). By taking inferences from the cobra study and adding results from this study, we can agree that the degree of anisotropy varies with respect to dorsoventral location on the body and orientation. However, we also find significant differences in circumferential-ventral comparisons, which were not found in Niitsuma et al.'s work.

5.2 Strain Rate Effects

Statistical comparisons showed that on the global scale, greater strength was seen with an increase in strain rate. This was also not localized to a single species, as the percent increase was similar in *E. guttata* and *C. ornata*. However, this does make sense in a biological perspective. If we consider a gliding snake, the force upon ground impact is proportional to the speed at which it impacts. By assuming the strain rate on impact to also be related to the landing speed, an increase in landing force can be correlated with an increased strain rate due to both friction and pressure. If this phenomenon occurred strictly in gliding snakes, it could be seen as a specialization. However, because it occurs in other non-gliding species as well, it may not necessarily be a specialization for gliding behavior, but simply a rate-dependent behavior, typical of viscoelastic biological tissues [46].

Because the energy absorption capabilities and modulus were significantly different in *E. guttata*, but not in *C. ornata*, this may indicate that the maximum strain affects these values more than maximum stress (as maximum stresses were found to be significant and maximum strains were not). However, variation in test response may also impact the statistics. When looking at gross differences in *C. ornata*, 12/18 paired comparisons yielded an increase in these values from normal to fast rates. This indicates that the number of comparisons may not be large enough to give an accurate assessment due to variability, as the majority of evaluations yielded a positive difference.

5.3 Hysteresis

To examine the energy return with cyclic loading and unloading, strain energy loss was computed between each of the first 9 loading and unloading cycles. By comparing the percentage energy loss, the return is generally constant across these cycles, even if the loading strain energy magnitude does decrease with each cycle. Energy return in all directions seems to be approximately 60-75% for an extension in any orientation, with circumferential loading having the greatest return (approximately 75%). This is encouraging, for if the energy return properties indicate efficiency, the skin can aid in passive undulation motion rather than active muscle activation; however, this remains untested. Based on comparisons with loading and unloading

curves of other animals using undulation as a method of locomotion, the energy return seems to be very high. By performing a simple estimation of strain loss from previous data on fish skin [27] and eel skin [29], it seems that energy losses of approximately 70-90% are reasonable estimates for these tissues, with greater loss in the circumferential direction in these tissues. Because of the low energy loss in the snake skin circumferential orientation compared to other similar tissues, this can be considered a further specialization for macrophagy as less energy is required to return the skin to the original configuration. The lower energy loss in the longitudinal direction may be a specialization for this particular mode of locomotion, but given the general constancy of loss across orientations, is more likely due to fiber orientation and other unknown factors common to both species.

5.4 Relaxation

Relaxation of biological tissue is often characterized by fitting the response to exponential decay equations whose time constants may be used in modeling (which is not attempted here). However, only basic characteristics of the relaxation behavior are detailed here. From the results previously shown, the load held by the skin decreases very rapidly to a stress value that is 20-30% of the peak stress value. This value did not seem to be dependent on species or orientation. Large decreases in stress seems abnormal when compared to some biological tissue (mesentery, in which the load only decreases by approximately 10-15% of the maximum value after relaxing for ~3 minutes [19]), but also seems to be similar to other tissues (cartilage, which decreases by approximately 85% of the maximum value within several minutes [47]). In most tests, after several minutes the value had decreased to approximately 30-40% of the initial stress, but had not reached a steady-state value, which was not the case with the two studies mentioned above.

When comparing relaxation rates calculated from a power law function fit, there seems to be very little difference in this value across different directions and snakes. Overall, ventral values seem to have a tighter grouping than the other orientations, but there are not enough samples to determine if this is statistically relevant. However, the relaxation rate calculated using this method is of the same order of magnitude for strains in the toe region of a tissue. Compared to values from Provenzano's work on ligaments [42], the strains with comparable rates are much lower (ligament strain < 1%) than those seen here, but the ligament failure strain is also much

lower. The differences in values appear to be a function of initial stress in the sample, rather than fundamental differences between orientations. This agrees with the data seen earlier indicating varying peak moduli in different orientations. However, the functional significance of these data is unknown, and is merely presented as a characterization of the tissue.

5.5 Creep

In this study, only the first two phases of creep were studied. When analyzing strain rates, the rate was shown to decrease from 1-4 x 10^{-4} strain/s by approximately one order of magnitude. Also, the switch from primary to secondary creep, as shown by a constant creep rate, occurred between 500 and 1000 seconds in the longitudinal and circumferential samples, and usually between 400 and 700 seconds in the ventral samples.

The creep response was also fit using the same power law used for the relaxation response. Overall, creep rates (i.e. the slope of the strain vs. time response plotted in log-log scale) were between approximately 0.01 and 0.16 log(strain)/log(s). Compared to other biological tissues tested in the toe region of the load-displacement curve [42], these seem to be reasonable values. This rate was also compared to the strain at the end of the initial ramp phase of the test. As the initial strain increased, the creep rate tended to decrease. The most noticeable decrease occurred in the longitudinal orientation, and the ventral samples seemed to show almost no decrease in creep rate with increasing initial strain. Circumferential samples had a very large range of creep rates, at least compared to the other orientations, but showed a slight decrease in creep rate with increasing strain.

This decrease in creep rate could be attributed to several things. First, it has been suggested that with increasing strains, more collagen fibers are recruited [42, 44], and thus the apparent stiffness of the material increases. This may cause a decrease in creep rate, and as the strain increased, further fibers would be recruited, causing the rate to decrease further as more load is applied. Differences in creep rates between orientations are most likely due to the orientation of collagen fibers with respect to the loading direction. Because the test is performed at a constant load, the effect of the toe region can be neglected (i.e. strain without substantial stress). If this assumption is made, it seems that fibers are oriented more in the longitudinal direction along the snake rather than circumferentially. Given the crossed orientation of fibers in many other animals

using undulation for locomotion (e.g. fish [27, 29], etc), we might predict that the fiber orientation in snakes is similar. This may explain the behavior of not only the creep response but other properties of the skin as well.

5.6 Summary

In conclusion, this study presents results that both agree and disagree with some values and conclusions from previous studies. Addressing the hypotheses presented, several conclusions can be made which indicate that *Chrysopelea ornata* skin does not seem to be specialized for gliding behavior. First, the overall strength of the skin is not greater than non-gliding species. Second, the energy absorbed and/or returned by the skin is not greater in the flying species, although this assumes terrestrial and aerial undulation occur at the same frequency. Flying snake skin also does not seem to be more extensible, comparing measured values of strain in the direction of load and analyzing the differences between Lagrangian and Eulerian stresses to see the change in area with load application, indicating that body shape change does not necessitate a change in material properties. Viscoelastic tests also showed no differences between species. However, what does seem to be of great importance is the significant change in properties with strain rate, specifically increased stress, strain energy, and stiffness. Although trends were similar between species, this may be an advantage employed by gliding snakes for greater efficiency and safety in gliding maneuvers that is not used by snakes whose skin doesn't operate at this higher rate. Finally, a comprehensive method of analysis which accounts for many commonly ignored aspects of biological tissues is presented that to date has only been used to analyze snake skin as a homogeneous structure, but has the capability of analyzing the tissue as a non-homogeneous structure with properties that vary depending on local content.

Chapter 6: Future Work

This chapter presents a brief overview of suggestions for work to be done in the future. To begin, the work needed to move this study further in the intended direction is presented. First, more testing should be performed on other species, particularly those indicated in Figure A-1. Second, the analysis method has the capability to look at skin in relation the scalation, but was not directly studied here. The strain analysis method should also be refined to focus on uniaxial strain to prevent some of the odd values seen in strain measurements of a single grid region (these made up a very small percentage of the total value in a particular strain calculation, so were not discarded). Of course, more tests should be run to improve the confidence in certain measurements, particularly dynamic properties and properties of *T. sirtalis*. Biaxial tests should also be performed to fully analyze the behavior of skin when stretched in multiple directions simultaneously. Finally, as strain rate dependence seemed to be the most interesting result from this study, this avenue of comparison should be further pursued.

Although this study presented a comprehensive approach to mechanical characterization of snake skin, there is still a fair amount of non-uniformity in the global test methodology of soft tissues that should be unified to provide comparisons between similar tissues.

References

1. Frolich, L.M., *The role of the skin in the origin of amniotes: permeability barrier, protective covering and mechanical support*, in *Amniote Origins*, S.S. Sumida and K.L.M. Martin, Editors. 1997, Academic Press: San Diego.
2. Licht, P. and A.F. Bennett, *A Scaleless Snake: Tests of the Role of Reptilian Scales in Water Loss and Heat Transfer.* Copeia, 1972. **1972**(4): p. 702-707.
3. Osorio, D. and M.V. Srinivasan, *Camouflage by Edge Enhancement in Animal Coloration Patterns and Its Implications for Visual Mechanisms.* Proceedings: Biological Sciences, 1991. **244**(1310): p. 81-85.
4. *Prana Open Source PIV Software* 2010; Available from: http://www.me.vt.edu/AEThER/prana.
5. Socha, J.J., T. O'Dempsey, and M. LaBarbera, *A 3-D kinematic analysis of gliding in a flying snake, Chrysopelea paradisi.* J Exp Biol, 2005. **208**(10): p. 1817-1833.
6. Socha, J.J., *Gliding flight in the paradise tree snake.* Nature, 2002. **418**(6898): p. 603-4.
7. Socha, J.J., *Turning a snake into a wing: Challenges of being a snake glider*, in *Society for Integrative and Comparative Biology*. 2011: Salt Lake City, UT.
8. Lillywhite, H.B., *Subcutaneous compliance and gravitational adaptation in snakes.* Journal of Experimental Zoology, 1993. **267**(6): p. 557-562.
9. Rivera, G., A.H. Savitzky, and J.A. Hinkley, *Mechanical properties of the integument of the common gartersnake, Thamnophis sirtalis (Serpentes: Colubridae).* J Exp Biol, 2005. **208**(15): p. 2913-2922.
10. Jayne, B.C., *Mechanical behaviour of snake skin.* Journal of Zoology, 1988. **214**(1): p. 125-140.
11. Socha, J.J., K. Miklasz, F. Jafari, and P.P. Vlachos, *Non-equilibrium trajectory dynamics and the kinematics of gliding in a flying snake.* Bioinspiration & Biomimetics, 2010. **5**(4): p. 045002.
12. Socha, J.J., *Becoming airborne without legs: the kinematics of take-off in a flying snake, Chrysopelea paradisi.* J Exp Biol, 2006. **209**(17): p. 3358-3369.
13. Miklasz, K., M. LaBarbera, X. Chen, and J. Socha, *Effects of Body Cross-sectional Shape on Flying Snake Aerodynamics.* Experimental Mechanics, 2010. **50**(9): p. 1335-1348.
14. Jackson, M.K. and H.W. Reno, *Comparative Skin Structure of Some Fossorial and Subfossorial Leptotyphlopid and Colubrid Snakes.* Herpetologica, 1975. **31**(3): p. 350-359.
15. Alibardi, L., *Differentiation of snake epidermis, with emphasis on the shedding layer.* Journal of Morphology, 2005. **264**(2): p. 178-190.
16. Gans, C. and E.A. Liner, *Biology of the reptilia*. Vol. 12. 1969, London; New York: Academic Press.
17. Hinkley, J.A., A.H. Savitzky, G. Rivera, and S.H. Gehrke, *Tensile Properties of Hydrogels and of Snake Skin.* 2002.
18. Fung, Y.C., *Biomechanics: Mechanical Properties of Living Tissues*. 2 ed. 1993, New York: Springer-Verlag.
19. Fung, Y.C., *Elasticity of soft tissues in simple elongation.* The American journal of physiology, 1967. **213**(6): p. 1532.

20. Vogel, H.G. and W. Hilgner, *The "step phenomenon" as observed in animal skin.* Journal of Biomechanics, 1979. **12**(1): p. 75-81.
21. Lee, M.S.Y., A.F. Hugall, R. Lawson, and J.D. Scanlon, *Phylogeny of snakes (Serpentes): combining morphological and molecular data in likelihood, Bayesian and parsimony analyses.* Systematics and Biodiversity, 2007. **5**(04): p. 371-389.
22. Niitsuma, K., S. Miyagawa, and S. Osaki, *Mechanical anisotropy in cobra skin is related to body movement.* European Journal of Morphology, 2005. **42**(4/5): p. 193-200.
23. Bauer, A.M., A.P. Russell, and R.E. Shadwick, *Mechanical Properties and Morphological Correlates of Fragile Skin in Gekkonid Lizards.* J Exp Biol, 1989. **145**(1): p. 79-102.
24. Bauer, A.M., A.P. Russell, and R.E. Shadwick, *Skin mechanics and morphology of the gecko Teratoscincus scincus.* Amphibia-Reptilia, 1993. **14**: p. 321-331.
25. Pabst, D.A., *Springs in Swimming Animals.* American Zoologist, 1996. **36**(6): p. 723-735.
26. Pabst, D.A., *Morphology of the subdermal connective tissue sheath of dolphins: a new fibre-wound, thin-walled, pressurized cylinder model for swimming vertebrates.* Journal of Zoology, 1996. **238**(1): p. 35-52.
27. Hebrank, M.R. and J.H. Hebrank, *The Mechanics of Fish Skin: Lack of an "External Tendon" Role in Two Teleosts.* Biol Bull, 1986. **171**(1): p. 236-247.
28. Swartz, S.M., M.S. Groves, H.D. Kim, and W.R. Walsh, *Mechancial properties of bat wing membrane skin.* Journal of Zoology, 1996. **239**(2): p. 357-378.
29. Hebrank, M.R., *Mechanical Properties and Locomotor Functions of Eel Skin.* Biol Bull, 1980. **158**(1): p. 58-68.
30. Eckstein, A. and P.P. Vlachos, *Digital particle image velocimetry (DPIV) robust phase correlation.* Measurement Science and Technology, 2009. **20**(5): p. 055401.
31. Sutton, M.A., X. Ke, S.M. Lessner, M. Goldbach, M. Yost, F. Zhao, and H.W. Schreier, *Strain field measurements on mouse carotid arteries using microscopic three-dimensional digital image correlation.* J Biomed Mater Res A, 2008. **84**(1): p. 178-90.
32. Zhang, D., C. Eggleton, and D. Arola, *Evaluating the mechanical behavior of arterial tissue using digital image correlation.* Experimental Mechanics, 2002. **42**(4): p. 409-416.
33. Zhang, J., G.C. Jin, L.B. Meng, L.H. Jian, A.Y. Wang, and S.B. Lu, *Strain and mechanical behavior measurements of soft tissues with digital speckle method.* J Biomed Opt, 2005. **10**(3): p. 034021.
34. Lok, T.S., T.C. Jui, and J. Goh Cho Hong. *Soft tissue strain measurement using an optical method*. 2008. Nanjing, China: SPIE.
35. Krehbiel, J.D. and T.A. Berfield, *Applying Digital Image Correlation to Biological Materials*. p. 53-61.
36. Wang, Y.Q., M.A. Sutton, H.A. Bruck, and H.W. Schreier, *Quantitative Error Assessment in Pattern Matching: Effects of Intensity Pattern Noise, Interpolation, Strain and Image Contrast on Motion Measurements.* Strain, 2009. **45**(2): p. 160-178.
37. Wang, X. and R. Ker, *Creep rupture of wallaby tail tendons.* J Exp Biol, 1995. **198**(3): p. 831-845.
38. Huang, H. and et al., *On errors of digital particle image velocimetry.* Measurement Science and Technology, 1997. **8**(12): p. 1427.
39. Pan, B. and et al., *Two-dimensional digital image correlation for in-plane displacement and strain measurement: a review.* Measurement Science and Technology, 2009. **20**(6): p. 062001.

40. Cinelli, A.R., *Calcium transients in the garter snake vomeronasal organ.* Journal of neurophysiology, 2002. **87**(3): p. 1449.
41. Sanpaz. *Deformation of a continuum body from an undeformed configuration to a deformed configuration*. 2008 [cited 2011 March 21]; Available from: http://en.wikipedia.org/wiki/File:Deformation.png.
42. Provenzano, P., R. Lakes, T. Keenan, and R. vanderby, *Nonlinear Ligament Viscoelasticity.* Annals of Biomedical Engineering, 2001. **29**(10): p. 908-914.
43. Kalcioglu, Z.I., M. Qu, K.V. Vliet, K. Strawhecker, and M. VanLindingham. *Multiscale Characterization of Relaxation Times of Tissue Surrogate Gels and Soft Tissues*. in *Army Science Conference*.
44. Thornton, G.M., N.G. Shrive, and C.B. Frank, *Ligament creep recruits fibres at low stresses and can lead to modulus-reducing fibre damage at higher creep stresses: a study in rabbit medial collateral ligament model.* J Orthop Res, 2002. **20**(5): p. 967-74.
45. Osaki, S., *Orientational distribution of collagen fibers in cobra skin.* Cellular and molecular biology, including cyto-enzymology, 2004. **50 Online Pub**: p. OL559-64.
46. Larrabee, W.F., *A finite element model of skin deformation. I. Biomechanics of skin and soft tissue: A review.* The Laryngoscope, 1986. **96**(4): p. 399-405.
47. Kenedi, R.M. and et al., *Tissue mechanics.* Physics in Medicine and Biology, 1975. **20**(5): p. 699.
48. Pyron, R.A., F.T. Burbrink, G.R. Colli, A.N.M. de Oca, L.J. Vitt, C.A. Kuczynski, and J.J. Wiens, *The phylogeny of advanced snakes (Colubroidea), with discovery of a new subfamily and comparison of support methods for likelihood trees.* Molecular Phylogenetics and Evolution, 2011. **58**(2): p. 329-342.
49. Foutz, T.L., E.A. Stone, and C.F. Abrams, Jr., *Effects of freezing on mechanical properties of rat skin.* Am J Vet Res, 1992. **53**(5): p. 788-92.

Appendix A: Snake Phylogeny

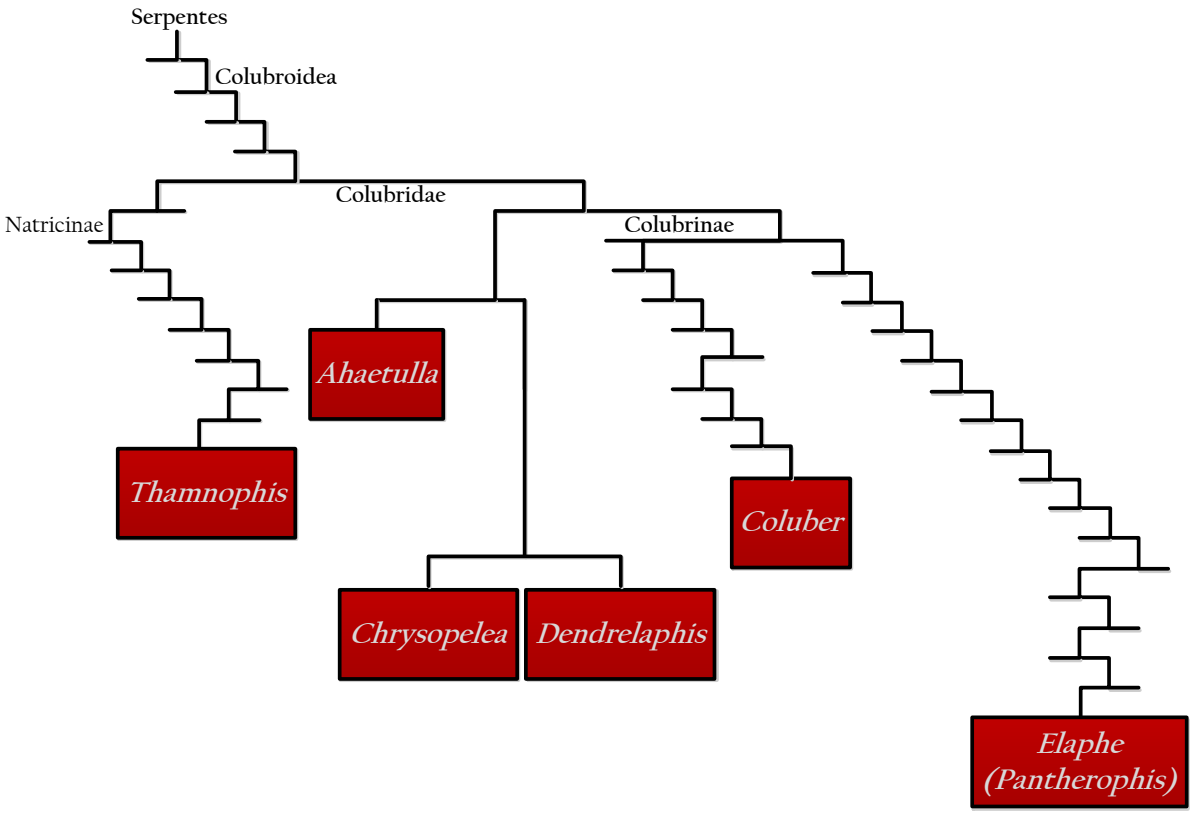

Figure A-1: Phylogeny of snakes used for this study, along with other snakes proposed for use. Derived from [48].

Appendix B: Testing Rationale and DIC Parameters

B.1. Thickness

To determine if thickness of a particular section of skin varied with the strain applied, thickness of the mid-section of a sample was measured at various extensions. Based on the plot below, after the initial 2-3 mm of extension, there does not seem to be any variability in thickness due to strain. For this reason, I have assumed thickness to be constant and equal to a value measured before testing.

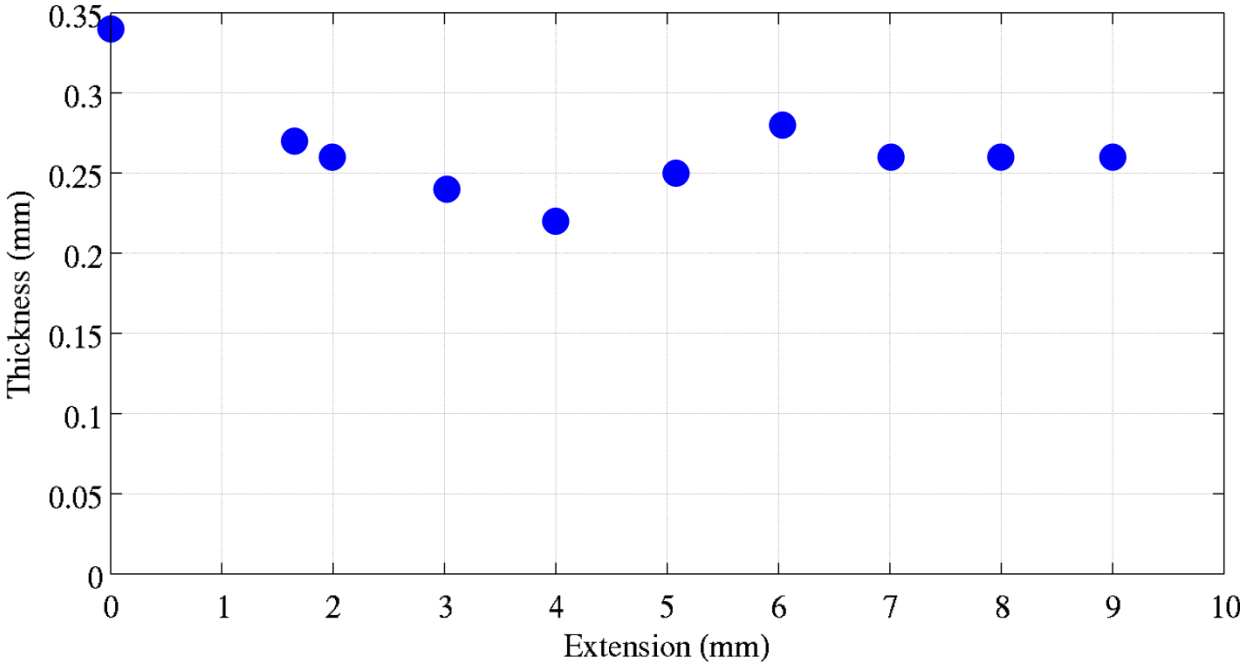

Figure B-1: Change in thickness with extension of sample.

B.2. Measurement Uncertainty and Error

By performing 5 independent thickness measurements on a single sample, the maximum uncertainty in repeated thickness measurements was 13.9% (for extremely thin samples, this may be slightly higher). The uncertainty in width measurements was determined by measuring the width of a sample at 5 points on the sample, with a value of 1.33%. The load uncertainty on the

tensile tester is 0.25% of the measured load, and error is 0.67% based on a static weight calibration. By comparing the displacement from a speckle-coated piece of paper displaced at 0.941 $mm \cdot s^{-1}$ to the output from the tensile tester, the error in DIC was calculated and found to range from 2-3.5% over the typical range of displacements seen.

B.3. Degradation Dependence

To analyze the effects of degradation, a series of tensile tests to failure was performed on samples from a single snake. The sample preparation and testing followed the protocol listed below. To determine the difference in properties with respect to time after euthanasia, *Elaphe guttata* 5 was divided into 3 sections (2 pre-pyloric and 1 post-pyloric) with 6 circumferential samples in each section. In each section, samples were tested at several time intervals over a period extending 72 hours after euthanasia (the intervals began at approximately 6.5, 20, 31, 48, and 72 hours). The sixth sample in each section was frozen. Maximum Lagrangian stress was compared, and there seemed to be no increase or decrease in stress with respect to time or freezing. Freezing has also been shown not to affect properties of rat skin [49].

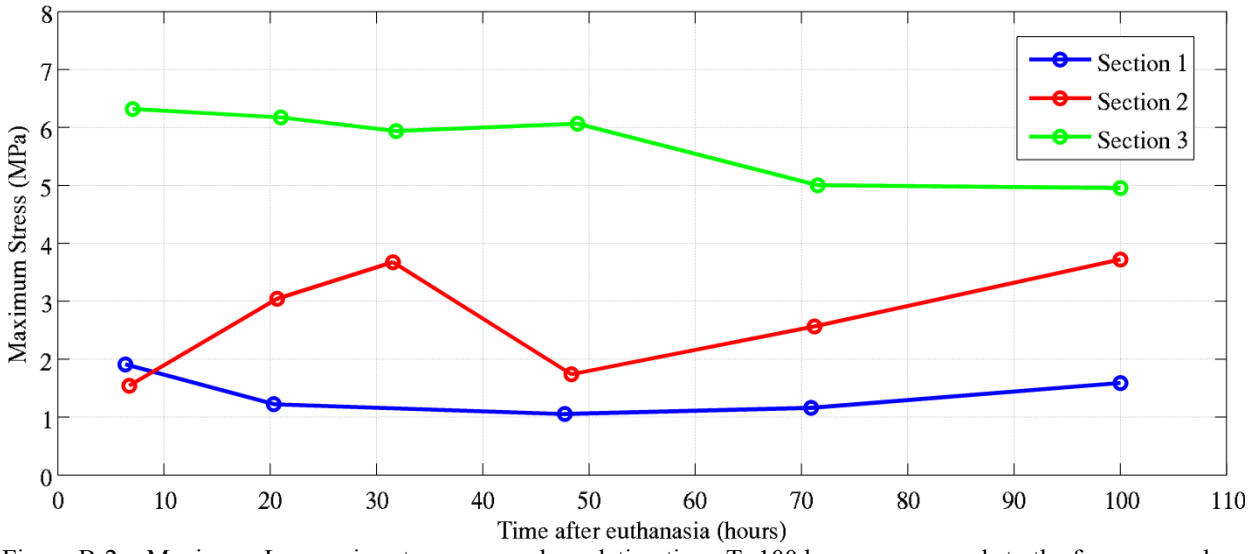

Figure B-2: : Maximum Lagrangian stress versus degradation time. T=100 hours corresponds to the frozen samples. Pre-pyloric: Sections 1 and 2; post-pyloric: Section 3. Although the samples were separated into three separate sections, sections 1 and 2 were combined in later experimentation as a general pre-pyloric region.

B.4. Prana Parameters

These parameters are used within Prana. A 3-pass multigrid approach with digital window offset is used. No data validation or correction is performed. The only difference in these parameters for different test types is seen in the image and correlation steps. For creep tests, the image step is 1, and in hysteresis, the steps change to 2 due to changes in data sampling rate. This creep step is used for frames 1-101, after which a step size of 100 is used (strain rates during this portion are very small, so this increases correlation accuracy). The hypothetical extension of the skin between consecutive image steps using these values is equal for all test cases.

Table B - 1: Digital Image Correlation parameters for normal and fast rate tests, along with the initial portion of relaxation tests. The only differences for creep and relaxation tests are changes in step sizes.

Parameter	*Value (pixels unless otherwise noted)*
Pass 1	
Window Size	128 x 128
Window Resolution	32 x 32
Pass 2	
Window Size	64 x 64
Window Resolution	16 x 16
Pass 3	
Window Size	32 x 32
Window Resolution	8 x 8
Outlier Detection	None
Image Step	10 (images)
Correlation Step	10 (images)

Appendix C: Additional Results and Figures

This Appendix presents the results from tensile tests. Table C-1 shows the linear strain before a significant load is applied. Tables are presented with the results of statistical comparisons using t-tests and ANOVAs. Significant comparisons are noted in each table by bold or italicized font. Figures are also given showing each test along with the average and standard deviation of each grouping.

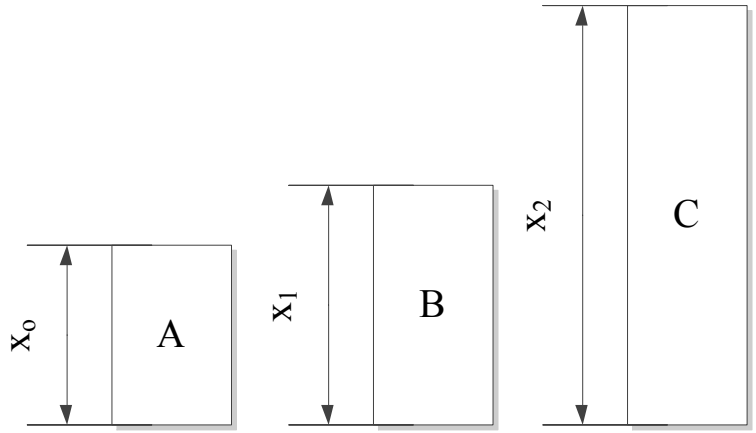

Figure C-1: Calculations of linear strains at various points. A = original configuration, B = configuration at 0.1 MPa, C = configuration at failure

The equations below show the derivation of the strain from configuration A to B with the values given for failure strains in the normalized and non-normalized configurations. By solving Equation 18.a for x_0 and Equation 18.b for x_1, these values can be substituted into Equation 18.c, yielding Equation 19. Because $\varepsilon_{A\text{-}C}$ and $\varepsilon_{B\text{-}C}$ are calculated values, and x_o is known, a value for $\varepsilon_{A\text{-}B}$ can be derived from these values.

$$\begin{aligned} \varepsilon_{A-C}^{'} &= \frac{x_2 - x_0}{x_0} \text{ (a)} \\ \varepsilon_{B-C}^{'} &= \frac{x_2 - x_1}{x_1} \text{ (b)} \\ E_{A-B}^{'} &= \frac{x_1 - x_0}{x_0} \text{ (c)} \end{aligned} \tag{C-1}$$

$$\varepsilon_{A-B}^{'} = \frac{\frac{x_2}{\varepsilon_{B-C}^{'} + 1} - \frac{x_2}{\varepsilon_{A-C}^{'} + 1}}{\frac{x_2}{\varepsilon_{A-C}^{'} + 1}} \tag{C-2}$$

By solving Equation 18.a for x_2 in terms of known values $\varepsilon_{A\text{-}C}$ and x_o and substituting into Equation 19, an equation for $\varepsilon_{A\text{-}B}$ is derived in terms of only the normalized and non-normalized maximum strains.

$$\varepsilon_{A-B}^{'} = \frac{\varepsilon_{A-C}^{'} + 1}{\varepsilon_{B-C}^{'} + 1} - 1 \tag{C-3}$$

Table C-1: Strain at 0.1 MPa for all snakes.

Strain at 0.1 MPa		*Longitudinal*	*Circumferential*	*Ventral*
C. ornata	Pre-Pyloric	0.19 (0.069)	0.44 (0.22)	0.22 (0.17)
	Post-Pyloric	0.19 (0.077)	0.15 (0.0011)	0.20 (0.061)
E. guttata	Pre-Pyloric	0.17 (0.090)	0.36 (0.12)	0.30 (0.060)
	Post-Pyloric	0.26 (0.078)	0.26 (0.16)	0.34 (0.034)
T. sirtalis	Pre-Pyloric	0.17 (0.020)	0.51 (0.23)	0.44 (0.035)
	Post-Pyloric	0.15 (-0.061)	0.23 (0.011)	0.33 (0.14)

Table C-2: *C. ornata* statistical comparison results. Region 1 = pre-pyloric, region 2 = post-pyloric. L=longitudinal, C=circumferential, V=ventral. Significant values ($p < 0.05$) are indicated in bold, and likely significant values ($p < 0.1$) are italicized.

Region 1	***Orientation 1***	***Region 2***	***Orientation 2***	***Lagrangian Stress***	***Eulerian Stress***	***Strain Energy***	***Linear Strain***	***Nonlinear Strain***	***Modulus***
1	**L**	**1**	**V**	**0.032**	**0.004**	**0.044**	0.146	*0.082*	0.209
1	**L**	**1**	**C**	**0.002**	**0.007**	**0.031**	0.773	**< 0.001**	**< 0.001**
1	**C**	**1**	**V**	0.118	0.889	0.928	0.118	**< 0.001**	**< 0.001**
2	**L**	**2**	**V**	**0.020**	*0.010*	**0.050**	**0.016**	**< 0.001**	0.162
2	**L**	**2**	**C**	0.914	0.965	0.144	**< 0.001**	**0.001**	0.573
2	**C**	**2**	**V**	*0.074*	*0.068*	**0.026**	**< 0.001**	**< 0.001**	0.731
1	**L**	**2**	**L**	*0.081*	**0.034**	0.217	0.933	*0.064*	0.307
1	**C**	**2**	**C**	*0.055*	*0.060*	**0.028**	**< 0.001**	0.009	0.192
1	**V**	**2**	**V**	0.749	0.784	0.824	0.968	0.789	**0.098**

Table C-3: Results of ANOVA on *C. ornata* data. F and p values are given. Significant values ($p < 0.05$) are indicated in bold, and likely significant values ($p < 0.1$) are italicized.

	Lagrangian Stress	*Eulerian Stress*	*Strain Energy*	*Linear Strain*	*Nonlinear Strain*	*Modulus*
Region	**F = 19.48**	**F = 25.81**	**F = 24.43**	**F = 4.89**	**F = 7.36**	F = 1.1
	P < 0.001	**P > 0.001**	**P < 0.001**	**P = 0.031**	**P = 0.009**	P = 0.299
Orientation	**F = 7.14**	**F = 9.90**	**F = 11.78**	**F = 12.48**	**F = 33.57**	*F = 2.7*
	P = 0.002	**P < 0.001**	**P < 0.001**	**P < 0.001**	**P < 0.001**	*P = 0.075*
Region·Orientation	**F = 6.11**	**F = 6.24**	**F = 11.98**	**F = 3.85**	F = 1.72	**F = 4.09**
	P = 0.004	**P = 0.003**	**P < 0.001**	**P = 0.026**	P = 0.188	**P = 0.021**

Table C-4: *E. guttata* statistical comparison results. Region 1 = pre-pyloric, region 2 = post-pyloric. L=longitudinal, C=circumferential, V=ventral. Significant values ($p < 0.05$) are indicated in bold, and likely significant values ($p < 0.1$) are italicized.

Region 1	***Orientation 1***	***Region 2***	***Orientation 2***	***Lagrangian Stress***	***Eulerian Stress***	***Strain Energy***	***Linear Strain***	***Nonlinear Strain***	***Modulus***
1	**L**	**1**	**V**	**< 0.001**	**< 0.001**	**< 0.001**	*0.077*	0.146	0.245
1	**L**	**1**	**C**	**< 0.001**	**< 0.001**	0.135	**0.036**	**< 0.001**	**< 0.001**
1	**C**	**1**	**V**	0.117	0.111	**0.001**	**0.003**	**< 0.001**	**0.042**
2	**L**	**2**	**V**	**< 0.001**	**< 0.001**	**< 0.001**	**< 0.001**	**< 0.001**	**< 0.001**
2	**L**	**2**	**C**	0.930	0.957	*0.080*	0.283	0.150	0.414
2	**C**	**2**	**V**	**< 0.001**	**< 0.001**	**< 0.001**	**< 0.001**	**< 0.001**	**0.001**
1	**L**	**2**	**L**	0.583	0.388	0.391	**0.015**	**< 0.001**	0.235
1	**C**	**2**	**C**	**< 0.001**	**< 0.001**	**0.001**	0.210	0.700	**0.002**
1	**V**	**2**	**V**	0.755	0.911	0.925	0.968	0.607	**0.032**

Table C-5: Results of ANOVA on *E. guttata* data. F and p (in parentheses) values are given. Significant values ($p < 0.05$) are indicated in bold, and likely significant values ($p < 0.1$) are italicized.

	Lagrangian Stress	*Eulerian Stress*	*Strain Energy*	*Linear Strain*	*Nonlinear Strain*	*Modulus*
Region	**F=6.53**	**F = 7.50**	**F = 7.79**	*F = 3.60*	**F = 5.87**	F = 1.00
	P = 0.012	**P = 0.007**	**P = 0.006**	*P = 0.061*	**P = 0.017**	P = 0.321
Orientation	**F = 19.40**	**F = 1.80**	**F = 13.66**	**F = 20.63**	**F = 29.19**	**F = 14.56**
	P < 0.001	**P < 0.001**	**P < 0.001**	**P < 0.001**	**P < 0.001**	**P < 0.001**
Region·Orientation	**F = 5.24**	**F = 4.54**	**F = 4.89**	F = 1.11	**F = 3.61**	**F = 9.56**
	P = 0.007	**P = 0.013**	**P = 0.009**	P = 0.332	**P = 0.030**	**P < 0.001**

Table C-6: *T. sirtalis* statistical comparison results. Region 1 = pre-pyloric, region 2 = post-pyloric. L=longitudinal, C=circumferential, V=ventral. Significant values ($p < 0.05$) are indicated in bold, and likely significant values ($p < 0.1$) are italicized.

Region 1	***Orientation 1***	***Region 2***	***Orientation 2***	***Lagrangian Stress***	***Eulerian Stress***	***Strain Energy***	***Linear Strain***	***Nonlinear Strain***	***Modulus***
1	**L**	**1**	**V**	*0.052*	0.108	0.203	0.575	0.267	**0.037**
1	**L**	**1**	**C**	0.133	0.196	0.795	**0.006**	**0.003**	**0.023**
1	**C**	**1**	**V**	0.136	0.192	0.132	**0.015**	**0.016**	0.328
2	**L**	**2**	**V**	0.433	0.440	0.539	0.714	0.558	0.327
2	**L**	**2**	**C**	0.639	0.613	0.627	*0.061*	*0.052*	0.383
2	**C**	**2**	**V**	*0.069*	*0.070*	*0.064*	**0.020**	**0.026**	0.216
1	**L**	**2**	**L**	0.585	0.569	0.609	0.787	0.637	0.634
1	**C**	**2**	**C**	*0.061*	*0.051*	*0.078*	0.237	0.474	**< 0.001**
1	**V**	**2**	**V**	0.116	*0.091*	0.287	0.604	0.661	0.650

Table C-7: Results of ANOVA on *T. sirtalis* data. F and p (in parentheses) values are given. Significant values ($p < 0.05$) are indicated in bold, and likely significant values ($p < 0.1$) are italicized.

	Lagrangian Stress	*Eulerian Stress*	*Strain Energy*	*Linear Strain*	*Nonlinear Strain*	*Modulus*
Region	**F = 4.7**	*F = 4.04*	**F = 6.63**	**F = 1.79**	F = 0.95	*F = 3.13*
	P = 0.046	*P = 0.062*	**P = 0.020**	**P = 0.200**	P = 0.343	*P = 0.096*
Orientation	**F = 4.83**	**F = 3.84**	**F = 4.43**	**F = 22.21**	**F = 19.82**	**F = 11.94**
	P = 0.023	**P = 0.043**	**P = 0.029**	**P < 0.001**	**P < 0.001**	**P < 0.001**
Region·Orientation	F = 0.39	F = 0.37	F = 1.36	F = 0.51	F = 0.04	F = 0.44
	P = 0.685	P = 0.699	P = 0.285	P = 0.611	P = 0.957	P = 0.651

Table C-8: Species statistical comparison results. Region 1 = pre-pyloric, region 2 = post-pyloric. L=longitudinal, C=circumferential, V=ventral. Significant values ($p < 0.05$) are indicated in bold, and likely significant values ($p < 0.1$) are italicized.

Region	***Orientation***	***Species 1***	***Species 2***	***Lagrangian Stress***	***Eulerian Stress***	***Strain Energy***	***Linear Strain***	***Nonlinear Strain***	***Modulus***
1	**L**	**CO**	**EG**	**0.002**	**0.003**	**0.019**	0.869	0.836	**< 0.001**
1	**C**	**CO**	**EG**	0.129	0.251	**0.003**	*0.078*	0.582	0.034
1	**V**	**CO**	**EG**	0.162	0.502	0.391	0.909	0.705	**0.989**
1	**L**	**CO**	**TS**	0.941	0.968	0.614	**0.001**	**0.011**	0.389
1	**C**	**CO**	**TS**	0.367	0.117	0.479	*0.094*	0.360	**0.025**
1	**V**	**CO**	**TS**	**0.007**	**0.011**	*0.087*	0.861	0.605	**0.002**
1	**L**	**TS**	**EG**	**0.028**	*0.059*	**0.037**	**0.003**	**0.016**	**0.068**
1	**C**	**TS**	**EG**	**0.029**	**0.011**	0.360	0.323	0.491	**< 0.001**
1	**V**	**TS**	**EG**	*0.052*	*0.037*	0.283	0.939	0.821	**0.015**
2	**L**	**CO**	**EG**	0.354	0.468	0.311	**0.028**	*0.080*	0.563
2	**C**	**CO**	**EG**	0.615	0.686	0.934	**0.021**	**0.026**	0.580
2	**V**	**CO**	**EG**	0.137	0.177	0.366	0.781	0.208	0.128
2	**L**	**CO**	**TS**	0.972	0.966	0.941	0.398	0.265	0.663
2	**C**	**CO**	**TS**	0.242	0.183	0.687	0.615	0.874	0.436
2	**V**	**CO**	**TS**	0.153	0.216	0.712	0.707	0.427	*0.089*
2	**L**	**TS**	**EG**	0.799	0.796	0.828	0.248	0.198	0.787
2	**C**	**TS**	**EG**	**0.012**	**0.006**	0.666	0.149	0.215	**0.003**
2	**V**	**TS**	**EG**	0.813	0.690	0.863	0.627	0.685	0.578

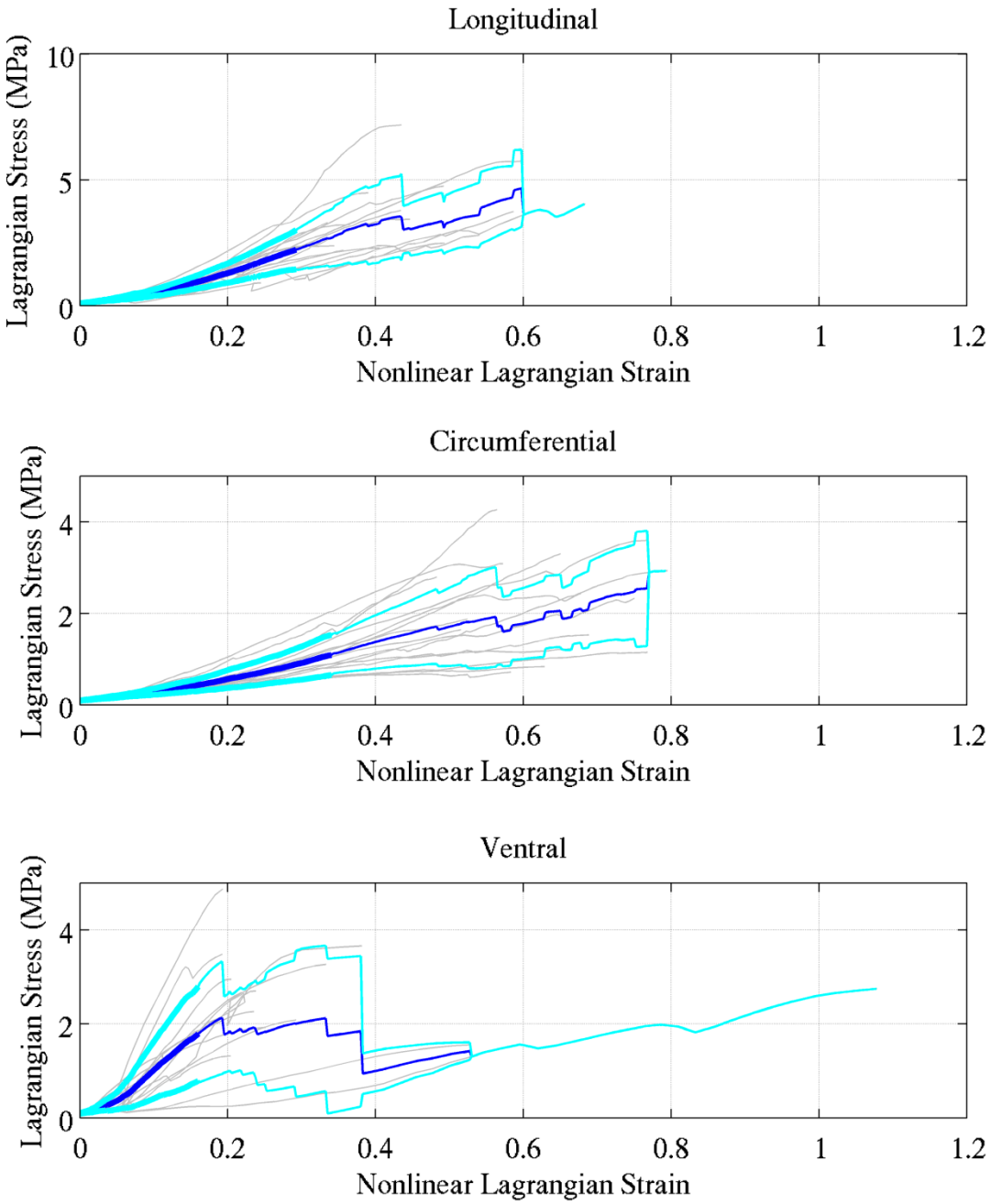

Figure C-2: *C. ornata* pre-pyloric samples. An average of all tests up to the least maximum strain is shown in dark blue, with one standard deviation shown in light blue. The finer lines show the same values, but may seem erratic due to decreasing sample numbers at higher strains.

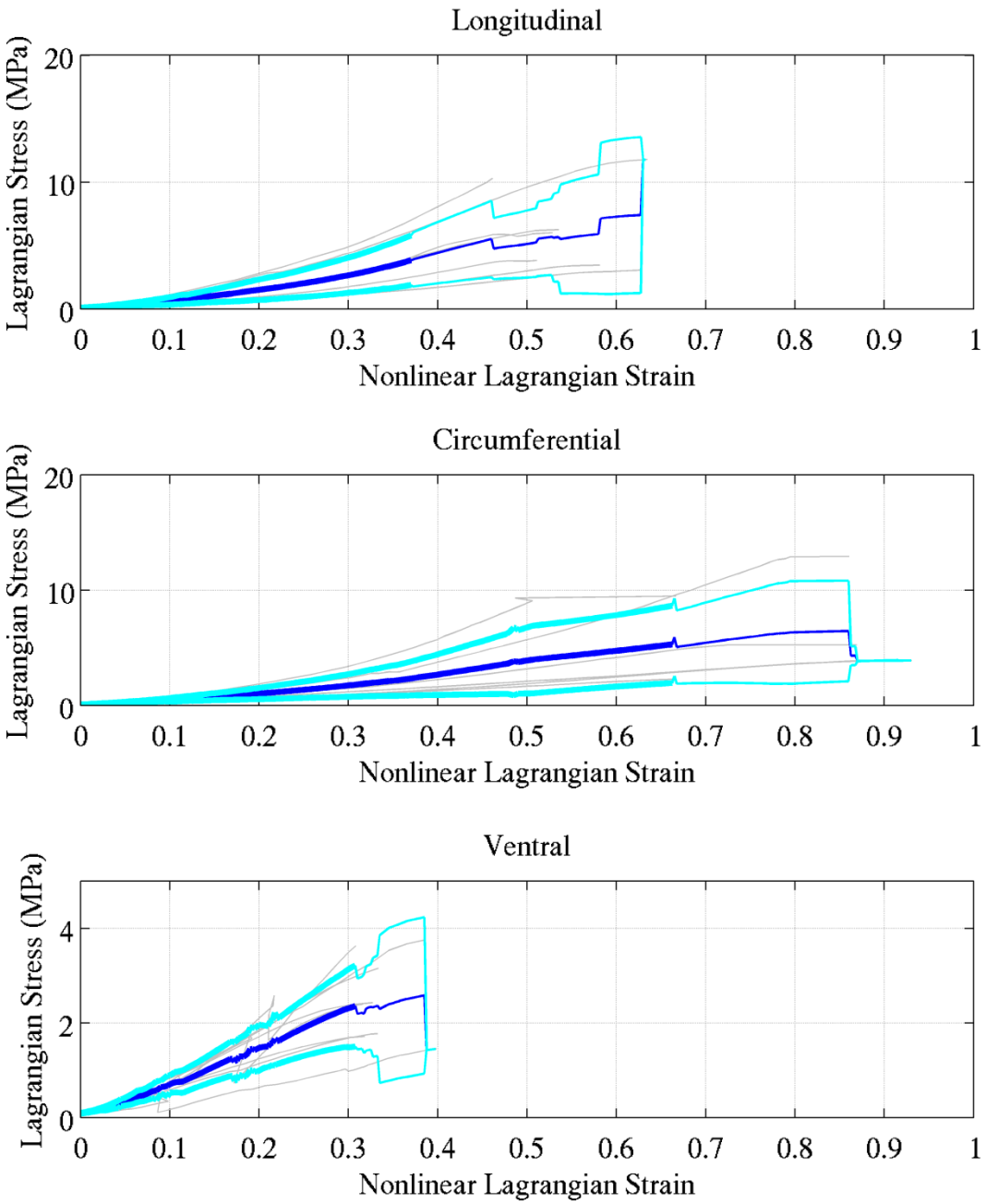

Figure C-3: *C. ornata* post-pyloric samples. An average of all tests up to the least maximum strain is shown in dark blue, with one standard deviation shown in light blue. The finer lines show the same values, but may seem erratic due to decreasing sample numbers at higher strains.

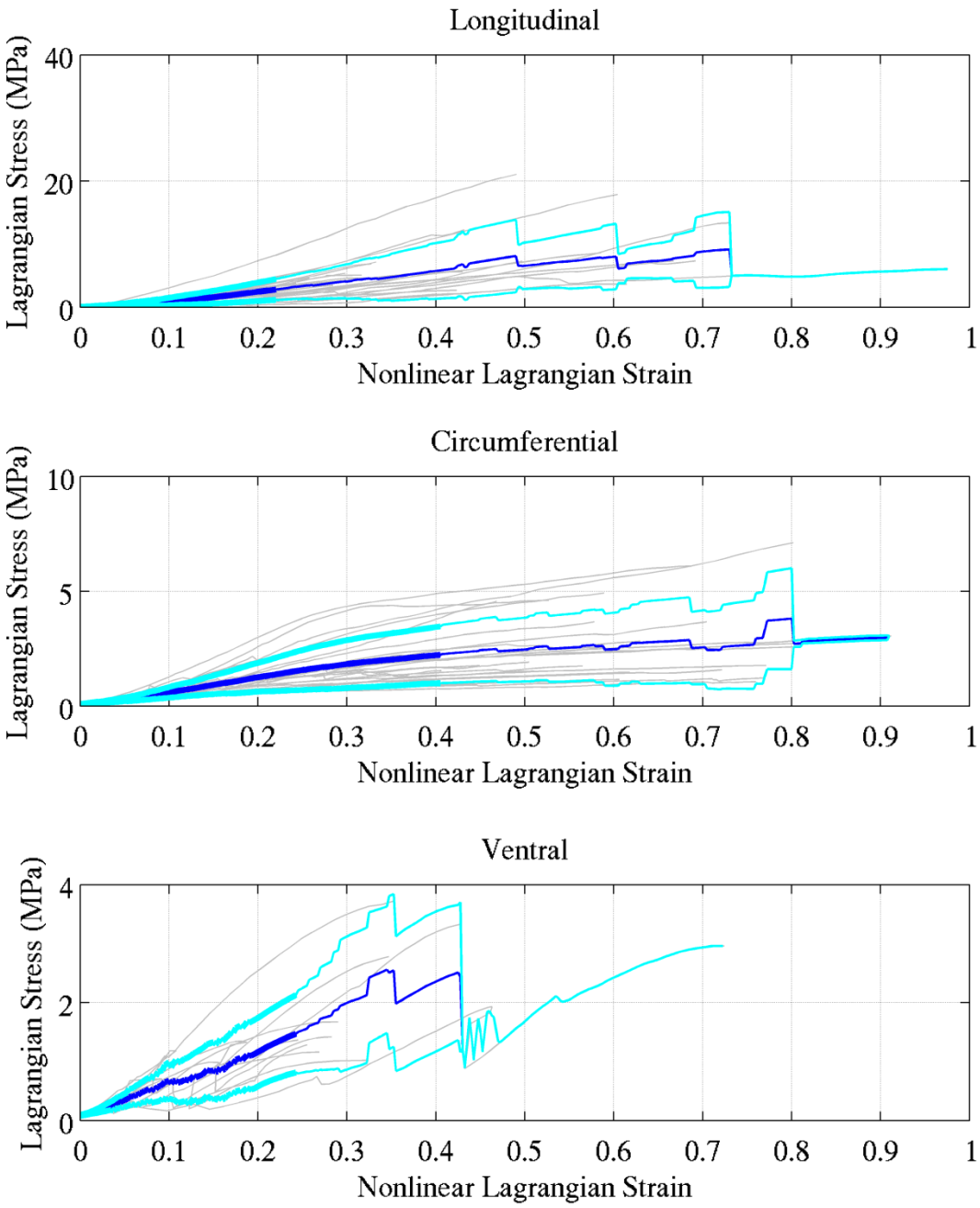

Figure C-4: *E. guttata* pre-pyloric samples. An average of all tests up to the least maximum strain is shown in dark blue, with one standard deviation shown in light blue. The finer lines show the same values, but may seem erratic due to decreasing sample numbers at higher strains.

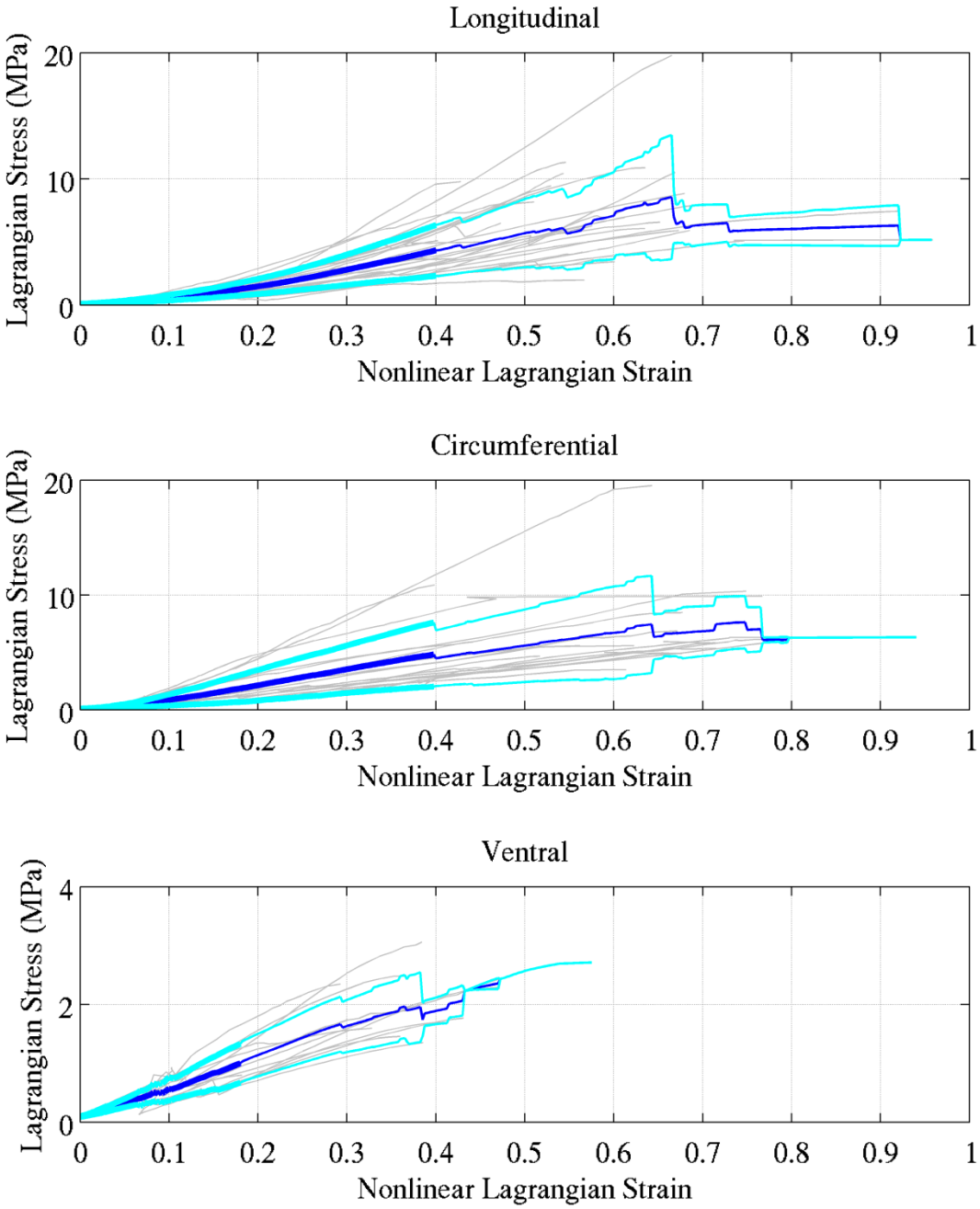

Figure C-5: *E. guttata* post-pyloric samples. An average of all tests up to the least maximum strain is shown in dark blue, with one standard deviation shown in light blue. The finer lines show the same values, but may seem erratic due to decreasing sample numbers at higher strains.

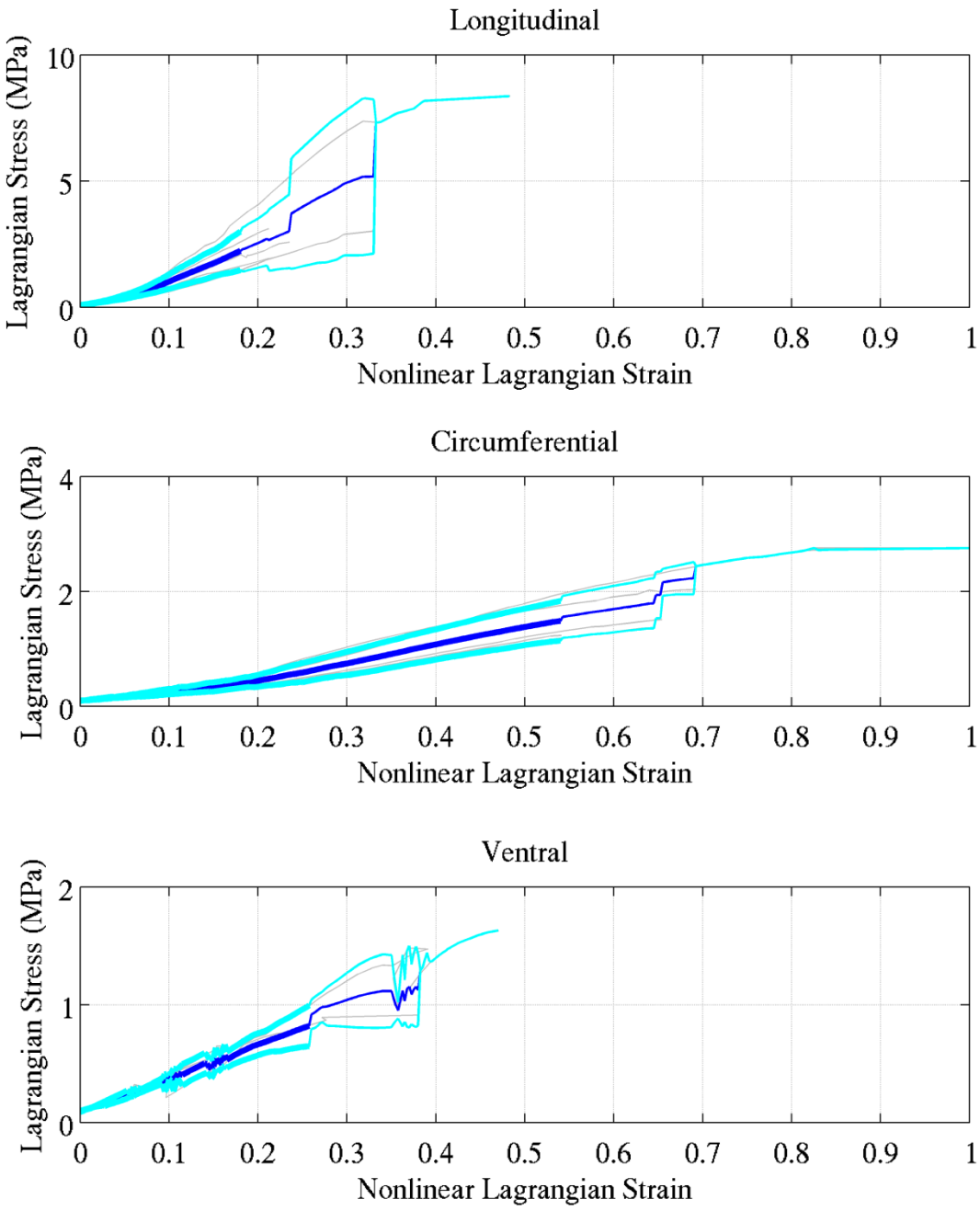

Figure C-6: *T. sirtalis* pre-pyloric samples. An average of all tests up to the least maximum strain is shown in dark blue, with one standard deviation shown in light blue. The finer lines show the same values, but may seem erratic due to decreasing sample numbers at higher strains.

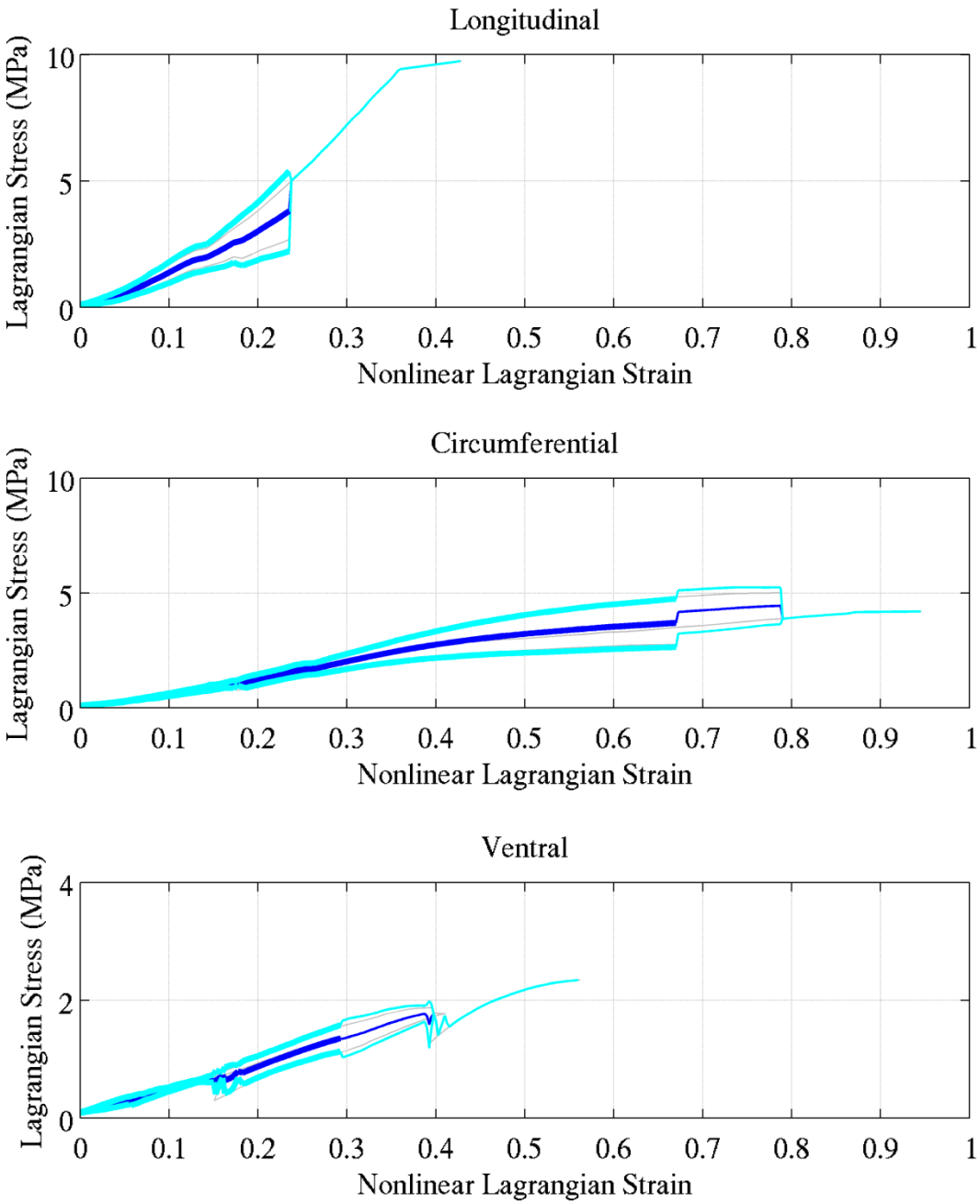

Figure C-7: *T. sirtalis* post-pyloric samples. An average of all tests up to the least maximum strain is shown in dark blue, with one standard deviation shown in light blue. The finer lines show the same values, but may seem erratic due to decreasing sample numbers at higher strains.

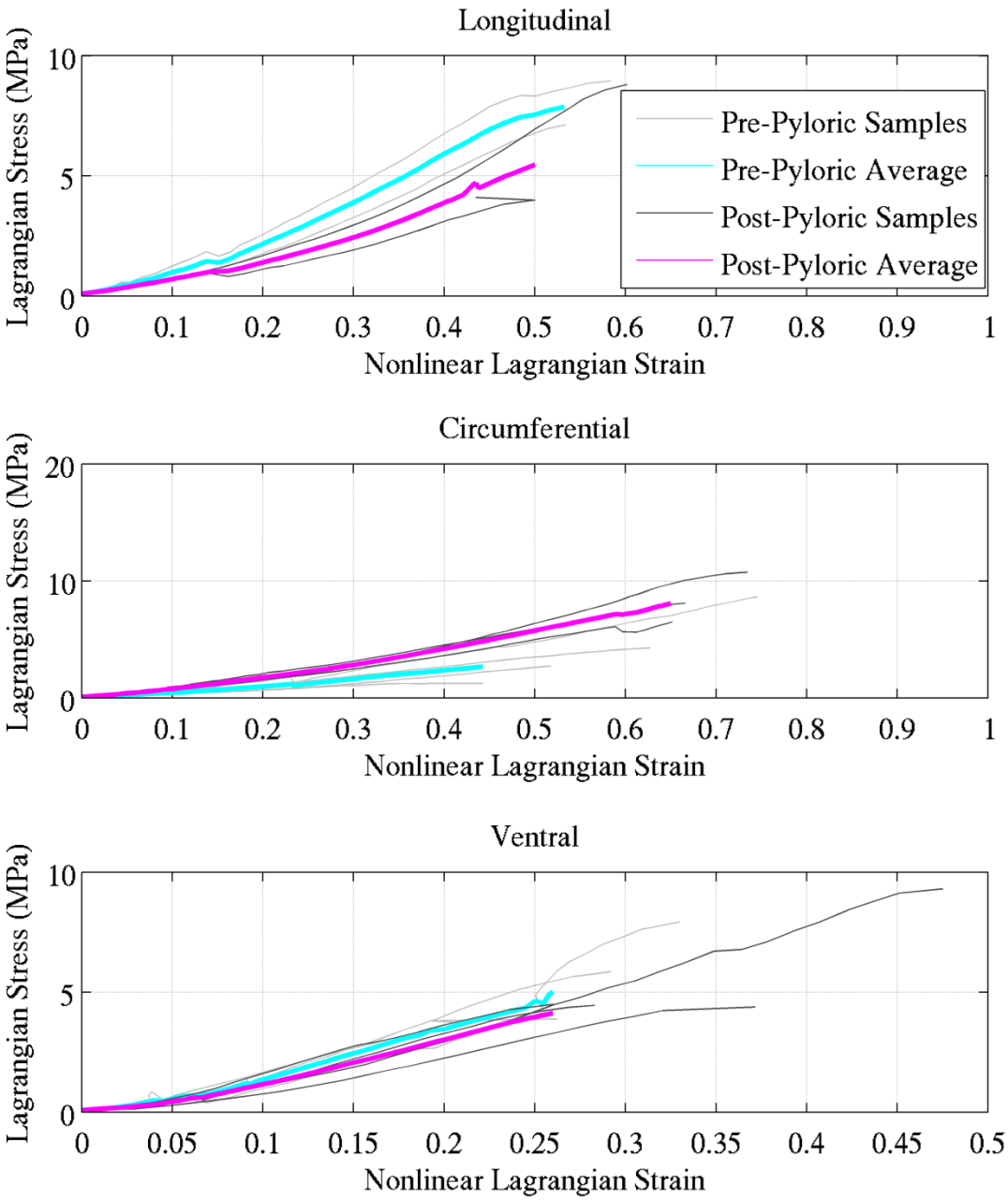

Figure C-8: *C. ornata* fast rate stress versus strain curves.

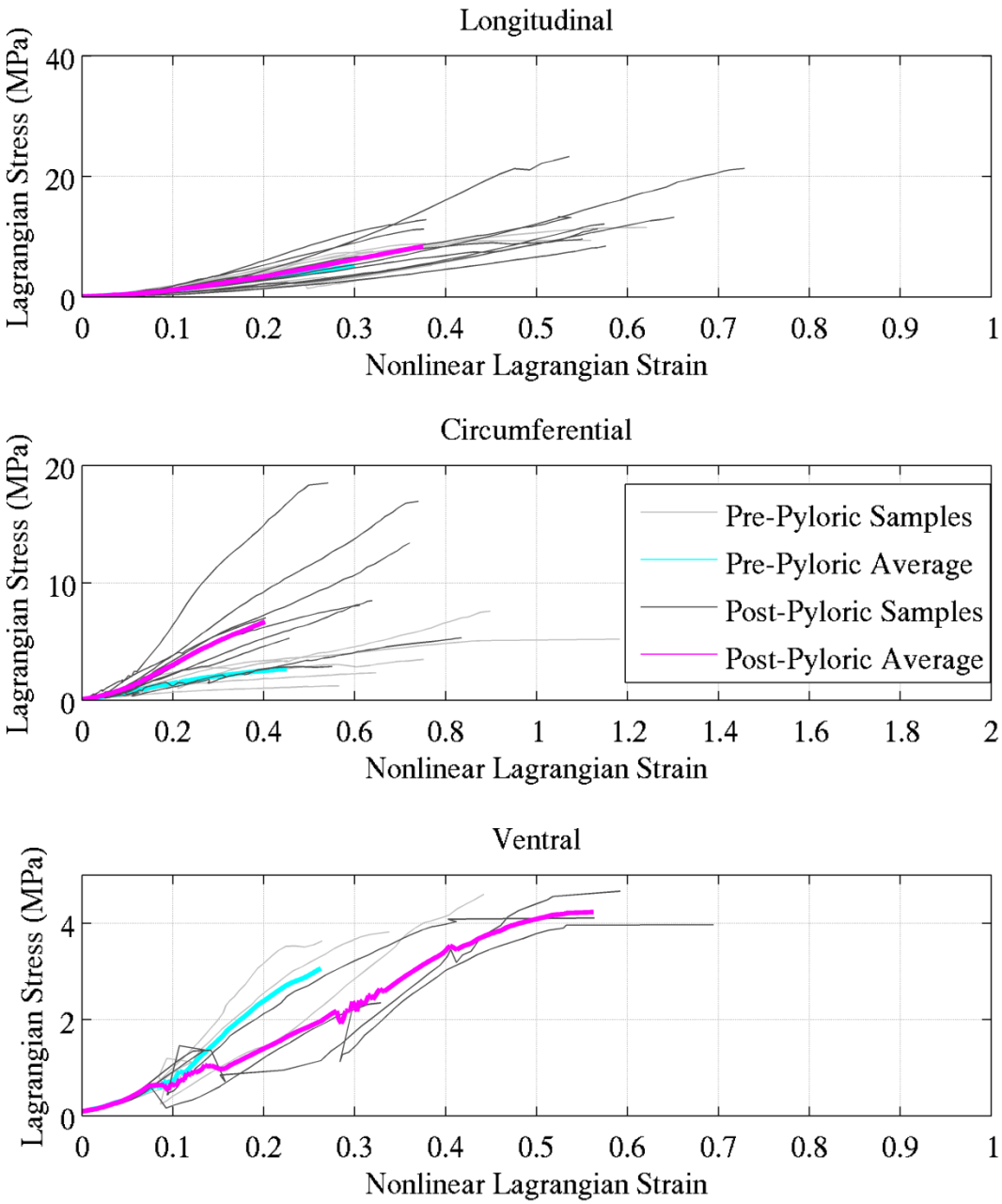

Figure C-9: *E. guttata* fast rate stress versus strain curves.